

A BROWN DWARF CENSUS FROM THE SIMP SURVEY

Jasmin Robert^{1,7}, Jonathan Gagné^{2,3}, Étienne Artigau⁴, David Lafrenière^{4,7}, Daniel Nadeau¹, René Doyon⁴, Lison Malo⁵, Loïc Albert⁴, Corinne Simard¹, Daniella C. Bardalez Gagliuffi⁶, Adam J. Burgasser⁶

Département de physique and Observatoire du Mont-Mégantic, Université de Montréal, Montréal,
QC H3C 3J7, Canada

Received _____; accepted _____

Accepted in *Astrophysical Journal*

¹Département de Physique, Université de Montréal, C.P. 6128 Succ. Centre-ville, Montréal, QC, H3C 3J7, Canada; jasmin@astro.umontreal.ca

²Carnegie Institution of Washington, 5241 Broad Branch Road, Washington, DC 20015, USA

³Sagan Fellow

⁴Institut de Recherche sur les Exoplanètes (iREx), Université de Montréal, Département de Physique, C.P. 6128 Succ. Centre-ville, Montréal, QC H3C 3J7, Canada

⁵Canada-France-Hawaii Telescope, 65-1238 Mamalahoa Hwy, Kamuela, HI 96743, USA

⁶Center for Astrophysics and Space Sciences, University of California San Diego, 9500 Gilman Dr., Mail Code 0424, La Jolla, CA 92093, USA

⁷Visiting Astronomer at the Infrared Telescope Facility, which is operated by the University of Hawaii under contract NNH14CK55B with the National Aeronautics and Space Administration.

ABSTRACT

We have conducted a near-infrared (NIR) proper motion survey, the Sondage Infrarouge de Mouvement Propre, in order to discover field ultracool dwarfs (UCD) in the solar neighborhood. The survey was conducted by imaging $\sim 28\%$ of the sky with the Caméra PAnoramique Proche-InfraRouge both in the southern hemisphere at the Cerro Tololo Inter-American Observatory 1.5 m telescope, and in the northern hemisphere at the Observatoire du Mont-Mégantic 1.6 m telescope and comparing the source positions from these observations with the Two Micron All-Sky Survey Point Source Catalog (2MASS PSC). Additional color criteria were used to further discriminate unwanted astrophysical sources. We present the results of an NIR spectroscopic follow-up of 169 M, L, and T dwarfs. Among the sources discovered are 2 young field brown dwarfs, 6 unusually red M and L dwarfs, 25 unusually blue M and L dwarfs, 2 candidate unresolved L+T binaries, and 24 peculiar UCDs. Additionally, we add 9 L/T transition dwarfs (L6–T4.5) to the already known objects.

Subject headings: brown dwarf, stars: low-mass, infrared: stars, proper motions, surveys, solar neighborhood

1. INTRODUCTION

Ever since the discovery of the high proper motion of Barnard’s star (Barnard 1916), proper motion has proved to be an effective method to identify faint stars in the solar neighborhood. Even thin disk stars, which are comoving with the Sun, have residual velocities of the order of tens of km s^{-1} . This arises mainly from the fact that, as stars age, they randomly interact with interstellar cloud complexes and spiral arms, which progressively increases their velocity dispersion. This leads to proper motions of about 100 mas yr^{-1} for stars up to $\sim 50 \text{ pc}$.

With the advent of sensitive near-infrared (NIR) hybrid mosaic detectors, the search for low-mass stars and substellar objects has become possible. Hundreds of ultracool dwarfs (UCDs; spectral type M7 or later; Kirkpatrick et al. 1995) have been discovered through large-scale red-optical ($0.6\text{--}1.0 \mu\text{m}$) surveys, such as the Sloan Digital Sky Survey (SDSS; York et al. 2000), the Canada–France Brown Dwarf Survey (Delorme et al. 2008), the Pan-STARRS1 3π Survey (PS1; Kaiser et al. 2010), along with large-scale and all-sky NIR ($1.0\text{--}2.5 \mu\text{m}$) surveys, e.g., the DEep Near Infrared Survey (DENIS; Epchtein et al. 1997), the Two Micron All Sky Survey (2MASS; Skrutskie et al. 2006), the UKIRT Infrared Deep Sky Survey (UKIDSS; Lawrence et al. 2007), the VISTA Hemisphere Survey (VHS; McMahon 2012) and the all-sky mid-infrared ($3.4\text{--}22 \mu\text{m}$) *Wide-Field Infrared Survey Explorer* (*WISE*; Wright et al. 2010) survey.

Most of these surveys used color-based criteria to identify UCDs (Delfosse et al. 1997; Kirkpatrick et al. 1999; Burgasser et al. 2002a; Hawley et al. 2002; Kirkpatrick et al. 2011). While this is an effective way of finding UCDs, it may overlook objects with peculiar colors, such as very low metallicity halo objects (subdwarfs; Burgasser et al. 2003; Sivarani et al. 2009).

Furthermore, an increase in opacity of the CH_4 , H_2O , and H_2 molecules in the atmosphere of L/T transition dwarfs (L6–T4.5) leads to NIR colors similar to those of M and early-L dwarfs (Leggett et al. 2000; Chiu et al. 2006). The ability to select transition dwarf candidates for spectroscopic follow-up is important to uncover a large sample of these objects and better

understand the processes causing condensate cloud disruption (Ackerman & Marley 2001; Burgasser et al. 2002b; Knapp et al. 2004), which is known to happen in their photosphere as they evolve and cool down. This effect has been demonstrated in several variability studies (Crossfield 2014 and references therein). While recent studies were able to discover some L/T transition dwarfs (Best et al. 2013; Scholz et al. 2014), it is likely that several more are still hiding in surveys such as 2MASS and *WISE*.

This could also be said of UCDs very close to the Sun. Previous studies (Metchev et al. 2008; Burningham et al. 2010; Reylé et al. 2010; Kirkpatrick et al. 2012) have suggested that the space density of brown dwarfs is below that of stars, with possibly a minimum at the L/T transition (Day-Jones et al. 2013 and references therein). However, the recent finding of the brown dwarf binary WISE J104915.57–531906.1 (Luhman 2013), and of the coldest brown dwarf known to date, WISE J085510.83–071442.5 (Luhman 2014), outclassing Wolf 359 and Lalande 21185 as the third and fourth closest systems to the Sun, provides evidence that the search for UCDs in the solar neighborhood is far from over. The proper motion method is the most efficient way of uncovering nearby ($\lesssim 50$ pc) UCDs in a color-unbiased search, just as it is for warmer stars.

While some surveys include multi-epoch observations that can lead to a detection of proper motion (Looper et al. 2008; Kirkpatrick et al. 2010), the small timespan (approximately one to two years) between individual observations is better suited for the detection of very large proper motions. This is the case for AllWISE (Kirkpatrick et al. 2014), released to track down high-proper motion objects in the *WISE* catalog. However, as noted by Kirkpatrick et al. (2014), AllWISE measures only the apparent motion on the sky, because most objects were observed only at two epochs separated by six months. This interval maximizes the effect of the parallax on the motion of the sources, hindering the calculation of their true proper motion.

Some studies have combined the different epochs of two or more of those surveys to search for high proper motion objects: DENIS and 2MASS (Artigau et al. 2010), 2MASS and SDSS

(Metchev et al. 2008; Sheppard & Cushing 2009; Geißler et al. 2011), 2MASS and UKIDSS (Deacon et al. 2009), and more recently 2MASS and *WISE* (Bihain et al. 2013; Pérez Garrido et al. 2014) or 2MASS and AllWISE (Gagné et al. 2015) and Pan-Starrs and AllWISE (Best et al. 2013). Others used several of those surveys to identify new candidates (Aberasturi et al. 2011; Scholz et al. 2012) or added a second epoch of *K*-band astrometry, such as the UKIDSS Galactic Plane Survey (GPS; Lucas et al. 2008), in which a new T5 dwarf and several other L and T dwarf candidates were recently discovered in the galactic plane (Smith et al. 2014).

It is in this context that the large area NIR proper motion survey Sondage Infrarouge de Mouvement Propre (SIMP) was initiated using the 2MASS Point Source Catalog (PSC¹) as a first epoch. This brings the possibility of discovering UCDs in the solar neighborhood that were missed in other searches, such as L/T transition dwarfs or UCDs with peculiar photometric colors. This survey is also suited for the discovery of wide binaries and members of young moving groups. Discovering more of these objects will help constrain the substellar mass function and the brown dwarf space density in the solar neighborhood. Furthermore, cataloging a large number of high-proper motion brown dwarfs will be useful for predicting microlensing events, enabling an independent and direct measurement of their masses (Evans 2014).

Since 2MASS and SIMP use similar filters and pixel scales and reach photometric comparable depths (see Section 2), cross-matching sources is straightforward. This survey has already enabled the discovery of several UCDs: a bright, nearby T2.5 dwarf (SIMP J013656.5+093347; Artigau et al. 2006), five very low-mass binaries (SIMP J1619275+031350AB & SIMP J1501530–013506AB; Artigau et al. 2011, 2MASS J10432513–1706065, 2MASS J11150150+1607026 & 2MASS J12594167+1001380; Baron et al. 2015), and a low-gravity L5 β/γ candidate member of the Argus association (SIMP J21543454–1055308; Gagné et al. 2014, 2015b). This paper presents the remaining UCDs

¹see <http://irsa.ipac.caltech.edu/>

discovered so far through the SIMP survey.²

The SIMP survey is described in detail in Section 2, and the spectroscopic and photometric follow-ups are presented in Section 3 and Section 4, respectively. We describe the method used to classify the candidates in Section 5 and we present the results in Section 6. We summarize and conclude in Section 7.

2. THE SIMP SURVEY

The SIMP survey was initiated in early 2005, when a newly developed wide-field NIR camera, the Caméra PAnoramique Proche Infra-Rouge (CPAPIR; Artigau et al. 2004), was installed at the Cerro Tololo Inter-American Observatory (CTIO) 1.5 m telescope, which is operated by the SMARTS consortium. CPAPIR uses a HAWAII-II 2048×2048 HgCdTe detector and is designed to image a large portion of the sky at once, making it one of the most efficient NIR survey instruments for small-class (up to 2 m) telescopes. At the CTIO, it has a pixel scale of 1.''03, yielding a field of view of 34'.8×34'.8. Two filter wheels contain 10 broad- and narrowband filters, within its 0.8–2.5 μm bandpass. CPAPIR was used at CTIO from 2005 February to 2007 March.

From 2007 August to 2009 November, the SIMP survey was conducted with CPAPIR at the Observatoire du Mont-Mégantic (OMM) 1.6 m telescope (Racine 1978). The OMM and CTIO survey procedures were similar (see below), except that the OMM field of view decreased to 30'×30', with a pixel scale of 0.''89.

The SIMP observations were obtained in the MKO *J* band ($\lambda_c = 1.25 \mu\text{m}$ and $\Delta\lambda = 0.16 \mu\text{m}$)

²A list of all known ultracool dwarfs is maintained at <http://www.astro.umontreal.ca/~gagne/listLTys.php>.

for two reasons: (1) to minimize the sky background level, which is the main source of noise for faint objects, and (2) to identify the T dwarfs, which have blue $J - H$ colors. At each sky position, three to five individual 8 s exposures were obtained, with a 7'' dither pattern along the declination axis. The survey was divided into stripes extending over 20° in declination, to minimize telescope dithering time, and it was highly automated with computer scripts. The number of exposures obtained at each sky position was adjusted in function of the observing conditions to reach a 5σ depth of $J = 17.2$.

Figure 1 shows the source count as a function of J magnitude for both the 2MASS and SIMP photometry of a 6.7 square degree area of the sky corresponding to one night of SIMP data. The SIMP and 2MASS source counts agree precisely up to $J = 16.4$. For $16.4 < J < 16.8$, the number of sources appears slightly but systematically larger in 2MASS than in SIMP. In the $16.6 < J < 16.8$ range, the SIMP source count is 94.0% of the 2MASS source count, but a SIMP counterpart is found for 97.2% of the 2MASS sources in that magnitude range, within 2'' (or 1 SIMP FWHM). The source count discrepancy is probably due to uncertainties on the magnitudes, and the plot is consistent with the SIMP source count being complete to $J = 17.2$. The SIMP survey is thus limited by the depth of the 2MASS Survey.

The SIMP survey has covered $\sim 28\%$ of the sky; the region surveyed was restricted to absolute galactic latitudes larger than 20° (except for a few specifically targeted nearby stars) to avoid source confusion when cross-matching with 2MASS.

The final SIMP survey contains more than 115,000 raw frames; a custom IDL pipeline was developed to reduce these data. Each individual frame is divided by a flat-field image obtained from on and off dome-flats taken either at the beginning or at the end of each night. A bad pixel mask is applied and a running median of 11 exposures is used to subtract sky emission before individual images are median combined.

An astrometric solution is obtained for each SIMP image based on the 2MASS PSC, and

the SIMP images are corrected for spatial distortion using a second-order polynomial in both directions, in order to minimize the residual errors between the PSC and SIMP positions. Figure 2 presents the positional uncertainty in R.A. and decl. as a function of J magnitude, for the same data subset as in Figure 1. The 2MASS uncertainties are plotted as given in the PSC. They amount to $\sim 0.^{\circ}06$ in each direction for $J < 15.7$, increasing to $\sim 0.^{\circ}2$ in each direction at $J = 16.7$. The SIMP curves show the 1σ positional uncertainty in R.A. and decl. obtained from the difference in position measured for those sources that were observed twice due to frame overlap. The SIMP uncertainties are $\sim 0.^{\circ}08$ in each direction for $J < 15.7$, increasing to $\sim 0.^{\circ}11$ at $J = 16.7$.

2.1. Candidate Selection

The SIMP survey being roughly half a magnitude more sensitive than the typical $J \sim 16.7$ limit of 2MASS, cross-matching between SIMP and 2MASS is done by searching in the SIMP images for a counterpart to the PSC sources that meet the following criteria: they must have a J -band photometric quality (ph_qual) of A, B, or C, an H -band photometric quality of A, B, C, or D, they must not be flagged as a minor planet (mp_flg = 0), and there must be no confusion (cc_flg = 0) or galaxy contamination (gal_contam = 0). A match is made with the nearest source in the SIMP image that is within $\Delta J = 0.6$ of the 2MASS source, is not already matched to another source, has a profile sharpness consistent with a gaussian, has a long to short axis ratio less than three, and is within a matching radius of $27''$.

The proper motion detection limit of the survey was derived from the astrometric uncertainties in both 2MASS and SIMP. Since 2MASS started in 1997 June and ended in 2001 February, the difference in epochs between SIMP and 2MASS varies between 4 and 12 years. For an average timespan of eight years, proper motions down to $\mu = 88 \text{ mas yr}^{-1}$ can be measured to 5σ for $J < 15.7$, increasing to $\mu = 200 \text{ mas yr}^{-1}$ at $J = 16.7$. For the $27''$ matching radius, the typical upper bound limit on proper motion is $\mu \simeq 3400 \text{ mas yr}^{-1}$.

The use of a photometric color criterion makes it possible to select UCD candidates with proper motions down to $\mu = 100 \text{ mas yr}^{-1}$ with minimal contamination by other sources. For this purpose, we used I -band photometry from the SuperCosmos Sky Survey (SSS; Hambly et al. 2001) or, if available, $ugriz$ photometry from SDSS. If neither of these surveys were available, follow-up i and z -band observations were obtained with MegaCam (Boulade et al. 2003) at the Canada-France-Hawaii Telescope (CFHT) by taking single 200 s exposures. The MegaCam photometry is in the AB system, like SDSS, and no color-dependent corrections were applied (see Delorme et al. (2008) for photometric corrections from SDSS to MegaCam). The resulting i magnitude for those candidates, which were confirmed spectroscopically, is presented in Table 5 of Section 6.

A target is selected as a candidate for further observation if any one of these criteria is met:

1. $\mu > 100 \text{ mas yr}^{-1}$ and detected in I with $I - J > 3.5$,
2. $\mu > 100 \text{ mas yr}^{-1}$, with a 3σ upper limit on I ($I_{3\sigma}$) such that $I_{3\sigma} - J > 3.0$, or
3. $\mu > 200 \text{ mas yr}^{-1}$ and undetected in I .

For a typical velocity dispersion of $\sim 25 \text{ km s}^{-1}$, stars with $\mu > 100 \text{ mas yr}^{-1}$ will be within 50 pc of the Sun. Dwarfs of type M8 V and earlier have $M_J < 11.5$ and $I - J < 3.4$ (Pecaut & Mamajek 2013). If such a star were closer than 50 pc to the Sun, it would be detected in the I band and rejected due to its blue $I - J$ color. Nevertheless, some M dwarfs were still selected because they were found to meet the third criterion (see Section 6 for more detail).

In Figure 3, the selection criteria are represented as a line on a plot of the $I - J$ color versus proper motion, for UCDs discovered in this work, other known UCDs with measured i magnitude and proper motion, and the SIMP survey sources from the same data subset as in Figure 1. For legibility, UCDs with $I - J > 10$ or a $\mu > 400 \text{ mas yr}^{-1}$ are omitted from the graph. For the data subset, the I -band magnitude was obtained from SSS, and if the source is undetected in the I band,

an $I-J$ color is calculated using the SSS survey limit, $I = 19.5$. For the UCDs discovered in this work and other known UCDs, the i -band magnitude was obtained from SDSS or Megacam when available. As shown in Figure 3, for a data subset typical of the whole survey, UCD selection criteria eliminate all but 11 candidates among the 27644 SIMP survey sources. However, all except one of the UCDs identified by other surveys, with measured $i-J$ color and proper motion, satisfy the color criteria. As expected, the SIMP survey will miss the low proper motion UCDs. A few SIMP UCDs are found outside the selection criteria as their proper motion or color, given in Table 5, have been updated with data posterior to the SIMP survey.

3. SPECTROSCOPIC OBSERVATIONS

Once a considerable list of candidates had been extracted from the SIMP survey, a spectroscopic follow-up to confirm their UCD nature and determine their spectral type, was conducted at four different telescopes, with as many NIR instruments, as described in the following subsections.

Limits on telescope time imposed a selection of the candidates to be observed spectroscopically, based on the magnitude of their proper motion, their optical-NIR colors, and airmass considerations. Table 1 presents a log of all spectroscopic observations, in order of increasing R.A. of the targets. Their 2MASS designation is given in Column 1; hereafter, the coordinate will be abbreviated to the first four digits of the R.A. and decl. (i.e. SIMP J23185497–1301106 becomes J2318–1301).

Columns 2–9 list the instruments used, the UT date of observation, the integration time in minutes, the mode used for the instrument (when applicable), the standard star observed and its spectral type, along with the weather, the mean airmass or any difficulty encountered during the observation.

In total, 197 spectra were obtained for 169 targets. In the next subsections, we detail the observing setups and data reduction processes for every instrument used. All spectra were corrected for telluric absorption by observing an A-type star immediately before or after the science target.

3.1. SIMON at OMM

The spectra of 50 candidates were obtained at the OMM 1.6 m telescope during 81 nights, from 2006 April to 2007 November, with the Spectromètre Infrarouge de Montréal (SIMON; Albert 2006), featuring a HAWAII-I 1024×1024 HgCdTe detector with a $0.^{\prime\prime}46 \text{ pixel}^{-1}$ scale. All observations were obtained with the Amici prism and a $1.^{\prime\prime}1$ wide slit (2.4 pixels) with a north–south orientation, resulting in a spectral resolution of $R \sim 40$ over the wavelength range from 0.9 to $2.4 \mu\text{m}$. The spectra were obtained in series of nine exposures using a $10''$ spacing five-position nod pattern along the slit.

An IDL pipeline was used first to divide each image by a flat-field and correct for bad pixels. Sky emission was removed by taking the difference of images obtained at adjacent nod positions. The spectra were extracted from each difference image, weighted according to their signal-to-noise ratio (S/N), and combined. White light recorded through the Paschen β or Brackett γ filters was used for wavelength calibration, in combination with the previously calibrated dispersion of the Amici prism. Some spectra with low-S/Ns were smoothed using a second order Savitzky–Golay polynomial filter (Press et al. 1992), with a width of five points, to help with the visual comparison of the spectra.

3.2. Gemini Near-Infrared Spectrograph (GNIRS) at Gemini South

Spectra for 56 of the fainter SIMP candidates were obtained at the Gemini South telescope from 2006 August to 2007 April with GNIRS (Elias et al. 2006). The cross-dispersed mode (XD), covering the wavelength range from 0.85 to $2.5\,\mu\text{m}$ across five orders, was used with the $32\,\text{l mm}^{-1}$ grating and a $0.^{\circ}3$ -wide slit, yielding a spectral resolution of $R \sim 1700$. A total of 8 to 33 individual exposures of 60 – 120 s were acquired for each target, using a $5''$ ABBA nod pattern along the slit.

A custom IDL pipeline, detailed in Albert (2011), was used to reduce all GNIRS data. An image acquired with a pinhole mask is used to correct for the distortion and to straighten up the cross-dispersed spectrum. Pairs of adjacent exposures from the ABBA pattern are subtracted from each other and the spectra extracted from each difference image are median combined. The resulting spectrum is wavelength calibrated using an Ar lamp, and the calibration is fine-tuned with OH lines from sky emission (Rousselot et al. 2000).

3.3. NIRI at Gemini North

Observations of 20 of the fainter SIMP candidates were obtained at the Gemini North telescope from 2008 February to 2008 November with the Near InfraRed Imager and Spectrometer (NIRI; Hodapp et al. 2003). The $f/6$ camera and the 6-pixel ($\sim 0.^{\circ}7$) centered slit were used with the KRS5 J , H , and K grisms, to obtain a spectral resolution of $R \sim 500$, sufficient to resolve the $1.25\,\mu\text{m}$ K I doublet. The J , H , and K bands of a target spectrum were obtained at different times, and sometimes on different nights, leading to large uncertainties in the relative calibration of the band fluxes. Using the 2MASS photometry to normalize the fluxes in each band was also not reliable since the uncertainties on the 2MASS photometry for most targets were higher than 0.1 mag. This led us to normalize each of the J , H and K bands independently to a

standard spectrum (at 1.00–1.35 μm , 1.40–1.80 μm , and 1.95–2.40 μm , respectively) in order to facilitate the visual classification. A total of 4 to 30 exposures of 60 s were obtained in each band with a 5'' nod along the slit. The reduction pipeline is described in Delorme et al. (2008).

3.4. SpeX at InfraRed Telescope Facility (IRTF)

Spectroscopic observations of 71 targets were obtained at the NASA IRTF for a total of nine nights grouped in three observing runs, in 2008 February–March, 2008 September, and 2009 April. The medium-resolution infrared spectrograph SpeX (Rayner et al. 2003) was used either in the cross-dispersed ShortXD mode (SXD, 0.8–2.46 μm coverage) with a 0.''8 \times 15'' slit, yielding a spectral resolution of $R \sim 750$, sufficient to resolve the K I doublet at 1.25 μm , or in the low-resolution prism mode (PRISM, 0.8–2.5 μm coverage) with 15''-long slits of width 0.''8 ($R \sim 75$), 0.''5 ($R \sim 120$), or 0.''3 ($R \sim 200$). The choice of resolution was based on target brightness and observing conditions. The orientation of the slit was maintained near the parallactic angle. For each candidate, a total of 6 to 22 exposures of 60–240 s were acquired using a 7.''5 ABBA nod pattern along the slit.

The SpeX data were reduced with version 3.4 of the SpeXtool package³ (Cushing et al. 2004). The adjacent image subtraction A–B reduction mode was used together with optimal spectrum extraction (Horne 1986). The resulting spectra were wavelength calibrated using Ar lamp calibration exposures. Telluric correction and flux calibration were achieved with the *xteLLcor* procedure that is included in the SpeXtool package (Vacca et al. 2003).

³Available at <http://irtfweb.ifa.hawaii.edu/~spex/>.

4. PHOTOMETRIC OBSERVATIONS

A photometric follow-up in the J , H and K bands was conducted in 2007 and 2008 for 28 targets with low precision 2MASS photometry. These observations were obtained at the OMM during the spectroscopic follow-up and SIMP survey runs, using SIMON and CPAPIR, respectively, to optimize telescope time when it would allow short photometric measurements, but was insufficient for the longer spectroscopic or survey observations. The photometry also provided supplementary astrometric epochs to refine the proper motion measurements of our targets.

The raw SIMON and CPAPIR images were processed using a custom IDL pipeline similar to the SIMP survey pipeline described in Section 2. Aperture photometry was performed, calibrated on 2MASS stars in the field of view, while masking the potentially saturated bright stars. Since the NIR colors of UCDs can vary by up to ~ 0.4 mag depending on the photometric system used (Stephens & Leggett 2004) and the filters in SIMON and CPAPIR conform with the Mauna Kea (MKO) system (Simon & Tokunaga 2002; Tokunaga et al. 2002), the 2MASS magnitudes were converted to the MKO system using polynomial relations from Leggett et al. (2006). Table 2 presents a log of the photometric observations and the results are presented in Table 5.

5. SPECTRAL CLASSIFICATION

All of the observed spectra were classified by the use of spectral indices as a first step, followed by visual comparison with NIR standard spectra, as described in the following subsections.⁴

Visual comparison is particularly useful for the low-resolution SIMON spectra, for some low

⁴All spectra are publicly available at <http://dx.doi.org/10.5281/zenodo.58501>.

S/N (~ 5) spectra, and for the identification of peculiar sources such as young or low-metallicity objects, and unresolved binaries. The spectral indices are most useful when a visual classification is ambiguous.

5.1. Spectral Indices

Over the years, multiple sets of NIR spectral indices have been defined to classify UCDs. Most of them measure the flux ratio in narrow bands subject to molecular absorption (H_2O , CH_4 , etc.) within the J , H or K bands. As any molecular absorption feature varies over a limited range of atmospheric conditions, most indices are restricted to a range of spectral types and become inaccurate outside this range. The broad spectral range of our objects, and the variety of instruments used for this campaign, led to the use of two sets of NIR spectral indices.

The first set is made of four indices determined by Allers & Liu (2013) to be spectral type sensitive for a broad range of M and L dwarfs while being insensitive to surface gravity. These indices and their respective valid spectral type range are H_2O (M5–L4), H_2OD (L0–L8), $\text{H}_2\text{O-1}$ (M4–L5), and $\text{H}_2\text{O-2}$ (M4–L2).

The second set of indices is from Burgasser et al. (2006b, with spectral type relations from Burgasser 2007) and is useful for the L and T dwarfs. These indices and their respective valid spectral type range are $\text{H}_2\text{O-}J$ (L0–T8), $\text{H}_2\text{O-}H$ (L0–T8), $\text{CH}_4\text{-}K$ (L0–T7), $\text{CH}_4\text{-}J$ (T0–T8), and $\text{CH}_4\text{-}H$ (T1–T8).

Table 3 lists a compilation of the indices for our targets, along with the calculated spectral type if within the index useful range. A median type is also given along with its uncertainty, both rounded to the nearest half-integer. The median type is calculated by iterative rejection of the types (put in brackets) that fall too far from the median, until it converges or the rounded uncertainty equals 0.5. This resulted in the most likely spectral type from all the useful indices.

Nevertheless, for some candidates, the indices give a broad range of spectral types or a spectral type that is far from the visual type, due to a lower quality spectrum, or to a peculiar object. These cases are discussed in Section 6.

5.2. Comparison with standard spectra

The most straightforward and accurate method of classifying stellar spectra is direct comparison with standard spectra (MK process; Morgan et al. 1943; Morgan & Keenan 1973). We therefore compare our J , H and K band spectra with the NIR spectral standard sequences listed in Table 2 of Burgasser et al. (2006b), for the T dwarfs, and in Table 4 of Kirkpatrick et al. (2010), for the M and L dwarfs. The NIR standard spectra extend from 0.7 to 2.5 μm and they are all available in the SpeX Prism Spectral Libraries⁵ (Burgasser 2014), except for M6 and earlier types. For those types, instead of using the NIR standards for the comparison, we used the NIR spectra of the equivalent optical standards, which are Gl 213 (M4), Gl 51 (M5), and Gl 406 (M6). Since only a handful of mid-M dwarfs were found, the use of optical standards should not increase the uncertainties. We have also used the M6–L5 spectral templates defined by Gagné et al. (2015b) to identify low-gravity UCDs, since their set of templates includes both field (α , implied) and low-gravity (β and γ) sequences, extending in the NIR the optical sequence of Cruz et al. (2009), which uses the nomenclature scheme introduced by Kirkpatrick (2005) and Kirkpatrick et al. (2006).

The method of choice to assign a spectral type is to visually compare each candidate spectrum with five neighboring spectra of the standard sequence. The parts of the candidate spectrum that exhibit a very low S/N are masked to avoid interfering with the comparison. The regions of strong telluric absorption (1.15–1.18 μm , 1.35–1.45 μm , and 1.8–1.95 μm) are also masked. If

⁵<http://www.brown dwarfs.org/spexprism>

the candidate and comparison spectra differ in spectral resolution, the higher resolution data are smoothed to the lower resolution. The candidate and standard spectra are normalized to the same average value over the waveband from 1.235 to $1.305\mu\text{m}$ (or over the complete range of each individual band in the case of NIRI spectra). A half-subtype is assigned to a target spectrum when it falls in between two adjacent standard spectra.

Following Kirkpatrick et al. (2010), the M and L spectra are classified by matching only the *J* band, while the *H* and *K* bands are used to ascertain whether the candidate has a blue or red NIR spectrum or one that shows other peculiarities. For the L dwarfs, the spectral types were also determined by a method developed by K. Cruz et al. (2016, in preparation) that uses, for each optically anchored spectral type, median-combined spectra reflecting the diversity of spectral morphologies present in each type. This method visually classifies the spectra using all three NIR bands, normalized separately to minimize the difference in NIR colors that a given type can display. The spectral types obtained with both methods agreed within their uncertainties and only the classification with the Kirkpatrick method is presented in Figure 4.

The visual comparison method yields a typical uncertainty of one subtype, though in some cases where the S/N is low or the spectrum displays peculiar features, the uncertainty increases to two subtypes. On the other hand, if the spectral index method agrees with the visual comparison within a 0.5 subtype, and the candidate spectrum matches the standard very closely, the uncertainty of the adopted spectral type is estimated to be a 0.5 subtype.

6. RESULTS

The spectral type of each target, resulting from the classification scheme described in Section 5 is presented in Table 4. The object name is given in column 1, and a code to the instrument used for the observations is given in column 2. Results from the observations of an

object with different instruments are presented as separate entries. Column 3 gives the spectral type obtained with the spectral indices, column 4 the type obtained from visual comparison, and column 5 the adopted spectral type based on both methods, and weighted according to their respective accuracy. A “:” is used for an adopted spectral type with an uncertainty of ± 1 subtype, while “::” indicates a larger uncertainty. Spectral types based on previous observations in the optical or the NIR are also presented in columns 6 and 7, respectively, along with the reference in column 8. The spectral type obtained from optical data may differ from the infrared spectral type because the two wavelength ranges probe different layers of the atmosphere and/or because the source is an unresolved binary.

The properties of all targets are presented in Table 5, which is subdivided into eight parts (normal UCDs, young UCDs, Hyades Candidates, unusually red UCDs, subdwarf, unusually blue UCDs, binary UCDs and peculiar UCDs). In each part, the targets are ordered according to their spectral type (column 2; from column 5 of Table 4). The adopted proper motion and its uncertainty are presented in columns 3 and 4. In order to get the most accurate proper motion possible, it was recalculated after the SIMP survey by including the object’s position in as many different surveys as available (column 5). The different epochs used are from 2MASS-PSC, SIMP, SDSS-DR9, CFHT Follow-up, OMM Follow-up, and AllWISE. To ensure that every position corresponds to the same moving object at different epochs, a visual inspection was performed in each survey. The adopted proper motion is the median of the values obtained in a 10^5 -step Monte Carlo simulation by linear regression over source positions randomly chosen around the astrometric measurements, according to a Gaussian distribution of width equal to each measurement uncertainty. The standard deviation of the simulated distribution determines the uncertainty on the adopted proper motion.

A photometric distance (d_{phot}), calculated with the *WISE W2* band (or *H* if *W2* was unavailable) and polynomial fits for M_{W2} (or M_H) from Dupuy & Liu (2012), is listed in column 7.

A tangential velocity (V_{\tan}), derived from the photometric distance and the proper motion, is listed in column 6. Source photometry from each available survey is presented in columns 8 to 19. This includes i and z from SDSS or CFHT; J , H , and K_s from 2MASS; MKO J , H , and K from OMM/SIMON and OMM/CPAPIR (this paper); and finally W1 and W2 from AllWISE. The different colors obtained from these measurements are plotted as a function of spectral type in Figure 5.

The 169 targets that were observed spectroscopically range from earlier than M0 to T6.5, including 16 normal M dwarfs, 62 normal L dwarfs, and 17 normal T dwarfs. The remainder of this section presents a detailed discussion of several unusual objects: 2 young M dwarfs, 3 Hyades candidates, 6 unusually red M and L dwarfs, 1 subdwarf, 30 unusually blue M and L dwarfs, 4 unresolved binaries, and 28 peculiar objects, which are discussed in subsections 6.1–6.6 respectively.

One object, J0136+0933 was discovered previously as part of the SIMP survey by Artigau et al. (2006). This paper presents an unpublished GNIRS spectrum. The adopted classification remains unchanged ($T2.5 \pm 0.5$).

Kirkpatrick et al. (2010) suggest to classify as peculiar (blue or red) any object whose 1.5–2.5 μm continuum is significantly bluer/red than expected and the cause is not obviously low metallicity for blue objects or low gravity for red objects, whereas Faherty et al. (2009), who did not obtain spectra for the objects studied, used a photometric color criterion only: the 2MASS color $J - K_s$ (or MKO $J - K$ converted to the 2MASS system) must be off by more than 2σ from the mean color of known field objects with the same spectral type.

We use both spectral and color information. For an object to be defined as a “pec red” or “pec blue,” in addition to the 1.5–2.5 μm continuum criterion, its 2MASS $J - K_s$ color (or the MKO photometric observations if observed with better precision) must be off by more than 1σ from the mean color of field objects of the same type, as can be seen in Figure 5. Objects with a peculiar

spectrum but an uncertain color, or objects with a definite abnormal color but an otherwise normal spectrum, are labelled as pec¹ (possibly red) or as pec² (possibly blue) and are discussed in subsection 6.6.

6.1. Young Candidates

Young late-M and L dwarfs are still contracting; they are larger and less massive than older dwarfs of the same spectral type and their spectra display peculiar features, such as weaker alkali and molecular absorption lines, a flatter 2.18–2.28 μm continuum and a triangular-shaped continuum in the H band due to a decrease of collision-induced absorption of molecular hydrogen, as a consequence of their low gravity. The properties of the young candidates found in the SIMP survey are presented in Table 5b. As displayed in Figure 6, their spectra were compared with NIR spectral templates of the β (intermediate-gravity) and γ (very low-gravity) classes for M and L dwarfs, constructed by K. Cruz et al. (2016, in preparation) and Gagné et al. (2015b). This visual comparison alone was used to identify an object as a young candidate. We also verify that the adopted spectral type is consistent with the four Allers & Liu (2013) indices that are gravity-insensitive, and we calculate their gravity class and score with the indices that are sensitive to surface gravity.

J0120+1518: this object, with a red $i - J$ color (SDSS: 1.84 ± 0.06 ; MegaCam: 1.64 ± 0.09), and a red $J - K_s$ color (2MASS: 1.82 ± 0.18), displays features of a young brown dwarf that match quite well (within one subtype) the M9 γ standard; J0120+1518 displays a triangular H band, as well as a flatter K band and weaker alkali lines than the field standard. While the M9: γ spectral type agrees with the type obtained from the gravity-insensitive indices of Allers & Liu (2013, M9.5), the gravity score yields an FLD-G (field) classification. This object was previously classified by optical spectroscopy (Zhang et al. 2009) as an M9.

J0357–1937: this young candidate has a spectrum that fits in-between the M7 γ and M8 γ types, leading us to adopt a classification of M7.5 $\gamma\pm1$. The INT-G gravity score suggests a β class, the lower S/N possibly explaining the difference with the visual classification.

6.1.1. Hyades Member Candidates

The SIMP survey recovered three objects that were previously identified as candidate members of the Hyades cluster, which has an estimated age of 625 \pm 50 Myr (Perryman et al. 1998). While this is young compared to the Sun and field stars in general, it makes the Hyades older than about 85% of the open clusters in the solar neighborhood (Cox 2000). The age of the Hyades is much higher than the age estimate for the γ gravity-class ($\log(\text{age})$ (years) \approx 7), and even at the higher limit of the age estimate of the β class ($\log(\text{age})$ (years) \approx 8)(Allers & Liu 2013).

The space motion of the Hyades cluster members is consistent with parallel motion with an internal velocity dispersion of 0.3 km s $^{-1}$ (Perryman et al. 1998), and an important test of cluster membership is provided by the comparison of a candidate SIMP proper motion with the cluster convergence point (CP) and velocity.

Figure 7 shows the proper motion trajectories of stars selected as members of the Hyades by Perryman et al. (1998), as calculated from their Hipparcos proper motion (Van Leeuwen 2007), giving a good measure of the location and extent of the area of convergence. Superimposed on this plot are the trajectories of the three SIMP Hyades cluster candidates, discussed below.

The cluster velocity divided by the magnitude of a candidate proper motion gives its kinematic distance (d_{kin} ; Lépine & Simon 2009). The Hyades cluster has a tidal radius of 10 pc and a central distance of 46.34 \pm 0.27 pc (Perryman et al. 1998) and a better test of membership may result from a comparison of the kinematic distance with the photometric distance (column 7

of Table 5) than with the cluster central distance.

J0358+1039: this Hyades candidate L dwarf was discovered by Hogan et al. (2008) and observations with the 10 m Keck II telescope revealed it to be a tight binary (Duchêne et al. 2013). Lodieu et al. (2014) obtained an optical spectrum, classified it as an M5 (known as candidate Hya05), and rejected it as a Hyades member. We obtained the first NIR spectrum of the unresolved system, which leads to a spectral type of $L2.5 \pm 1$, in sharp contrast to the optical classification. The SIMP proper motion path is in very good agreement with the Hyades CP, as shown in Figure 7, and the kinematic distance obtained from this proper motion (31.8 ± 0.6 pc) is consistent with the photometric distance of the candidate (36.2 ± 5.9 pc). Based on this evidence, J0358+1039 may well be a member of the Hyades.

J0410+1459: the SpeX spectrum of this object yields a classification of L1 with no sign of youth (and a gravity score of FLD-G), but it is redder than the standard, which matches the 2MASS $J - K_s$ color (1.580 ± 0.093). This object, discovered by Hogan et al. (2008), is located $\sim 1.^{\circ}9$ from another source whose low proper motion suggests that it is a background object (Duchêne et al. 2013). Lodieu et al. (2014) classified J0410+1459 as an L0.5 (known as candidate Hya03) using optical spectroscopy, and confirmed it as a member of Hyades. The SIMP proper motion measurement ($\mu_{\alpha} \cos \delta = 100.1 \pm 9.9$ mas yr $^{-1}$, $\mu_{\delta} = -18.3 \pm 10.1$ mas yr $^{-1}$) gives a trajectory in excellent agreement with the Hyades CP, as shown in Figure 7, and the kinematic distance (46.0 ± 1.0 pc) agrees with the cluster distance and is within 1σ of the photometric distance (53.6 ± 8.7 pc). This evidence supports the Hyades membership of J0410+1459.

J0417+1634: our proper motion measurement ($\mu_{\alpha} \cos \delta = 83.5 \pm 7.4$ mas yr $^{-1}$ & $\mu_{\delta} = -60.1 \pm 7.3$ mas yr $^{-1}$) gives a value near the center of the range of proper motions for members of the Hyades (see Fig. 4 of Bouvier et al. 2008), and outside the range of proper motions for members of the Taurus–Auriga association (Frink et al. 1997). Accordingly, the kinematic distance, assuming J0417+1634 shares the Hyades velocity, is 45.5 ± 0.7 pc, in agreement with

the distance to the center of the Hyades cluster; if the Taurus velocity is assumed, the kinematic distance comes out as 34.2 ± 0.6 pc, far from the 137 ± 20 pc distance to Taurus (Torres et al. 2007). On the other hand, the proper motion path falls in between the two cluster CPs, 2.8σ from the Hyades CP (Figure 7) and 2.6σ from the Taurus CP (Figure 8). As shown on Figure 8, some Taurus members have proper motion paths similar to that of J0417+1634. As shown in Figure 6c, this object has a spectrum similar to the template for the L0 γ type. The Allers & Liu (2013) gravity score, calculated from the SpeX spectrum, yields INT-G, which agrees better with the intermediate age β class than the younger γ class. An L0: γ classification is consistent with the previous identification of this object by Gizis et al. (1999) as a probable young M8 UCD, and with its classification by Luhman (2006) as a likely intermediate age UCD. If confirmed, a young age would tend to exclude this object from membership in the 625 Myr old Hyades. If J0417+1634 were a field object, its photometric distance would be 30 ± 3 pc on the basis of the L0 absolute magnitudes determined by Dupuy & Liu (2012). A difference of 3.1 magnitudes is found, however, between the absolute magnitudes for a field M9 object (Dupuy & Liu 2012) and those of the pre-main sequence M9 star LH 0429+17 (Reid & Hawley 1999) for which a parallax was obtained by Harris et al. (1999). This magnitude difference increases the photometric distance to 125 ± 12 pc, in agreement with the distance to Taurus. With the data presently available, it is not possible to determine if J0417+1634 is a member of either cluster.

6.2. Unusually Red Objects

UCDs that show enhanced flux in the H and K bands as compared with the NIR standard, when their spectrum is normalized in the J band, and have unusually red 2MASS $J - K_s$ or MKO $J - K$ colors (see Figure 5), but lack the characteristics of low gravity UCDs, are considered to be peculiar (red) and their properties are presented in Table 5d. Objects that satisfy one but not both of the spectral and photometric criteria are classified as peculiar and possibly red, and they are

discussed in Section 6.6.

Table 5d presents 6 pec (red) objects that were recovered in the SIMP survey. We list here the spectral type, 2MASS $J-K_s$ color, and MKO $J-K$ color when MKO photometry was obtained, for the following objects: *J0026–0936* (M9, 1.35 ± 0.14), *J0432–0639* (L2, 1.65 ± 0.07), *J1307–0558* (L3::, 2.10 ± 0.21 , 1.82 ± 0.10), and *J2245+1722* (L0.5:, 1.72 ± 0.12). The remaining two objects are presented below.

J0307+0852: this source is classified as an L1.5: pec (red) UCD. The MKO and 2MASS colors are red for this spectral type ($J - K = 1.72 \pm 0.04$, $J - K_s = 1.73 \pm 0.14$). Its spectrum features a small bump on the blue side of the H band but otherwise fits in between the L1 and L2 standards. Although such an H -band feature could suggest the presence of an unresolved T-type companion, the combination of two standard UCD spectra, as described in Section 6.5, did not improve the fit to its spectrum peculiarities. It was also discovered in a proper motion survey by Schneider et al. (2016) to be a candidate UCD but no spectrum was obtained.

J0421–1133: this source is classified as an L3: pec (red). It displays extreme flux enhancements in the H and K bands when compared with early L standards, as well as a red 2MASS $J-K_s$ color of 1.78 ± 0.14 . The Allers & Liu (2013) gravity score is INT-G, but we do not classify it as a β dwarf because its spectrum matches the field standard better than an intermediate age spectrum.

6.3. Subdwarfs

Subdwarfs are UCDs with a low metallicity and a higher surface gravity and atmospheric pressure. This causes an increase of the collision-induced absorption by H₂ in the H and K bands, hence an unusually blue $J-K_s$ color. They also have stronger hydride bands (CaH, CrH, FeH), since the metal–metal molecules (TiO, VO) are less abundant, leaving the absorption by hydride

molecules more prominent. Metal (Ti I and Ca I) and alkali (Na I, K I, Cs I, and Rb I) Na I lines also remain important at lower temperatures since condensate formation is delayed due to the less frequent interactions of the rarefied atoms. Finally, as part of the galactic halo, they move with high transverse velocities ($\sim 200 \text{ km s}^{-1}$) and are easily detectable in proper motion surveys.

One such object, J1158+0435, was recovered in the SIMP survey. This blue ($J - K_s = 1.17 \pm 0.08$), very high proper motion object has an adopted spectral type of sdL7 ± 2 , its spectrum displaying strongly suppressed H and K bands and a strong FeH band around $1.24 \mu\text{m}$. This subdwarf was first identified by Zhang et al. (2009) as an L3 candidate through SDSS colors. Our result agrees with the sdL7 classification by Kirkpatrick et al. (2010), based on both optical and NIR spectra.

6.4. Unusually Blue Objects

Objects with a 2MASS $J - K_s$ color significantly bluer than the color of field UCDs (see Figure 5), and a $1.5\text{--}2.5 \mu\text{m}$ continuum significantly bluer than the best-matching field standard, while not showing obvious signs of low metallicity such as hydride bands, are classified as peculiar (blue) and are presented in Table 5f. Objects that have either a blue color or a blue spectrum, but not both, are flagged as peculiar and possibly blue and are presented in Section 6.6.

Table 5f presents 30 pec (blue) objects that were recovered in the SIMP survey. We list here the spectral type, 2MASS $J - K_s$ color, and MKO $J - K$ color when MKO photometry was obtained, for the following objects: *J0357+1529* (L1::, 1.11 ± 0.08), *J0421-1950* (M9::, 1.00 ± 0.13), *J0429+0607* (L0::, 0.89 ± 0.11 , 0.99 ± 0.03), *J0430+1035* (M9::, 1.28 ± 0.23 , 0.94 ± 0.11), *J0946+0922* (M9.5::, < 1.5 , 0.89 ± 0.11), *J0956-1910* (L6.5::, 1.36 ± 0.07), *J1014+1900* (L0.5::, 0.92 ± 0.12), *J1041-0429* (L2.5::, 1.34 ± 0.18 , 1.33 ± 0.14), *J1052+1722* (L2::, 1.18 ± 0.20), *J1058+1339* (L1.5::, 0.55 ± 0.26 , 1.09 ± 0.06), *J1130+2341* (L2.5::, 0.90 ± 0.22), *J1218-1332*

(L4::, 1.08 ± 0.19), *J1308+0432* (M9.5::, 0.49 ± 0.26), *J1510–1147* (L4:, 1.40 ± 0.10), *J1708+2606* (L4:, 1.05 ± 0.19), *J1811+2728* (L3:, 1.31 ± 0.14), *J2203–0301* (M9:, 0.96 ± 0.17), *J2248–0126* (L1.5:, 0.87 ± 0.27), and *J2257–0140* (L1::, 0.99 ± 0.20). The remaining 11 objects are presented individually below.

J0148+3712: we adopt an L1: pec (blue) spectral type for this source. Its spectrum displays a small bump on the blue side of the *H* band and overall suppressed flux in both the *H* and *K* bands. This led us to investigate a possible binary nature of the source, but no pair of UCD spectra could reproduce its spectrum satisfactorily. With a blue 2MASS $J - K_s$ color of 1.03 ± 0.13 , it is similar to 2MASS J1440–1303, which is classified as an L1 pec (sl. blue) by Kirkpatrick et al. (2010).

J0921–1534: we adopt a spectral type of L5:: pec (blue) for this source; its MKO $J - K = 1.37 \pm 0.07$ is bluer than a standard L5. Its spectrum has features in its *H* and *K* bands that could be due to an unresolved binary, but it could not be fit by a combination of two UCD spectra.

J1004–1318: we classify this object as an L3: pec (blue) UCD, since its spectrum displays peculiarities in the *H* and *K* bands as well as a slightly blue continuum, consistent with its 2MASS $J - K_s$ color of 1.33 ± 0.06 . It was first classified by Martín et al. (2010) as an L0 dwarf based on optical spectroscopy at the Nordic Optical Telescope. Marocco et al. (2013) classify it as an L1 dwarf from a fit, over the $1.2\text{--}2.3\,\mu\text{m}$ range, to a spectrum obtained with the Ohio State Infrared Imager/Spectrometer at the 4.1 m Southern Astrophysical Research telescope.

J1036+0306: the adopted classification for this object is L3.5: pec (blue). Our MKO photometry ($J - K = 1.40 \pm 0.07$) and the 2MASS $J - K_s$ color (1.15 ± 0.16) are bluer than field L3-L4 dwarfs. There is an unresolved discrepancy between our SIMON spectrum, which has all the characteristics of an L3 standard, and our GNIRS spectrum, which is similar to the L3 standard but for a suppressed flux in the *H* and *K* bands. This object was discovered by Luhman & Sheppard (2014) through its high proper motion in AllWISE data, and they classified it as a blue L4 dwarf based on a SpeX spectrum.

J1150+0520: we have obtained NIR spectra from both NIRI and SpeX, and classify this object as an L5.5: pec (blue), as its spectral continuum is blue, and so is its 2MASS $J - K_s = 1.24 \pm 0.23$. It was discovered by Zhang et al. (2009) and classified with optical SDSS spectroscopy as an L5.5 dwarf, while Schmidt et al. (2010) determined a spectral type of L6, also using SDSS spectroscopy.

J1343–1216: our classification, based on three distinct spectra and a blue 2MASS color $J - K_s = 1.05 \pm 0.20$, yields a spectral type of L5.5: pec (blue). Luhman & Sheppard (2014) classified this object as an $L6.5 \pm 2$ pec (blue) and found it to be a good match to 2MASS J11263991–5003550 (L6.5 pec; Burgasser et al. 2008b).

J1411+2948: our adopted classification for this object is L6:: pec (blue). The peculiar spectrum that we obtained corresponds to a visual type of $L5 \pm 2$, but an index-based type of $L8.0 \pm 2$. Its blue continuum is consistent with its 2MASS color $J - K_s = 1.10 \pm 0.14$. It was previously classified as an L3.5 by Zhang et al. (2009) from SDSS colors. Some features in the spectrum could be due to an unresolved binary, and an L3+T5 pec binary solution yields a match comparable to a single L5.

J1452+1114: we infer a spectral type of L2.5 pec (blue), from the visual match of the *J* band of its SpeX spectrum to the L2 (± 1) standard, its index-based spectral type of $L2.5 \pm 0.5$, and a 2MASS color $J - K_s = 1.18 \pm 0.12$ that is blue for this spectral type. It was found by Deacon et al. (2009) to be a UKIDSS candidate and classified optically by Zhang et al. (2010) as an L2 dwarf. Bardalez Gagliuffi et al. (2014) assigned a spectral type of L3 to this object from a SpeX spectrum.

J1756+2815: the adopted spectral type for this object is L1.5: pec (blue) since its 2MASS color ($J - K_s = 0.90 \pm 0.05$) is bluer than that of L1.5 field dwarfs. Kirkpatrick et al. (2010) discovered this object through its large proper motion and obtained optical (sdL1) and NIR spectroscopy (L1 pec (blue)), not classifying it as a subdwarf in the NIR because the FeH bands

have a strength similar to that of the L1 standard.

J2250+0808: we classify this UCD as an L3.5:: pec (blue). The SpeX spectrum, of low S/N, is visually most similar to the L3 standard and the calculated indices correspond to a spectral type of $L4.0 \pm 1.5$. Its blue continuum is consistent with its 2MASS color $J - K_s = 1.03 \pm 0.10$, as well as the UKIDSS color $J - K = 0.99$ presented by Day-Jones et al. (2013). These authors visually classified this source (identified as BRLT317) as an L1, from a NIR spectrum obtained with the X-shooter (Vernet et al. 2011) at the Very Large Telescope, though the Burgasser et al. (2006b) spectral indices yielded spectral types between L4.5 and L6.

J2322–1407: our adopted classification of L2: pec (blue) for this UCD results from an index-based spectral type of $L4.0 \pm 1$ and $L2 \pm 2.0$ for the NIRI and SpeX spectra, respectively, and a visual classification of $L1.5 \pm 2$ for both spectra. This object has a blue 2MASS color $J - K_s = 0.89 \pm 0.15$. It is classified as an L1 pec (blue) dwarf by Luhman & Sheppard (2014).

6.5. Unresolved Binary Candidates

The follow-up of our candidates revealed several spectra displaying peculiarities that could be attributed to the combined emission from two unresolved UCDs. In particular, the combined spectrum of a T dwarf and an earlier-type UCD features bumps where the flux of the T dwarf emerges between the strong H₂O and CH₄ absorption bands, the most prominent being around $1.58\,\mu\text{m}$. We searched for such binaries in our sample using the visual inspection method described in Bardalez Gagliuffi et al. (2014), which combines spectra from the SpeX library and performs a chi-square per degree of freedom fit to see if the combination of two spectral types results in a better match than any single object spectrum. This section presents the cases where a two-object combination yields a better match to the observed spectrum, but we emphasize that these sources remain binary candidates until this hypothesis is confirmed either by high-resolution imaging or a

radial velocity follow-up. This is especially the case for J0006–1319 and J0006–0852, where the T dwarf spectrum is at the noise level, leading to a small (<1) chi-square.

The adopted spectral types listed in Table 4 take into account the comparison with a two-object combination, as seen in Figure 9, while the visual classification listed in the same table is based only on the comparison with single standards.

J0006–1319: the two spectra that we obtained yield a single-standard visual classification of L6 \pm 2 pec with some features hinting at an unresolved binary. We analyzed the GNIRS spectrum with the method described above and found that an L6: and T7: combination ($\chi^2 = 0.16$) is a slightly better match to our spectrum than the best single object fit (L8, $\chi^2 = 0.22$). Luhman & Sheppard (2014) previously classified this object as an L5 pec and mentioned that its peculiar spectrum could be due to an unresolved binary, comparing it to 2MASS J17114573+2232044, a strong L5.5+T5.5 binary candidate (Bardalez Gagliuffi et al. 2015 and references therein).

J0006–0852: this binary candidate has a spectrum well matched by a combination of an M9: and a T6: pec ($\chi^2 = 0.29$), while the match to a single object gives an M9 classification but with a $\chi^2 = 0.51$. It was previously confirmed as an M8.5+T5 binary by radial velocity variability (named SDSS J0006–0852 AB; Burgasser et al. 2012). It may form a triple system with the M7 dwarf LP 704-48, on the basis of a common proper motion (Burgasser et al. 2012).

J0013–1816: the strange shape of this object SpeX spectrum, and the fact that the single-object index-based classification (L3.5 \pm 1.5) differs significantly from the visual classification (L6.5 pec) led us to investigate the possible binary nature of this source. Indeed, a better match is obtained with two objects of spectral types L3: and T4: ($\chi^2 = 1.04$). Baron et al. (2015) discovered this object by its common proper motion with NLTT 687 (M3 \pm 0.5), obtained a GMOS spectrum, and classified J0013–1816 as an L1 \pm 0.5 in the optical. It was also classified in the NIR as an L5 pec with SpeX spectroscopy by Best et al. (2015, named PSO J003.4–18), and identified it as a possible early L + early T binary.

J2249–1628: this source spectrum displays peculiarities that make it a strong binary candidate. The combined spectra of an L4 and a T1 give the best match to the observed spectrum ($\chi^2 = 1.07$) and this match is much better than any fit to a single spectrum of the SpeX libraries (L4:, $\chi^2 = 4.31$) or the standard sequence (L5.5±1). Best et al. (2015) previously classified this object (named as PSO J342.3–16) as an L5: and mentioned that the morphology of its spectrum could be due to an unresolved L+T binary.

6.6. Other Peculiar Objects

Objects that do not fit in any of the previous categories while still presenting anomalies are listed in Table 5h. This includes objects classified as pec¹ (possibly red) and pec² (possibly blue), that did not meet all the criteria required to be listed in subsection 6.2 or 6.4.

J0006–2158: this source is classified as an M9:: pec because the *H* and *K* band NIRI spectra differ from the M8-9 standards (bump on the blue side of the *H* band, suppressed flux in the center of the *K* band), while its 2MASS color $J - K_s = 1.39 \pm 0.25$ is red for an M9.

J0532–3253: the adopted classification for this source is M9.5: pec² due to a blue 2MASS color $J - K_s = 0.89 \pm 0.26$ which is unconfirmed by its GNIRS spectrum. It features a blue slant in the *H* band, but a binary analysis could not find a better match to the spectrum.

J0552+0210: this peculiar object is probably a reddened K dwarf, given its strange spectrum, rather low proper motion, and red NIR colors (2MASS: $J - K_s = 1.12 \pm 0.29$; MKO: $J - K = 1.50 \pm 0.10$).

J0858+2710: this object has a classification of L1.5: pec because of the suppressed blue part and enhanced red part of the *J* band, the weaker CO drop at $\sim 2.3 \mu\text{m}$ and the blue slant of the *H* band, but a normal 2MASS color $J - K_s = 1.38 \pm 0.07$. A binary analysis was performed on this object but yielded no good match. West et al. (2008) used an optical SDSS spectrum automatically

processed with the HAMMER stellar spectral-typing facility (Covey et al. 2007), which is limited to the M0–L0 spectral types, to classify this object as an L0. It was also classified as an L0 with SDSS spectroscopy by Schmidt et al. (2010), and Zhang et al. (2010) found it to be a candidate wide binary with LP 312-49 (M4). Baron et al. (2015) obtained a GMOS spectrum and classified this object as an L0±1 in the optical, while confirming that it is comoving with LP 312-49.

J1039+2440: the spectrum of this source is peculiar and somewhat similar to the L5 γ template; however, its *H* band is not as triangular as the template and, while its Na I and K I lines are weaker than usual, its FeH lines are normal. Since this candidate cannot be confidently confirmed as young, we adopt a spectral type of L5:: pec.

J1118–0856: our spectra from three different facilities are all consistent with an L6.5 classification. The SpeX spectrum is blue, while the SIMON spectrum shows a normal continuum. Because of this ambiguity and the fact that the 2MASS $J - K_s = 1.56 \pm 0.12$ is within the 1σ blue limit of the mean ($J - K_s = 1.73 \pm 0.22$), this object is classified as pec². It was previously discovered by Kirkpatrick et al. (2010) and was classified as an L6 pec (blue) with a SpeX spectrum.

J1132–3809: we adopt a spectral type of L8: pec for this source. The blue side of its *H* band displays enhanced flux compared to the standard L8–L9. An analysis for binarity could not identify a good match to this spectrum.

J1143+1905: the peculiar spectrum obtained here, especially in the *J* band, is classified visually as an L8±2. We mainly used the *H* and *K* bands for this classification, but the spectral indices yield an earlier type of L5.5±1.0, resulting in an adopted NIR classification of L7:: pec. This object was classified by Zhang et al. (2009) as an L9 on the basis of its SDSS colors.

J1256–1002: this object’s peculiar spectrum displays a *K* band flux level higher than the standards, and a very peculiar *J* band, leading to a classification of M8:: pec. It also has a very

red 2MASS color $J - K_s = 1.81 \pm 0.22$. The Allers & Liu (2013) gravity score of VL-G (γ type) indicates that it could be young, though the spectrum does not match any of the young M templates of Gagné et al. (2015b).

J1455+2619: we classify this object as an L2: pec. With its 2MASS color $J - K_s = 1.27 \pm 0.08$ and its suppressed flux in the H and K bands (which match the L1 standard almost perfectly), it could be a blue L dwarf; however, the blue part of its J band is suppressed, not enhanced, compared to the L2 standard. Schmidt et al. (2010) previously classified it as an L1 UCD using SDSS spectroscopy.

J1631-1922 this peculiar object, with red NIR colors (2MASS $J - K_s = 1.53 \pm 0.08$) is probably a reddened M dwarf.

J2351+3010: the adopted classification for this source is L5.5:. Our SpeX spectrum matches almost perfectly the L6 standard, except for a slightly enhanced K band flux, while the spectral indices yield a type of L5 \pm 1.5. Schneider et al. (2014) classified this object as an L6.5 dwarf. However, Kirkpatrick et al. (2010) and Gagné et al. (2015b) classified it as an L5 pec (red) and L5 pec respectively.

7. SUMMARY

A sample of 169 spectra have been obtained from different observatories for UCD candidates found through proper motion detection by comparing source position from the SIMP survey to 2MASS. From this sample, 164 UCDs, with spectral types from M8 to T6.5, were found, including 2 young field brown dwarfs, 6 unusually red M and L dwarfs, 25 unusually blue M and L dwarfs, 2 candidate unresolved L+T binaries and 24 other peculiar UCDs. We also discovered 9 L/T transition dwarfs (L6-T4.5), which helps better populate this interesting range of spectral type, often the target of variability studies.

This work demonstrates that many undiscovered UCDs remain to be found in preexisting surveys, including several peculiar objects. Proper motion has proved to be an efficient method to uncover those missed objects. Furthermore, most objects found are relatively bright ($J < 16$), enabling follow-up studies (parallax, variability, binarity, etc.).

We thank the referee for suggestions that led to significant improvement of the manuscript. This work was supported in part through grants from the Fonds de Recherche Québécois-Nature et Technologie and the Natural Science and Engineering Research Council of Canada. This research has benefited from the SpeX Prism Spectral Libraries, maintained by Adam Burgasser at <http://pono.ucsd.edu/~adam/brown dwarfs/spexprism>, as well as the M, L, T, and Y dwarf compendium housed at <http://DwarfArchives.org> and maintained by Chris Gelino, Davy Kirkpatrick, and Adam Burgasser, whose server was funded by a NASA Small Research Grant, administered by the American Astronomical Society. This research made use of the SIMBAD database and VizieR catalog access tool, operated at the Centre de Données astronomiques de Strasbourg, France (Wenger et al. 2000); data products from the Two Micron All Sky Survey (2MASS; Skrutskie et al. 2006), which is a joint project of the University of Massachusetts and the Infrared Processing and Analysis Center (IPAC)/California Institute of Technology (Caltech), funded by the National Aeronautics and Space Administration (NASA) and the National Science Foundation; data products from the *Wide-field Infrared Survey Explorer* (WISE; Wright et al. 2010), which is a joint project of the University of California, Los Angeles, and the Jet Propulsion Laboratory (JPL)/Caltech, funded by NASA; the NASA/IPAC Infrared Science Archive (IRSA), which is operated by JPL, Caltech, under contract with NASA; the Infrared Telescope Facility (IRTF), which is operated by the University of Hawaii under Cooperative Agreement NNX-08AE38A with NASA, Science Mission Directorate, Planetary Astronomy Program; the Database of Ultracool Parallaxes maintained by Trent Dupuy (Dupuy & Liu 2012). Based on observations obtained at the Gemini Observatory through program

numbers GS-2006B-Q19, GS-2007A-Q-28, GN-2008A-Q-51, and GN-2008B-Q-80. The Gemini Observatory is operated by the Association of Universities for Research in Astronomy, Inc., under a cooperative agreement with the National Science Foundation (NSF) on behalf of the Gemini partnership: the NSF (United States), the National Research Council (Canada), CONICYT (Chile), the Australian Research Council (Australia), Ministério da Ciência, Tecnologia e Inovação (Brazil), and Ministerio de Ciencia, Tecnología e Innovación Productiva (Argentina). Some data were acquired through the Canadian Astronomy Data Center. This publication uses observations obtained at IRTF through program numbers 2008A085, 2008B054, and 2009A065. The authors recognize and acknowledge the very significant cultural role and reverence that the summit of Mauna Kea has always had within the indigenous Hawaiian community. We are most fortunate to have the opportunity to conduct observations from this mountain.

Facilities: IRTF (SpeX), Gemini:South (GNIRS), Gemini:Gillett (NIRI), OMM (SIMON), OMM (CPAPIR), CTIO:1.5 m (CPAPIR), CFHT (MegaCam).

REFERENCES

- Aberasturi, M., Solano, E., & Martín, E. L. 2011, A&A, 534L, 7
- Ackerman, A. S., & Marley, M. S. 2001, ApJ, 556, 872
- Albert, L. 2006, PhD thesis, Université de Montréal, 13
- Albert, L., Artigau, É., Delorme, P., et al. 2011, AJ, 141, 203
- Allers, K. N., & Liu, M. C. 2013, ApJ, 772, 79
- Artigau, É., Doyon, R., Lafrenière, D., et al. 2006, ApJ, 651, L57
- Artigau, É., Doyon, R., Vallée, P., Riopel, M., & Nadeau, D. 2004, Proc. SPIE, 5492, 1479
- Artigau, É., Lafrenière, D., Doyon, R., et al. 2011, ApJ, 739, 48
- Artigau, É., Radigan, J., Folkes, S., et al. 2010, ApJ, 718, L38
- Bardalez Gagliuffi, D. C., Burgasser, A. J., Gelino, C. R., et al. 2014, ApJ, 794, 143
- Bardalez Gagliuffi, D. C., Gelino, C. R., & Burgasser, A. J. 2015, AJ, 150, 163
- Barnard, E. E. 1916, AJ, 29, 181
- Baron, F., Lafrenière, D., Artigau, É., et al. 2015, ApJ, 802, 37
- Bertout, C., & Genova, F. 2006, A&A, 460, 499
- Best, W. M. J., Liu, M. C., Magnier, E. A., et al. 2013, ApJ, 777, 84
- Best, W. M. J., Liu, M. C., Magnier, E. A., et al. 2015, ApJ, 814, 118
- Bihain, G., Scholz, R. D., Storm, J., & Schnurr, O. 2013, A&A, 557, 43
- Boulade, O., Charlot, X., Abbon, P., et al. 2003, Proc. SPIE, 4841, 72

- Bouvier, J., Kendall, T., Meeus, G., et al. 2008, A&A, 481, 661
- Burgasser, A. J. 2007, ApJ, 659, 655
- Burgasser, A. J. 2014, in Astronomical Society of India Conf. Ser. 11, International Workshop on Stellar Spectral Libraries, in press (arXiv:1406.48870)
- Burgasser, A. J., Burrows, A., & Kirkpatrick, J. D. 2006a, ApJ, 639, 1095
- Burgasser, A. J., Cruz, K. L., Cushing, M., et al. 2010, ApJ, 710, 1142
- Burgasser, A. J., Geballe, T. R., Leggett, S. K., Kirkpatrick, J. D., & Golimowski, D. A 2006b, ApJ, 637, 1067
- Burgasser, A. J., Kirkpatrick, J. D., Brown, M. E., et al. 2002a, ApJ, 564, 421
- Burgasser, A. J., Kirkpatrick, J. D., Burrows, A., et al. 2003, ApJ, 592, 1186
- Burgasser, A. J., Liu, M. C., Ireland, M. J., Cruz, K. L., & Dupuy, T. J. 2008a, ApJ, 681, 579
- Burgasser, A. J.,Looper, D. L., Kirkpatrick, J. D., Cruz, K. L., & Swift, B. J. 2008b, ApJ, 674, 451
- Burgasser, A. J.,Looper, D. L., Kirkpatrick, J. D., & Liu, M. C. 2007, ApJ, 658, 557
- Burgasser, A. J., Luk, C., Dhital, S., et al. 2012, ApJ, 757, 110
- Burgasser, A. J., Marley, M. S., Ackerman, A. S., et al. 2002b, ApJ, 571, L151
- Burgasser, A. J., & McElwain, M. W. 2006, AJ, 131, 1007
- Burgasser, A. J., McElwain, M. W., Kirkpatrick, J. D., et al. 2004, AJ, 127, 2856
- Burningham, B., Pinfield, D. J., Lucas, P. W., et al. 2010, MNRAS, 406, 1885
- Chiu, K., Fan, X., Leggett, S. K., et al. 2006, AJ, 131, 2722

- Covey, K. R., Ivezić, Ž., Schlegel, D., et al. 2007, AJ, 134, 2398
- Cox, A. N. 2000, Allen’s Astrophysical Quantities (4th ed.; New York: Springer)
- Crossfield, I. J. M. 2014, A&A, 566, 130
- Cruz, K. L., Burgasser, A. J., Reid, I. N., & Liebert, J. 2004, ApJ, 604, L61
- Cruz, K. L., Kirkpatrick, J. D., & Burgasser, A. J. 2009, AJ, 137, 3345
- Cushing, M. C., Vacca, W. D., & Rayner, J. T. 2004, PASP, 116, 362
- Day-Jones, A. C., Marocco, F., Pinfield, D. J., et al. 2013, MNRAS, 430, 1171
- Deacon, N. R., Hambly, N. C., King, R. R., & McCaughrean, M. J. 2009, MNRAS, 394, 857
- Deacon, N. R., Liu, M. C., Magnier, E. A., et al. 2011, AJ, 142, 77
- Deacon, N. R., Liu, M. C., Magnier, E. A., et al. 2014, ApJ, 792, 119
- Delfosse, X., Tinney, C. G., Forveille, T., et al. 1997, A&A, 327, 25
- Delorme, P., Willott, C. J., Forveille, T., et al. 2008, A&A, 484, 469
- Duchêne, G., Bouvier, J., Moraux, E., et al. 2013, A&A, 555, 137
- Dupuy, T. J., & Liu, M. C. 2012, ApJS, 201, 19
- Elias, J. H., Joyce, R. R., Liang, M., et al. 2006, Proc. SPIE, 6269, 62694C
- Epchtein, N., de Batz, B., Capoani, L., et al. 1997, The Messenger, 87, 27
- Evans, N. W. 2014, Mem. Soc. Astron. Italiana, 85, 704
- Faherty, J. K., Burgasser, A. J., Cruz, K. L., et al. 2009, AJ, 137, 1
- Frink, S., Röser, S., Neuhäuser, R., & Sterzik, M. F. 1997, A&A, 325, 613

- Gagné, J., Faherty, J. K., Cruz, K. L., et al. 2015b, *ApJS*, 219, 33
- Gagné, J., Lafrenière, D., Doyon, R., et al. 2014, *ApJ*, 792, L17
- Gagné, J., Lafrenière, D., Doyon, R., Malo, L., & Artigau, É. 2015, *ApJ*, 798, 73
- Geißler, K., Metchev, S., Kirkpatrick, J. D., Berriman, G. B., &Looper, D. 2011, *ApJ*, 732, 56
- Gizis, J. E., Reid, I. N., & Monet, D. G. 1999, *AJ*, 118, 997
- Hambly, N. C., Davenhall, A. C., Irwin, M. J., & MacGillivray, H. T. 2001, *MNRAS*, 326, 1315
- Harris, H. C., Vrba, F. J., Dahn, C. C., et al. 1999, *AJ*, 117, 339
- Hawley, S. L., Covey, K. R., Knapp, G. R., et al. 2002, *AJ*, 123, 3409
- Hodapp, K. W., Jensen, J. B., Irwin, E. M., et al. 2003, *PASP*, 115, 1138
- Høg, E., Fabricius, C., Makarov, V. V., et al. 2000, *A&A*, 355, 27
- Hogan, E., Jameson, R. F., Casewell, S. L., Osbourne, S. L., & Hambly, N. C. 2008, *MNRAS*, 388, 495
- Horne, K. 1986, *PASP*, 98, 609
- Itoh, Y., Tamura, M., Hayashi, M., et al. 2008, *PASJ*, 60, 209
- Kaiser, N., Burgett, W., Chambers, K., et al. 2010, *Proc. SPIE*, 7733, 12
- Kellogg, K., Metchev, S., Geißler, K., et al. 2015, *AJ*, 150, 182
- Kirkpatrick, J. D. 2005, *ARA&A*, 43, 195
- Kirkpatrick, J. D., Barman, T. S., Burgasser, A. J., et al. 2006, *ApJ*, 639, 1120
- Kirkpatrick, J. D., Cushing, M. C., Gelino, C. R., et al. 2011, *ApJS*, 197, 19

- Kirkpatrick, J. D., Cushing, M. C., Gelino, C. R., et al. 2012, *ApJ*, 753, 156
- Kirkpatrick, J. D., Henry, T. J., & Simons, D. A. 1995, *AJ*, 109, 797
- Kirkpatrick, J. D.,Looper, D. L., Burgasser, A. J., et al. 2010, *ApJS*, 190, 100
- Kirkpatrick, J. D., Reid, I. N., Liebert, J., et al. 1999, *ApJ*, 519, 802
- Kirkpatrick, J. D., Schneider, A., Fajardo-Acosta, S., et al. 2014, *ApJ*, 783, 122
- Knapp, G. R., Leggett, S. K., Fan, X., et al. 2004, *AJ*, 127, 3553
- Lawrence, A., Warren, S. J., Almaini, O., et al. 2007, *MNRAS*, 379, 1599
- Leggett, S. K., Currie, M. J., Varricatt, W. P., et al. 2006, *MNRAS*, 373, 781
- Leggett, S. K., Geballe, T. R., Fan, X., et al. 2000, *ApJ*, 536, L35
- Lépine, S., & Simon, M. 2009, *AJ*, 137, 3632
- Lodieu, N., Boudreault, S., & Bejar, V. J. S. 2014, *MNRAS*, 445, 3908
- Looper, D. L., Kirkpatrick, J. D., & Burgasser, A. J. 2007, *AJ*, 134, 1162
- Looper, D. L., Kirkpatrick, J. D., Cutri, R. M., et al. 2008, *ApJ*, 686, 528
- Lucas, P. W., Hoare, M. G., Longmore, A., et al. 2008, *MNRAS*, 391, 136
- Luhman, K. L. 2006, *ApJ*, 645, 676
- Luhman, K. L. 2013, *ApJ*, 767, L1
- Luhman, K. L. 2014, *ApJ*, 786, L18
- Luhman, K. L., & Sheppard, S. S. 2014, *ApJ*, 787, 126
- Mace, G. N., Kirkpatrick, J. D., Cushing, M. C., et al. 2013, *ApJS*, 205, 6

- Marocco, F., Andrei, A. H., Smart, R. L., et al. 2013, AJ, 146, 161
- Martín, E. L., Phan-Bao, N., Bessell, M., et al. 2010, A&A, 517, 53
- Mauron, N., Gigoyan, K. S., Berlitz-Arthaud, P., & Klotz, A. 2014, A&A, 562, 24
- McMahon, R. 2012, in Science from the Next Generation Imaging and Spectroscopic Surveys, 37
- Metchev S. A., Kirkpatrick, J. D., Berriman, G. B., &Looper, D. 2008, ApJ, 676, 1281
- Morgan, W. W., & Keenan, P. C. 1973, ARA&A, 11, 29
- Morgan, W. W., Keenan, P. C., & Kellman, E. 1943, An Atlas of Stellar Spectra, with an Outline of Spectral Classification (Chicago, IL: Univ. Chicago Press)
- Pecaut, M. J., & Mamajek, E. E. 2013, ApJS, 208, 9
- Pérez Garrido, A., Lodieu, N., Béjar, V. J. S., et al. 2014, A&A, 567, 6
- Perryman, M. A. C., Brown, A. G. A., Lebreton, Y., et al. 1998, A&A, 331, 81
- Press, W. H., Teukolsky, S. A., Vetterling, W. T., & Flannery, B. P. 1992, Numerical Recipes in C (2nd ed.; Cambridge: Cambridge Univ. Press)
- Racine, R., 1978, JRASC, 72, 324
- Rayner, J. T., Toomey, D. W., Onaka, P. M., et al. 2003, PASP, 115, 362
- Reid, I. N., & Hawley, S. L. 1999, AJ, 117, 343
- Reid, I. N., Cruz, K. L., Kirkpatrick, J. D., et al. 2008, AJ, 136, 1290
- Reid, I. N., Lewitus, E., Burgasser, A. J., & Cruz, K. L. 2006, ApJ, 639, 1114
- Reylé, C., Delorme, P., Willott, C. J., et al. 2010, A&A, 522, 112

- Rousselot, P., Lidman, C., Cuby, J.-G., Moreels, G., & Monnet, G. 2000, A&A, 354, 1134
- Schmidt, S. J., West, A. A., Hawley, S. L., & Pineda, J. S. 2010, AJ, 139, 1808
- Schneider, A. C., Cushing, M. C., Kirkpatrick, J. D., et al. 2014, AJ, 147, 34
- Schneider, A. C., Greco, J., Cushing, M. C., et al. 2016, ApJ, 817, 112
- Scholz, R. D., Bihain, G., Schnurr, O., & Storm, J. 2012, A&A, 541, 163
- Scholz, R. D., Bihain, G., & Storm, J. 2014, A&A, 567, 43
- Simons, D. A., & Tokunaga, A. T. 2002, PASP, 114, 169
- Sivarani, T., Lépine, S., Kembhavi, A. K., & Gupchup, J. 2009, ApJ, 694, L140
- Skrutskie, M. F., Cutri, R. M., Stiening, R., et al. 2006, AJ, 131, 1163
- Sheppard, S. S., & Cushing, M. C. 2009, AJ, 137, 304
- Smith, L., Lucas, P. W., Bunce, R., et al. 2014, MNRAS, 443, 2327
- Stephens, D. C., & Leggett, S. K. 2004, PASP, 116, 9
- Thompson, M. A., Kirkpatrick, J. D., Mace, G. N., et al. 2013, PASP, 125, 809
- Tokunaga, A. T., Simons, D. A., & Vacca, W. D. 2002, PASP, 114, 180
- Torres, R. M., Loinard, L., Mioduszewski, A. J., & Rodríguez, L. F. 2007, ApJ, 671, 1813
- Vacca, W. D., Cushing, M. C., & Rayner, J. T. 2003, PASP, 115, 389
- Van Leeuwen, F. 2007, A&A, 474, 653
- Vernet, J., Dekker, H., D’Odorico, S., et al. 2011, A&A, 536, 105
- Wenger, M., Ochsenbein, F., Egret, D., et al. 2000, A&AS, 143, 9

West, A. A., Hawley, S. L., Bochanski, J. J., et al. 2008, AJ, 135, 785

Wright, E. L., Eisenhardt, P. R. M., Mainzer, A. K., et al. 2010, AJ, 140, 1868

York, D. G., Adelman, J., Anderson, J. E., et al. 2000, AJ, 120, 1579

Zacharias, N., Urban, S. E., Zacharias, M. I., et al. 2003, yCat, 1289, 0

Zacharias, N., Finch, C. T., Girard, T. M., et al. 2012, yCat, 1322, 0

Zhang, Z. H., Pinfield, D. J., Day-Jones, A. C., et al. 2010, MNRAS, 404, 1817

Zhang, Z. H., Pokorny, R. S., Jones, H. R. A., et al. 2009, A&A, 497, 619

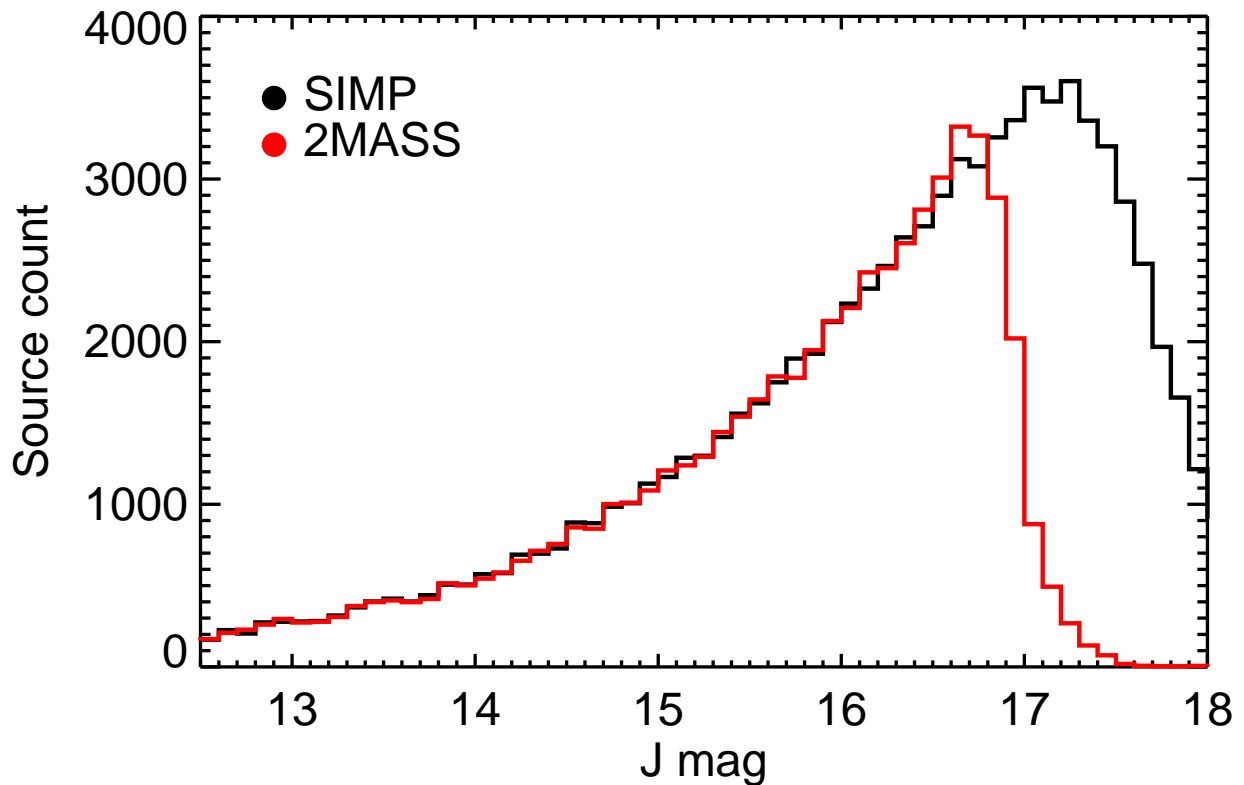


Fig. 1.— Distribution of J magnitude for the sources from the 2MASS PSC (red) and the SIMP images (black) for a 6.7 square degree area of the SIMP survey.

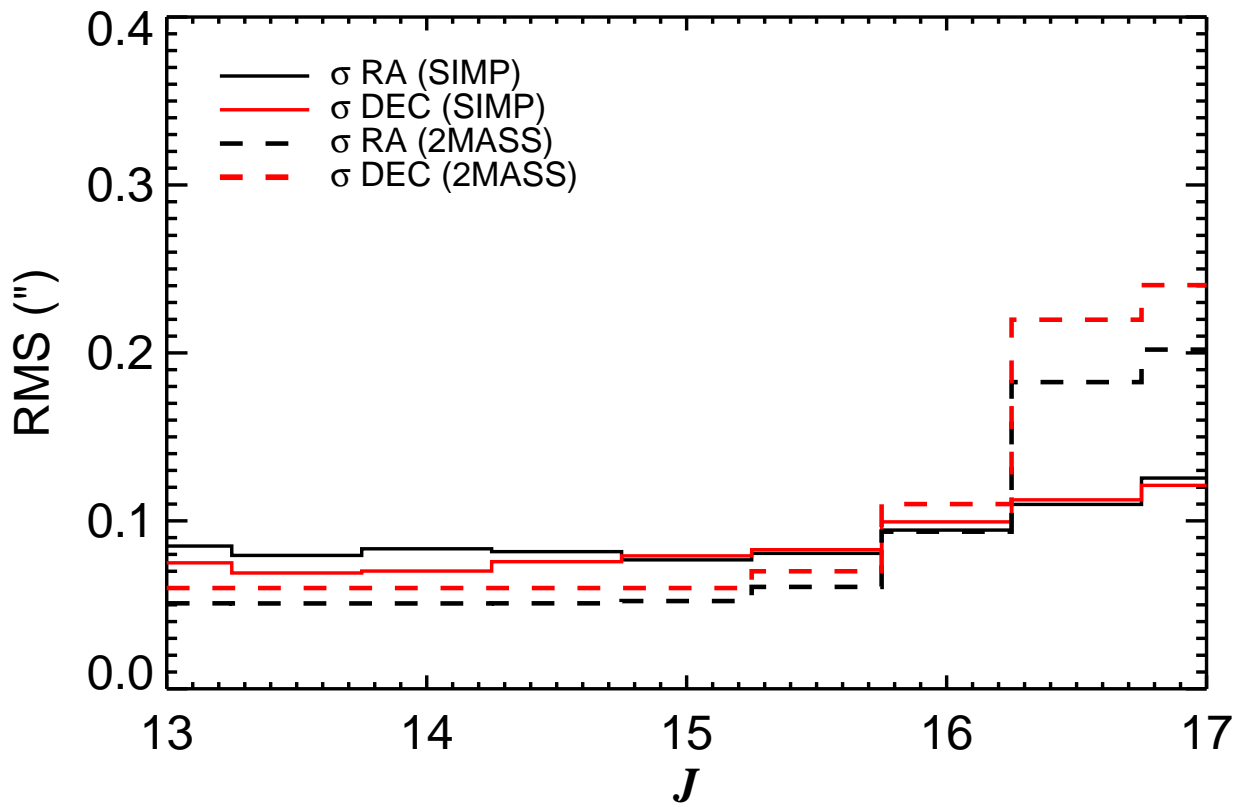


Fig. 2.— Mean R.A. (black) and decl. (red) uncertainties for SIMP (solid line) and 2MASS (dashed line) versus *J* magnitude for the same data subset as in Figure 1.

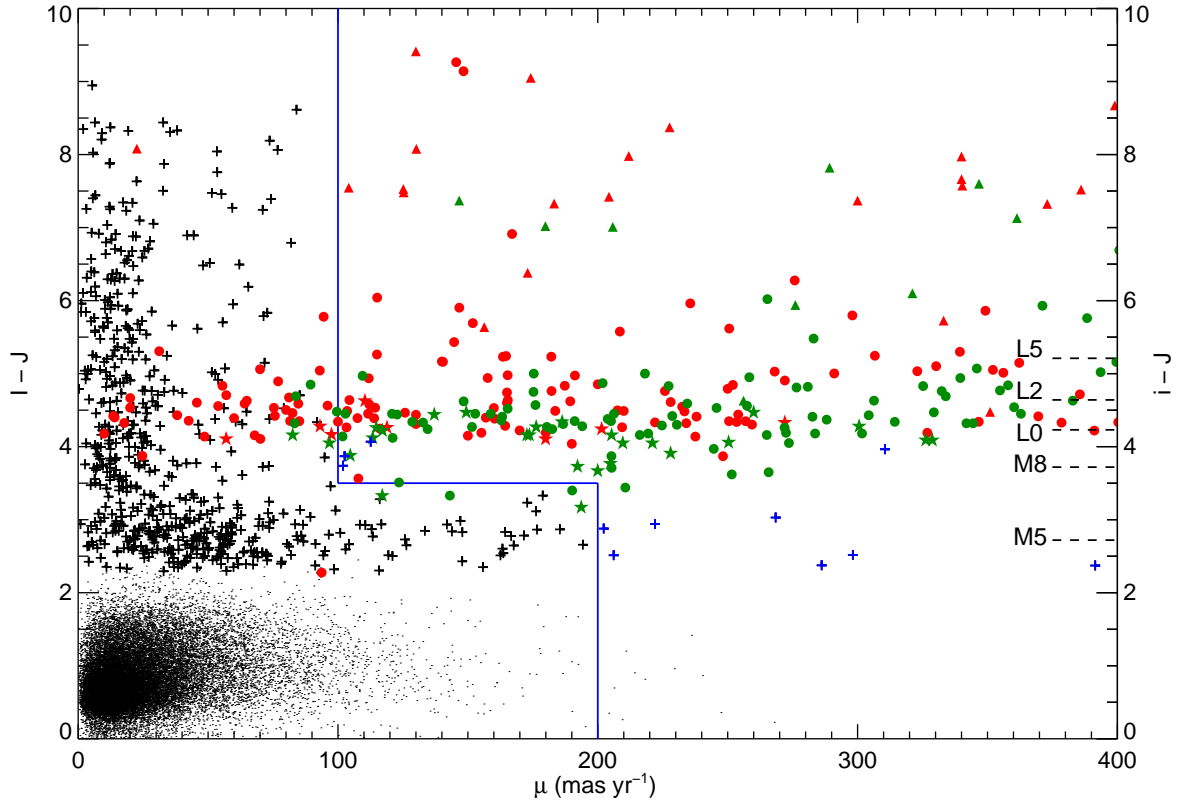


Fig. 3.— UCD candidate selection criteria represented as a blue line on a plot of $I-J$ color versus proper motion for the SIMP survey sources from the same data subset as in Figure 1. These are shown as small black dots if they have a measured I magnitude. If undetected in I , they are shown as black crosses, or blue for the 11 sources meeting the selection criteria, and are located on the plot by assigning the value $I = 19.5$ as a lower limit. Shown in green are the UCDs discovered in this work and in red other UCDs with measured $i-J$ color and proper motion (from <http://www.astro.umontreal.ca/~gagne/listLTYS.php>), M dwarfs as stars, L dwarfs as dots, and T dwarfs as triangles. On the right-hand scale is indicated the $i-J$ color of spectral types from M5 to L5 (Hawley et al. 2002).

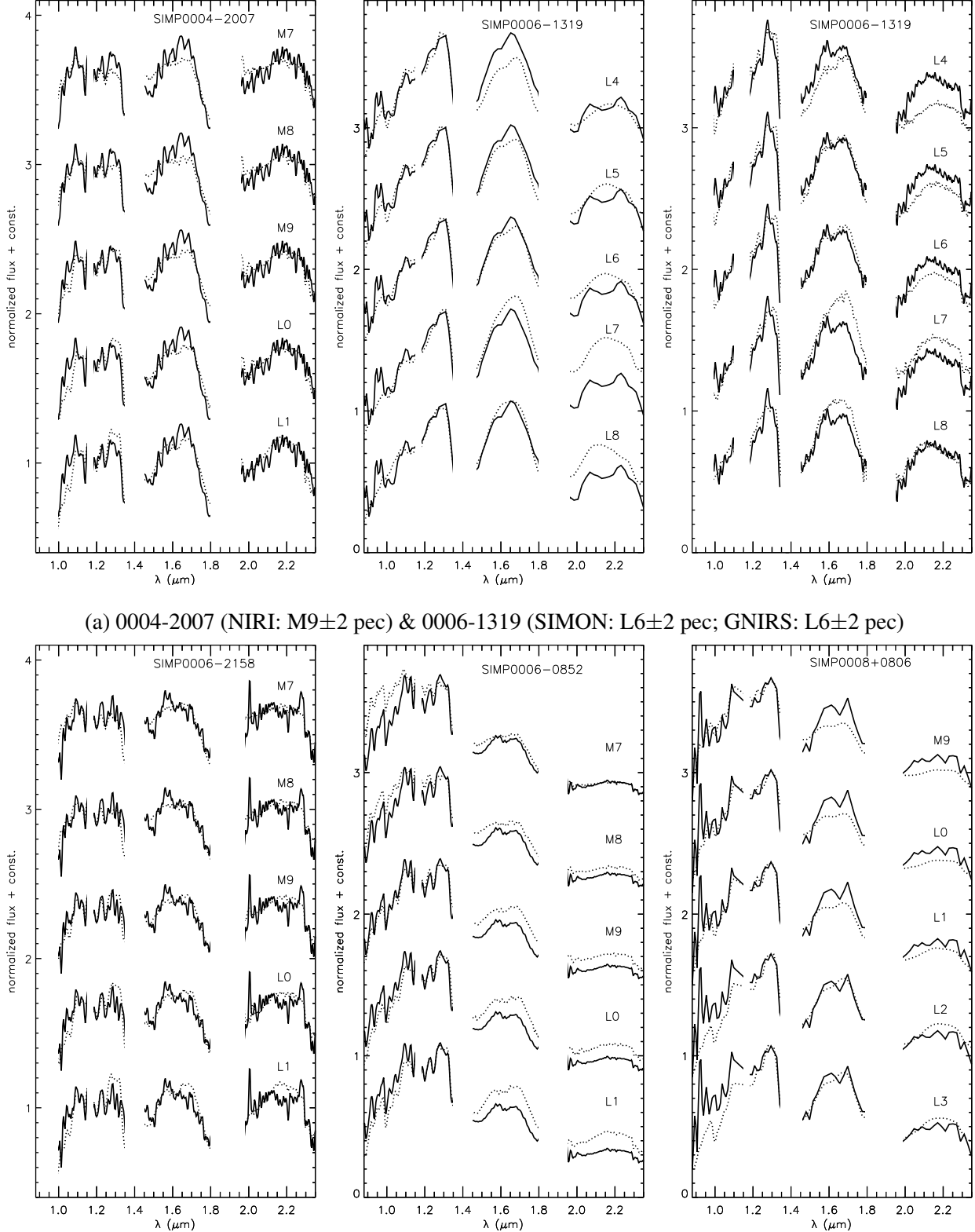


Fig. 4.— Comparison of the spectra of the targets (solid lines) to the M, L, or T dwarf standards (dotted lines). All spectra (publicly available at

Fig. 4.— <http://dx.doi.org/10.5281/zenodo.58501>) are normalized to the average flux in the 1.235–1.305 μm region (or over the complete range of each individual band in the case of NIRI spectra) and the target spectrum is offset by a constant in each panel. The spectral standards are VB 8 (M7; Burgasser et al. 2008a), VB 10 (M8; Burgasser et al. 2004), LHS 2924 (M9; Burgasser & McElwain 2006), 2MASSP J0345432+254023 (L0; Burgasser & McElwain 2006), 2MASSW J2130446–084520 (L1; Kirkpatrick et al. 2010), Kelu-1 (L1; Burgasser et al. 2007), 2MASSW J1506544+132106 (L3; Burgasser 2007), 2MASS J21580457–1550098 (L4; Kirkpatrick et al. 2010), SDSS J083506.16+195304.4 (L5; Chiu et al. 2006), 2MASSI J1010148–040649 (L6; Reid et al. 2006), 2MASSI J0103320+193536 (L7; Cruz et al. 2004), 2MASSW J1632291+190441 (L8; Burgasser 2007), DENIS-P J0255–4700 (L9; Burgasser et al. 2006b), SDSS J120747.17+024424.8 (T0;Looper et al. 2007), SDSS J015141.69+124429.6 (T1; Burgasser et al. 2004), SDSSp J125453.90-012247.4 (T2; Burgasser et al. 2004), 2MASS J12095613-1004008 (T3; Burgasser et al. 2004), 2MASSI J2254188+312349 (T4; Burgasser et al. 2004), 2MASS J15031961+2525196 (T5; Burgasser et al. 2004), SDSSp J162414.37+002915.6 (T6; Burgasser et al. 2006a), 2MASSI J0727182+171001 (T7; Burgasser et al. 2006a), and 2MASSI J0415195-093506 (T8; Burgasser et al. 2004).

(The complete figure set (197 images) is available in the online journal.)

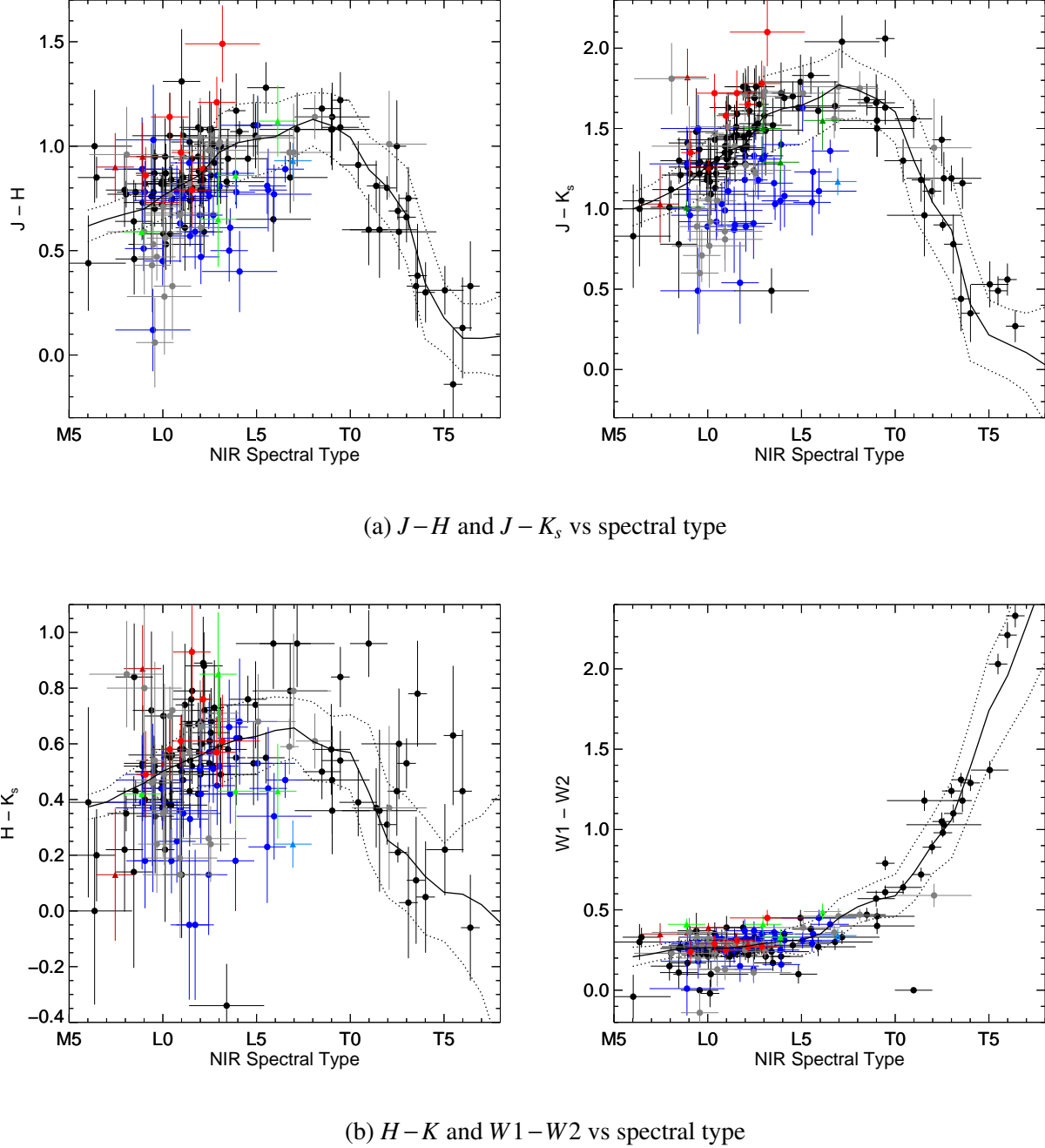
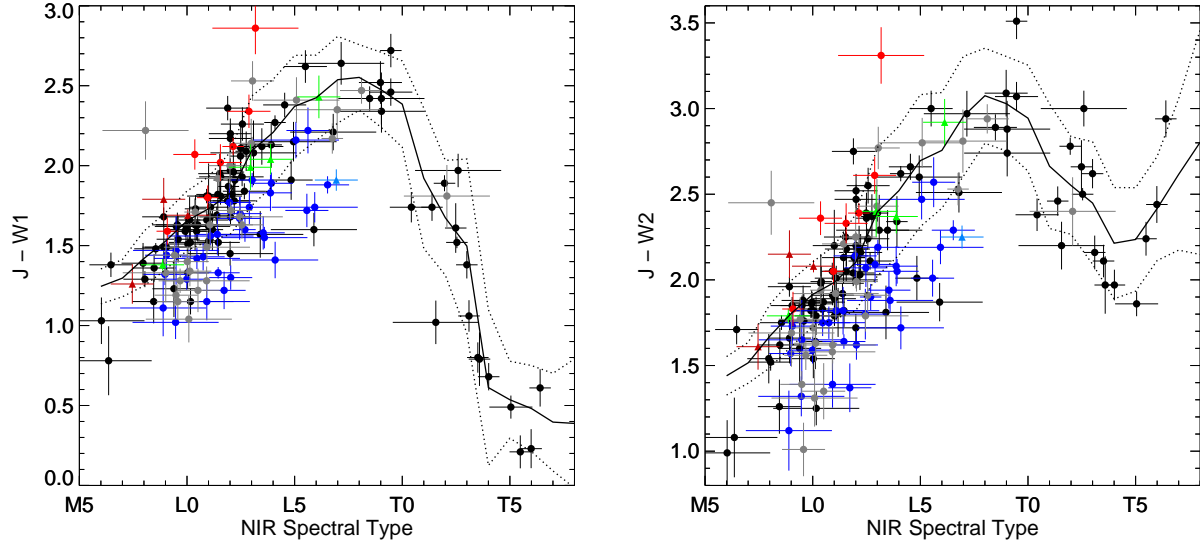
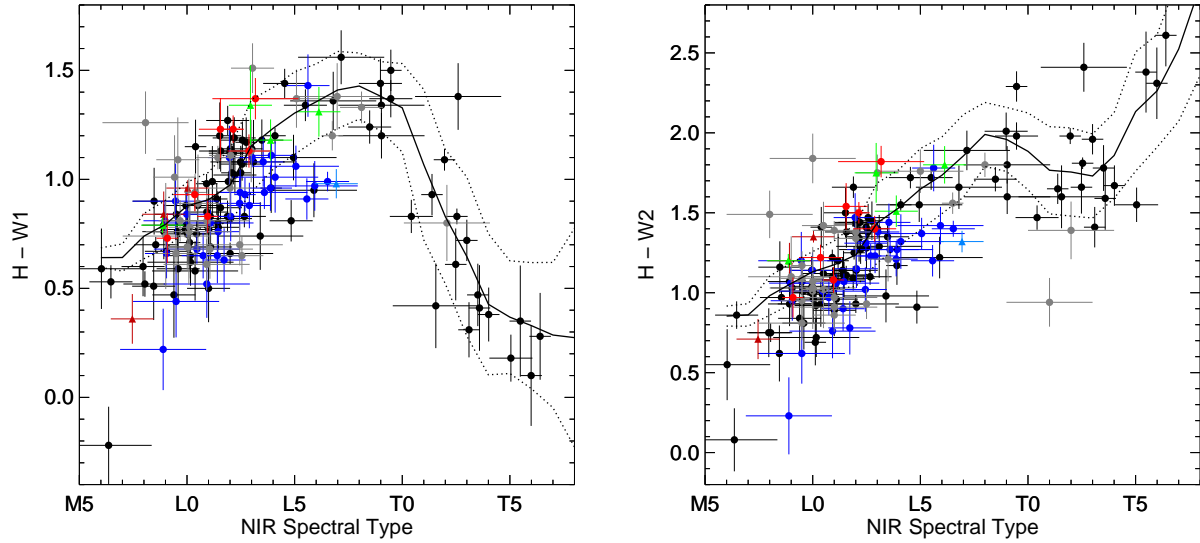


Fig. 5.— Color-NIR spectral type sequences for UCDs found in this work (black circles for non-peculiar; blue circles for blue dwarfs; light blue triangle for the subdwarf; red circles for red dwarfs; dark red triangles for young dwarfs; dark green triangles for binary dwarfs and gray circles for other peculiar dwarfs). Random noise smaller than 0.25 subtype was added to the spectral types for visibility. The uncertainties on spectral type were taken as ± 1 for “.” and ± 2 for “::.” The color distribution (black line) and 1σ dispersion (dotted line) were calculated from the median color

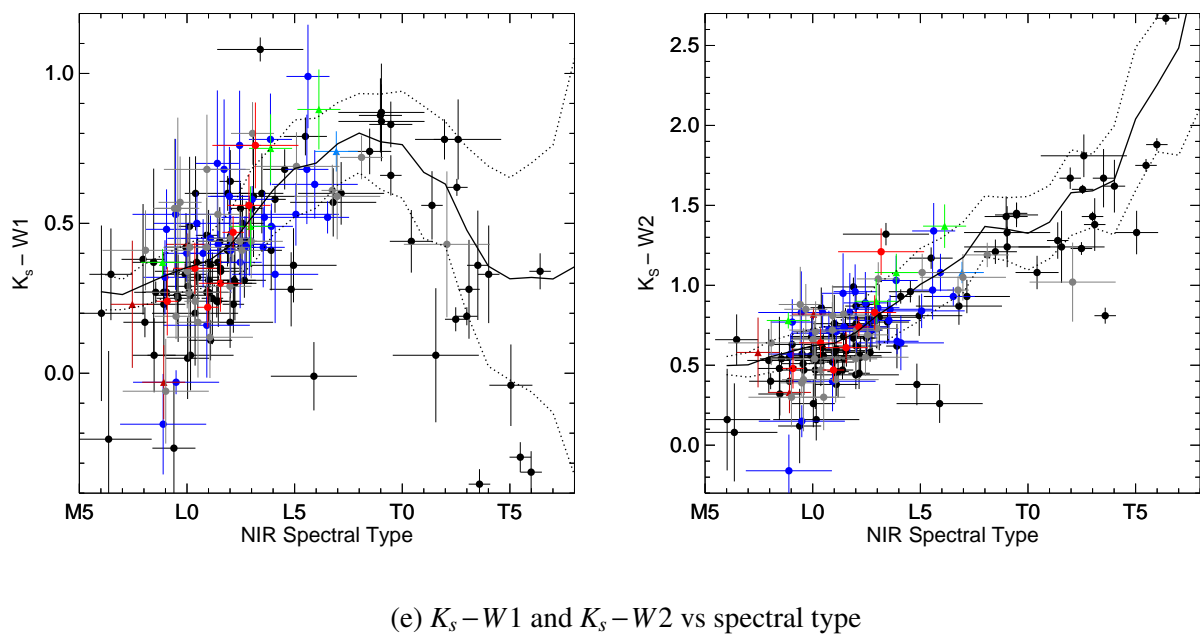


(c) $J - W1$ and $J - W2$ vs spectral type



(d) $H - W1$ and $H - W2$ vs spectral type

Fig. 5.— (Continued) and dispersion within 1 spectral type of non-peculiar known UCDs using 2MASS data taken from <http://www.astro.umontreal.ca/~gagne/listLTYs.php>.



(e) $K_s - W1$ and $K_s - W2$ vs spectral type

Fig. 5.— (Continued)

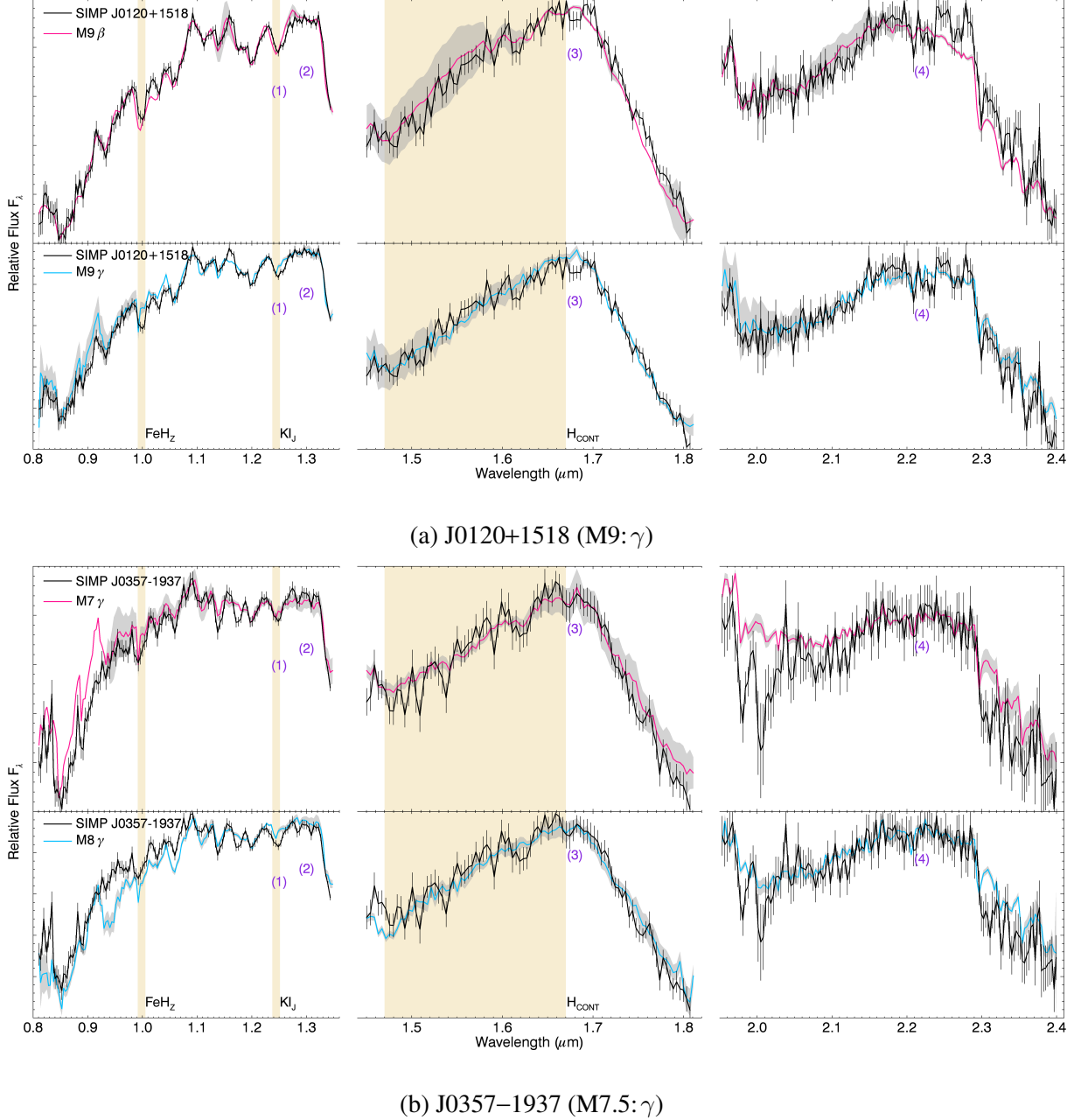
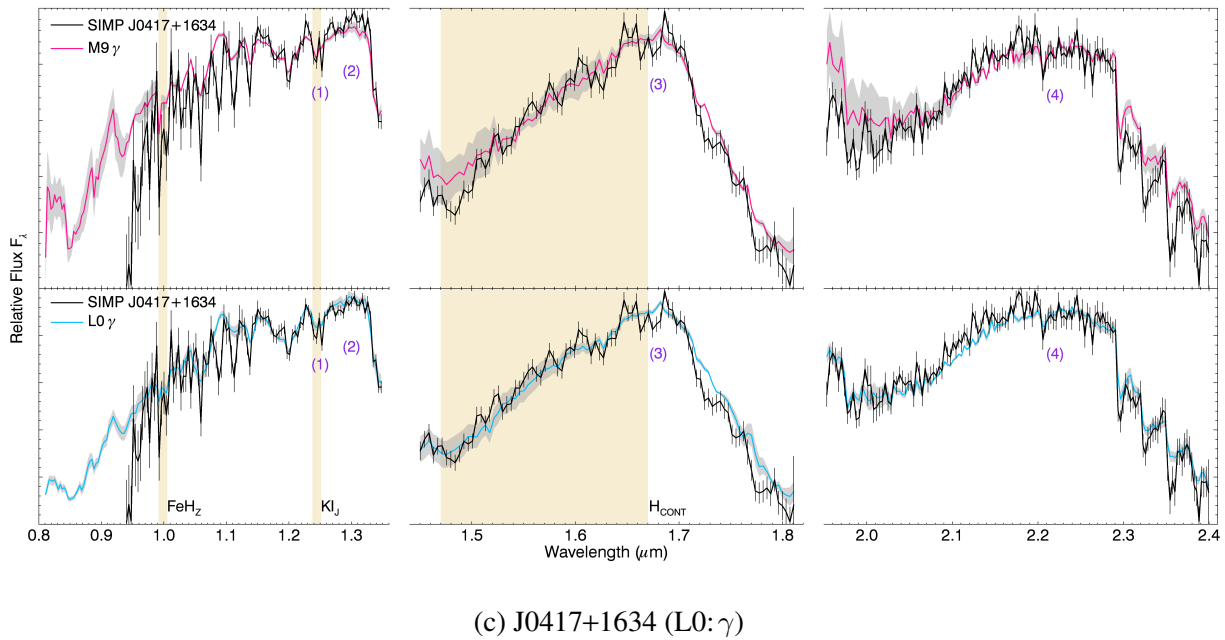


Fig. 6.— NIR spectrum (black) of the SIMP candidates, compared with low- and very-low-gravity template spectra. Each band was normalized individually. The gray shaded region represents the scatter of the individual objects used to create the templates and the black vertical lines represent the measurement uncertainty on each bin of the observed spectrum. Beige shaded regions correspond to the locations of gravity-sensitive spectral indices defined by Allers & Liu (2013). We denote regions useful to differentiate between the low- and very-low-gravity templates with purple numbers.



(c) J0417+1634 (L0: γ)

Fig. 6.— (Continued)

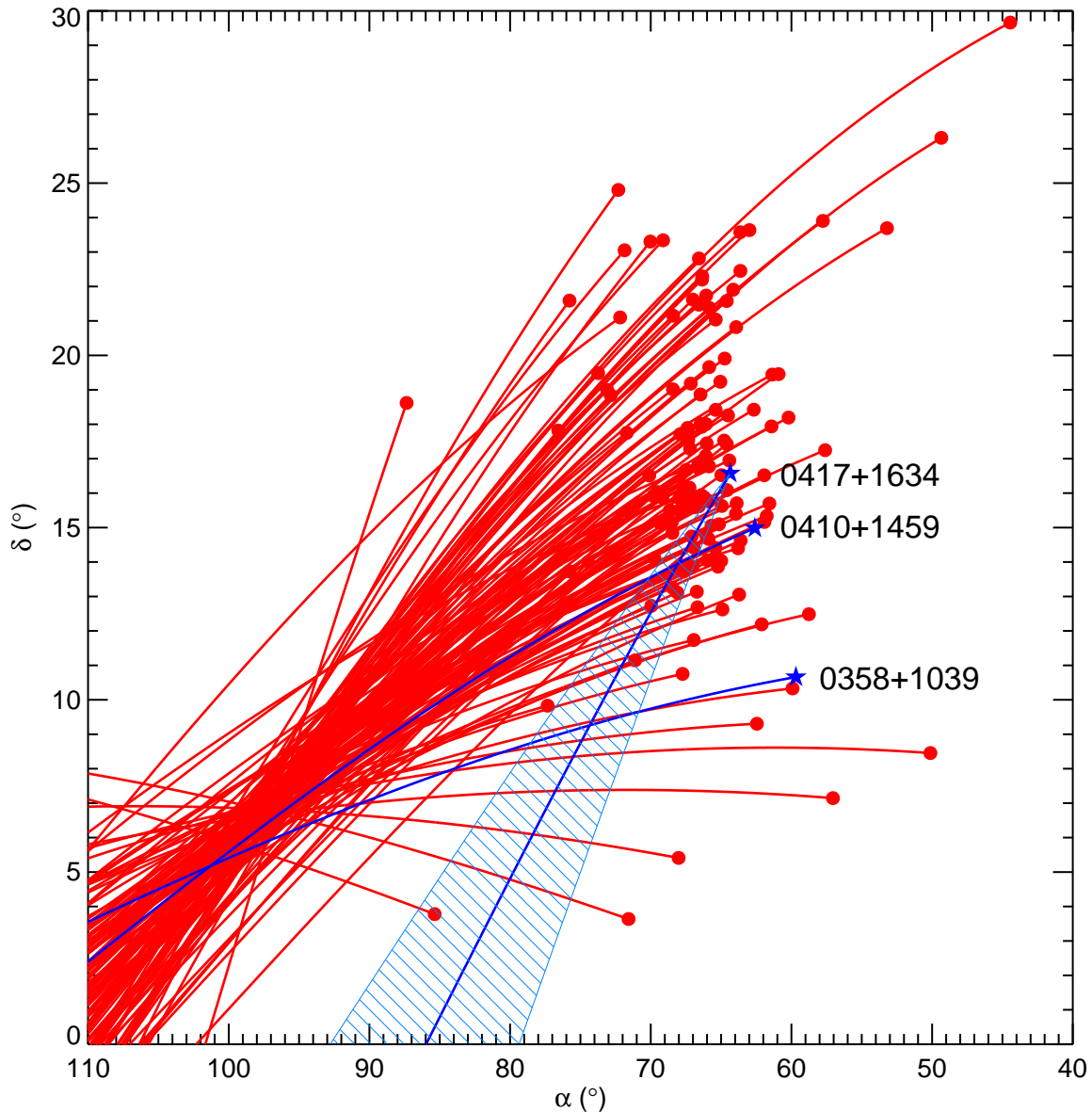


Fig. 7.— Proper motion paths for the three SIMP Hyades candidates (blue), including the 1σ uncertainty for SIMPJ0417+1634, and for the Hyades members taken from Perryman et al. (1998, red) with proper motion from Van Leeuwen (2007).

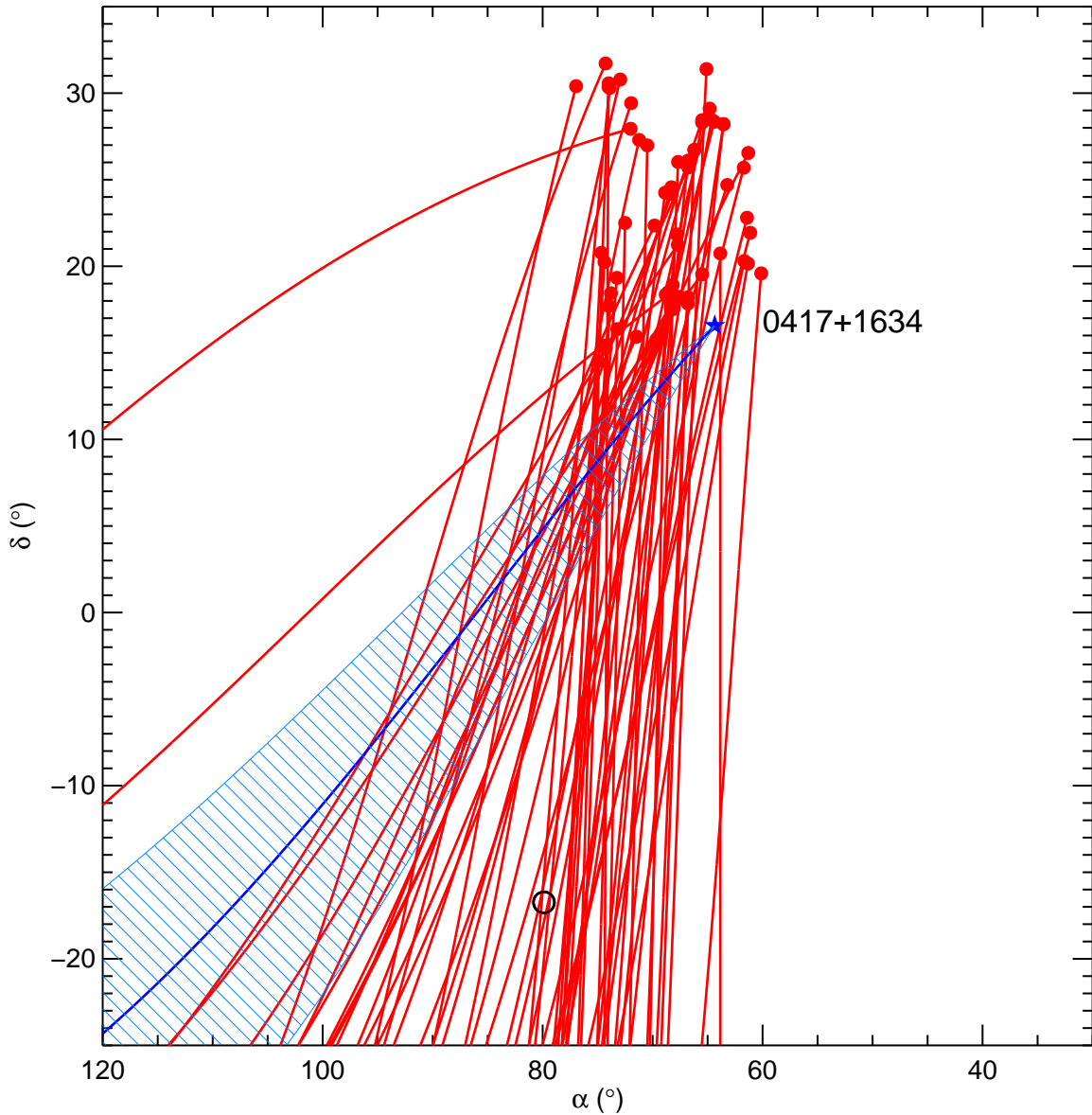
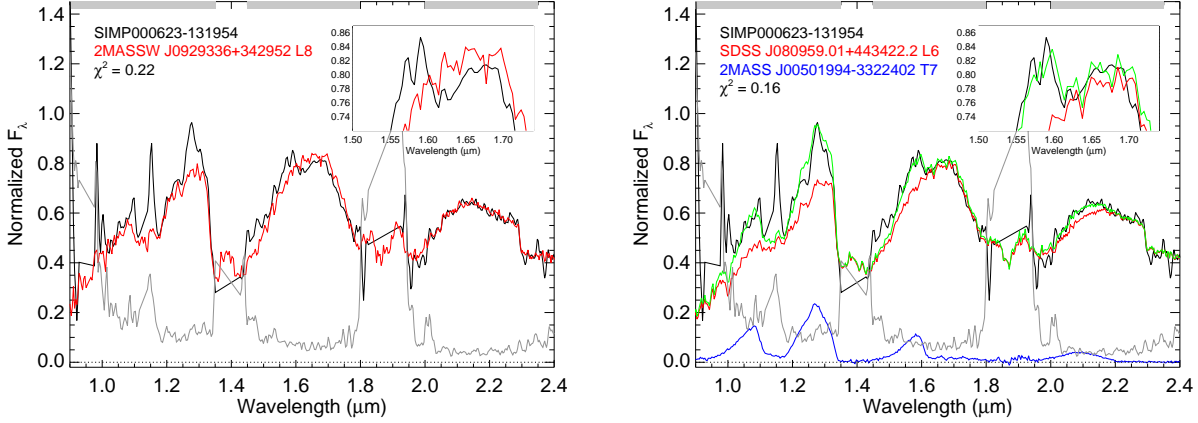
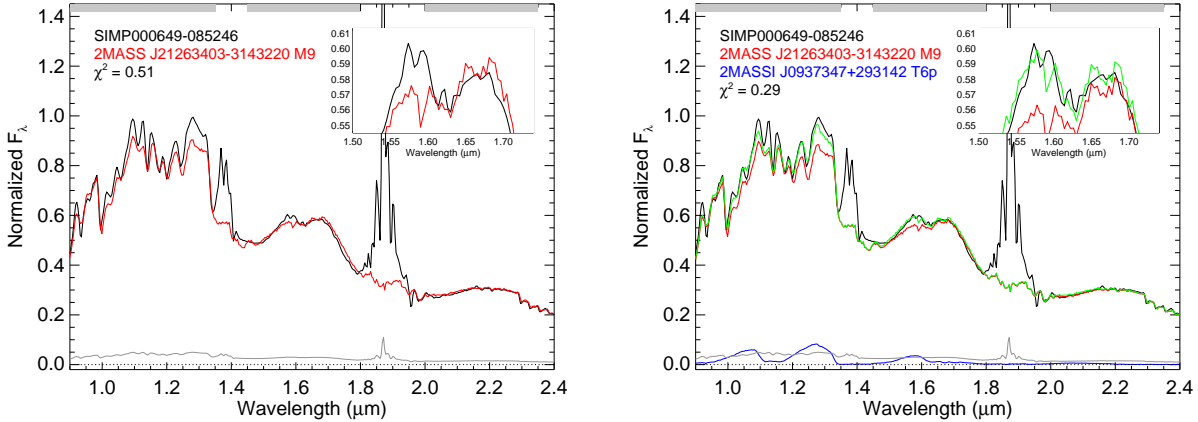


Fig. 8.— Proper motion path for SIMP J0417+1634 (blue, with 1σ uncertainty) and for the Taurus-Auriga members taken from Frink et al. (1997, red) with proper motion from Frink et al. (1997), Høg et al. (2000), Zacharias et al. (2003), Van Leeuwen (2007), Itoh et al. (2008), and Zacharias et al. (2012). The CP (black circle) of a core Taurus moving group was defined in Bertout & Genova (2006).

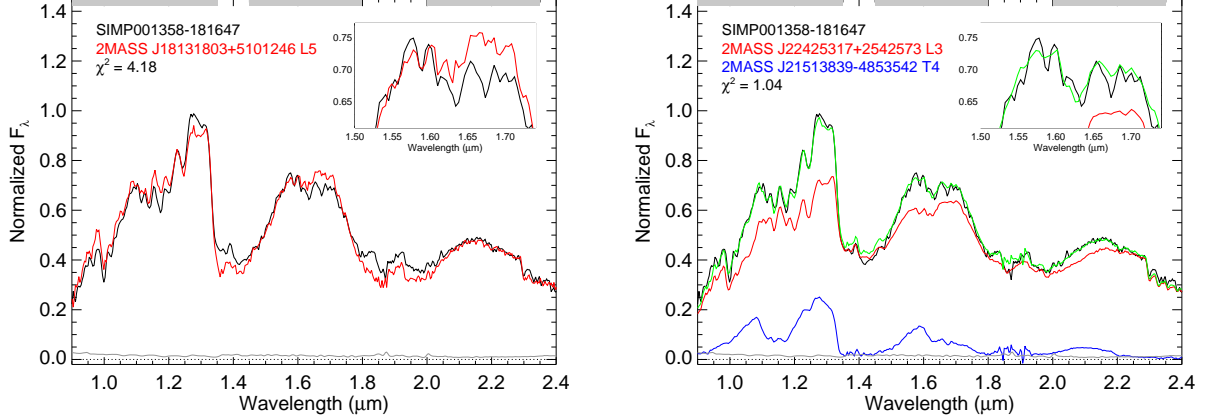


(a) J0006–1319 (L6+T7). Data for 2MASSW J0929336+342952, SDSS J080959.01+443422.2, and 2MASS J00501994-3322402 are from Burgasser et al. (2010), A. Burgasser, and Burgasser et al. (2006a), respectively.

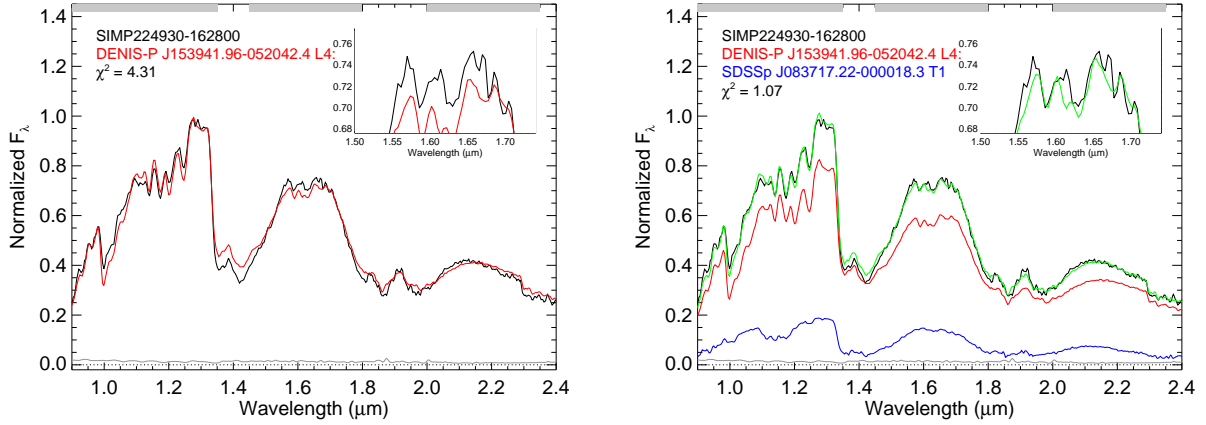


(b) J0006–0852 (M9+T6). Data for 2MASSW J21263403-3143220 and 2MASS J0937347+293142 are from A. Burgasser and Burgasser et al. (2006a), respectively.

Fig. 9.— Best fits to single (left) and binary (right) templates for our binary candidates. The black line shows the candidate spectrum. For the single fits, the red line is the best single template. For the binary fits, the green line is the best binary template, which is the addition of the red (primary) and blue (secondary) lines. The gray line represents the uncertainty in the candidate spectrum. The gray horizontal bars at the top of the figures mark the parts of the spectrum being fit, while water absorption dominates the gaps. Even with the high uncertainties, a significant fitting improvement is observed on the binary fits as compared to the single fits, particularly around the methane absorption feature centered at $1.63\ \mu\text{m}$ (see inset).



(c) J0013–1816 (L3+T4). Data for 2MASSW J18131803+5101246, SDSS J22425317+2542573, and 2MASS J21513839-4853542 are from Kirkpatrick et al. (2010), Burgasser et al. (2010), and Burgasser et al. (2006b), respectively.



(d) J2249–1628 (L4+T1). Data for DENIS-P J153941.96-052042.4 and SDSSp J083717.22-000018.3 are from A. Burgasser and Burgasser et al. (2006b), respectively.

Fig. 9.— (Continued)

Table 1 – Log of SIMP spectroscopic follow-up

SIMP name	Facility/ Instr.	Obs. Date (UT)	Int. Time (m)	Mode/ Slit	Standard Star	Standard Type ^a	Weather Conditions ^c	Airmass	Comment ^d
SIMP J00044599–2007410	G-N/NIRI	2008 Sep 12	25/0/0 ^b	Grism/0."/7	HD 9399	A1V	...	1.32	...
...	G-N/NIRI	2008 Sep 30	0/7/7 ^b	Grism/0."/7	HD 9399	A1V	...	1.31	...
SIMP J00062287–1319503	OMM/SIMON	2006 Sep 11	40	Prism/1."/1	HD 9930	A1V	Good	1.98	2
...	G-S/GNIRS	2007 Jan 06	31	XD/0."/3	HD 822	A1V	...	1.53	...
SIMP J00063158–2158225	G-N/NIRI	2008 Sep 14	20/7/14 ^b	Grism/0."/7	HD 214172	A1V	...	1.48	...
SIMP J00064916–0852457	G-S/GNIRS	2006 Nov 30	18	XD/0."/3	HD 1160	A0V	...	1.12	...
SIMP J00081285+0806441	OMM/SIMON	2006 Sep 12	12	Prism/1."/1	HD 18571	A0V	Clouds	1.36	...
SIMP J00132128+0841006	OMM/SIMON	2006 Sep 10	28	Prism/1."/1	HD 1160	A0V	Good	1.29	1,2
SIMP J00135882–1816462	IRTF/SpecX	2008 Sep 18	18	Prism/0."/5	HD 3604	A0V	Good	1.27	...
SIMP J00265329–0936267	IRTF/SpecX	2008 Sep 18	15	Prism/0."/5	HD 3604	A0V	Good	1.17	...
SIMP J00492826+0440575	G-S/GNIRS	2006 Aug 19	18	XD/0."/3	HD 1160	A0V	...	1.22	...
SIMP J01020186+0355405	G-S/GNIRS	2006 Aug 16	18	XD/0."/3	HD 1160	A0V	...	1.22	...
SIMP J01031050+1940463	IRTF/SpecX	2008 Sep 17	24	Prism/0."/5	HD 7215	A0V	Good	1.00	...
SIMP J01205253+1518277	IRTF/SpecX	2008 Sep 17	18	Prism/0."/5	HD 7215	A0V	Good	1.01	...
SIMP J01352531+0205232	OMM/SIMON	2006 Sep 11	41	Prism/1."/1	HD 12307	A0	Good	1.45	2
SIMP J01365662+0933473	G-S/GNIRS	2006 Aug 06	15	XD/0."/3	HD 9560	A0V	...	1.34	...
SIMP J01383648–0322181	OMM/SIMON	2007 Oct 02	32	Prism/1."/1	HD 18571	A0V	Fog,Clouds	1.52	...
SIMP J01481626+3712421	IRTF/SpecX	2008 Sep 16	18	Prism/0."/5	HD 9711	A0V	Good	1.06	...
SIMP J01500997+3827259	IRTF/SpecX	2008 Mar 01	16	Prism/0."/5	HD 13869	A0V	Good	1.57	...
SIMP J01512665+3824122	IRTF/SpecX	2008 Sep 18	18	SXD/0."/8	HD 13869	A0V	Good	1.08	...
SIMP J01550354+0950003	G-S/GNIRS	2006 Aug 16	18	XD/0."/3	HD 1160	A0V	...	1.32	...
...	OMM/SIMON	2007 Nov 19	90	Prism/1."/1	HD 19431	A0	PS,Fog	1.24	...
SIMP J02110979–1427349	IRTF/SpecX	2008 Sep 18	20	SXD/0."/8	HD 15130	A0V	Good	1.23	...
SIMP J02512861–0818254	OMM/SIMON	2006 Sep 10	26	Prism/1."/1	HD 1160	A0V	Good	1.70	1,2
SIMP J03070255+0852139	G-S/GNIRS	2007 Feb 19	16	XD/0."/3	HD 21985	A1V (AT)	...	1.77	...
SIMP J03162759+2650277	IRTF/SpecX	2008 Sep 16	24	Prism/0."/5	HD 23258	A0V	Good	1.08	...
SIMP J03314657+1944246	OMM/SIMON	2007 Oct 04	44	Prism/1."/1	HD 33303	A1V	Good	1.17	1
SIMP J03570493+1529270	G-S/GNIRS	2007 Feb 24	16	XD/0."/3	HD 27227	A1V	...	1.85	...
SIMP J03574959–1937538	IRTF/SpecX	2008 Sep 17	18	Prism/0."/5	HD 25754	A0V	Good	1.31	...
SIMP J03584293+1039396	OMM/SIMON	2006 Sep 12	50	Prism/1."/1	HD 287150	A2V	Clouds	1.23	2
SIMP J04005763–1322024	G-S/GNIRS	2007 Mar 18	16	XD/0."/3	HD 31411	A0V	...	1.65	...
SIMP J04102390+1459104	IRTF/SpecX	2008 Sep 18	15	Prism/0."/3	HD 23258	A0V	Good	1.01	...
SIMP J04144834+1529007	IRTF/SpecX	2008 Mar 01	16	Prism/0."/5	HD 27761	A0V	Good	1.15	...
SIMP J04172478+1634364	OMM/SIMON	2007 Nov 19	24	Prism/1."/1	HD 34080	A0V	Clouds	1.15	...
...	IRTF/SpecX	2008 Mar 01	12	SXD/0."/8	HD 27761	A0V	Good	1.65	...
SIMP J04173264–1345388	IRTF/SpecX	2008 Mar 01	12	Prism/0."/5	HD 29573	A0V	Good	1.61	...

Table 1 – *Continued*

SIMP name	Facility/ Inst.	Obs. Date (UT)	Int. Time (m)	Mode/ Slit	Standard Star	Standard Type ^a	Weather Conditions ^c	Airmass	Comment ^d
SIMP J04175143–1838320	IRTF/SpeX	2008 Sep 16	24	Prism/0."5	HD 24157	A0V	Good	1.30	...
SIMP J04182001+1121129	IRTF/SpeX	2008 Mar 01	12	SXD/0."8	HD 27761	A0V	Good	1.47	...
SIMP J04210053–1950245	G-S/GNIRS	2007 Feb 15	16	XD/0."3	HD 35388	A0V	...	1.58	...
SIMP J04210695–1133431	G-S/GNIRS	2007 Jan 06	15	XD/0."3	HD 27985	A2V	...	1.45	...
SIMP J04223054+0723448	IRTF/SpeX	2008 Sep 18	15	Prism/0."3	HD 31411	A0V	Good	1.02	...
SIMP J04223302+1033189	OMM/SIMON	2007 Nov 18	62	Prism/1."1	HD 74721	A0V (HB)	PS,Fog	1.31	...
...	IRTF/SpeX	2008 Feb 29	25	SXD/0."8	HD 31411	A0V	Good	1.19	...
SIMP J04232040+1212118	G-S/GNIRS	2007 Feb 25	16	XD/0."3	HD 31411	A0V	...	1.60	...
SIMP J04253602–1900022	G-S/GNIRS	2007 Feb 25	16	XD/0."3	HD 23164	A1V	...	1.38	...
SIMP J04292691+0607368	G-S/GNIRS	2007 Feb 25	16	XD/0."3	HD 31411	A0V	...	1.60	...
...	OMM/SIMON	2007 Oct 04	48	Prism/1."1	HD 33303	A1V	Good	1.32	...
SIMP J04302219+1035438	G-S/GNIRS	2007 Feb 24	14	XD/0."3	HD 31411	A0V	...	1.72	...
SIMP J04323767–0639501	IRTF/SpeX	2008 Sep 18	20	Prism/0."3	HD 34317	A0V	Good	1.12	...
SIMP J05320830–3253328	G-S/GNIRS	2007 Jan 29	16	XD/0."3	HD 35388	A0V	...	1.19	...
SIMP J05522359+0210585	G-S/GNIRS	2007 Mar 24	16	XD/0."3	HD 259639	A2V	...	1.32	...
SIMP J08125319+3721048	IRTF/SpeX	2009 Apr 28	24	Prism/0."5	HD 71906	A0V	Cirrus	1.13	...
SIMP J08511977+1043470	G-S/GNIRS	2007 Jan 08	15	XD/0."3	HD 74721	A0V	...	1.34	...
SIMP J08580549+2214582	OMM/SIMON	2006 Apr 19	52	Prism/1."1	HD 74721	A0V	Good	1.20	...
SIMP J08583693+2710518	G-S/GNIRS	2007 Jan 05	18	XD/0."3	BD+21 1974	A0V	...	1.85	...
SIMP J09155650+0514212	IRTF/SpeX	2008 Feb 28	44	Prism/0."5	HD 79108	A0V	Clouds	1.05	...
SIMP J09213274–1534290	G-S/GNIRS	2007 Jan 07	32	XD/0."3	HD 80750	A0V	...	1.18	...
SIMP J09363433+0528243	G-S/GNIRS	2007 Jan 29	16	XD/0."3	HD 86986	A1V (HB)	...	1.28	...
SIMP J09404793+2946534	IRTF/SpeX	2009 Apr 29	40	SXD/0."8	HD 71906	A0V	Clouds	1.03	...
SIMP J09455513–0757441	IRTF/SpeX	2008 Mar 01	18	Prism/0."5	HD 88025	A0V	Good	1.35	...
SIMP J09463358+1808211	OMM/SIMON	2007 Mar 25	98	Prism/1."1	HD 73210	A5V	Clouds	1.16	...
SIMP J09465378+0922432	G-S/GNIRS	2007 Jan 07	33	XD/0."3	HD 86986	A1V (HB)	...	1.43	...
SIMP J09475068+0617139	OMM/SIMON	2007 Mar 21	88	Prism/1."1	HD 60275	A1V	PS,Clouds	1.40	...
SIMP J09514402–1343474	OMM/SIMON	2007 Mar 30	30	Prism/1."1	HD 73873	A1V	Good	2.04	1,2
SIMP J09560810–1447065	IRTF/SpeX	2008 Mar 01	18	Prism/0."5	HD 90606	A0V	Good	1.30	...
SIMP J09564583–1910227	IRTF/SpeX	2008 Feb 29	24	SXD/0."8	HD 89911	A0V	Good	1.29	...
SIMP J10035482–1441534	OMM/SIMON	2007 Mar 20	64	Prism/1."1	HD 80750	A0V	PS	2.07	...
...	IRTF/SpeX	2008 Feb 29	24	SXD/0."8	HD 90606	A0V	Good	1.32	...
SIMP J10043728–1127342	G-S/GNIRS	2007 Jan 06	32	XD/0."3	HD 86986	A1V (HB)	...	1.17	...
SIMP J10044030–1318186	G-S/GNIRS	2007 Mar 31	16	XD/0."3	HD 88683	A0V	...	1.21	...
SIMP J10091160+1559289	G-S/GNIRS	2007 Jan 06	31	XD/0."3	HD 86986	A1V (HB)	...	1.49	...
SIMP J10135847–1946546	G-S/GNIRS	2007 Jan 26	16	XD/0."3	HD 88683	A0V	...	1.05	...

Table 1 – *Continued*

SIMP name	Facility/ Inst.	Obs. Date (UT)	Int. Time (m)	Mode/ Slit	Standard Star	Standard Type ^a	Weather Conditions ^c	Airmass	Comment ^d
SIMP J10144907+1900041	G-S/GNIRS	2007 Jan 29	24	XD/0."/3	BD+21 1974	A0V	...	1.59	...
SIMP J10315064+3349595	IRTF/SpeX	2009 Apr 29	40	Prism/0."/5	HD 89239	A0V	Clouds	1.06	...
SIMP J10355478+3655420	IRTF/SpeX	2008 Feb 28	18	Prism/0."/5	HD 89239	A0V	Clouds	1.16	...
SIMP J10360307+0306160	OMM/SIMON	2007 Mar 29	48	Prism/1."/1	HD 109860	A1V	Good	1.51	...
...	G-S/GNIRS	2007 Apr 01	16	XD/0."/3	HD 88683	A0V	...	1.43	...
SIMP J10390264–2829293	G-N/NIRI	2008 Mar 20	24/7/7 ^b	Grism/0."/7	HD 99613	A0/A1V	...	1.59	...
SIMP J10390822+2440446	G-N/NIRI	2008 Jun 10	30/7/7 ^b	Grism/0."/7	HD 89774	A1V	...	1.42	...
SIMP J10391406–1904471	IRTF/SpeX	2008 Mar 01	24	Prism/0."/5	HD 88025	A0V	Clouds	1.51	...
SIMP J10414238–0429259	G-S/GNIRS	2007 Mar 10	16	XD/0."/3	HD 88285	A1V	...	1.11	...
SIMP J10441549+0620138	OMM/SIMON	2007 Mar 31	80	Prism/1."/1	HD 80613	A1V	Good	1.44	...
SIMP J10520466+1722433	OMM/SIMON	2007 Mar 31	58	Prism/1."/1	HD 80613	A1V	Good	1.17	...
...	G-S/GNIRS	2007 Apr 06	24	XD/0."/3	HD 86986	A1V (HB)	...	1.50	...
SIMP J10580444+1339474	G-S/GNIRS	2007 Jan 08	15	XD/0."/3	HD 74721	A0V	...	1.66	...
...	OMM/SIMON	2007 Nov 18	10	Prism/1."/1	HD 74721	A0V (HB)	PS	1.43	...
SIMP J11021199+1629393	G-S/GNIRS	2007 Jan 08	15	XD/0."/3	HD 101060	A0V	...	1.45	...
SIMP J11082735+0838026	G-S/GNIRS	2007 Apr 04	16	XD/0."/3	HD 101060	A0V	...	1.28	...
SIMP J11171536+1857037	G-S/GNIRS	2007 Jan 30	24	XD/0."/3	HD 101060	A0V	...	1.65	...
SIMP J11181292–0856106	OMM/SIMON	2007 Mar 23	62	Prism/1."/1	HD 95423	A1V	PS,Clouds	1.90	...
...	IRTF/SpeX	2008 Feb 28	24	Prism/0."/5	HD 97585	A0V	Clouds	1.14	...
...	G-N/NIRI	2008 Apr 06	21/6/6 ^b	Grism/0."/7	HD 88683	A0V	...	1.51	...
SIMP J11220855+0343193	OMM/SIMON	2007 Mar 29	78	Prism/1."/1	HD 109860	A1V	Good	1.39	...
SIMP J11272648+1234310	G-S/GNIRS	2007 Jan 07	32	XD/0."/3	HD 86986	A1V (HB)	...	1.63	...
SIMP J11303803+2341480	IRTF/SpeX	2009 Apr 28	30	Prism/0."/8	HD 105388	A0V	Cirrus	1.01	...
SIMP J11322058–3809562	G-N/NIRI	2008 Apr 17	21/6/6 ^b	Grism/0."/7	HD 79293	B9V	...	1.89	...
SIMP J11384458+0748213	OMM/SIMON	2007 Mar 21	10	Prism/1."/1	HD 60275	A1V	PS,Clouds	1.39	...
SIMP J11411438+1941149	G-S/GNIRS	2007 Feb 15	16	XD/0."/3	HD 101060	A0V	...	1.55	...
SIMP J11430272+1905440	G-N/NIRI	2008 Mar 02	4/6/6 ^b	Grism/0."/7	HD 89774	A1V	...	1.05	...
SIMP J11470302–1032547	G-S/GNIRS	2007 Jan 08	15	XD/0."/3	HD 102948	A1V	...	1.18	...
SIMP J11473434+2153590	IRTF/SpeX	2009 Apr 28	30	Prism/0."/8	HD 105388	A0V	Cirrus	1.00	...
SIMP J11501322+0520124	G-N/NIRI	2008 Feb 28	24/9/9 ^b	Grism/0."/7	HD 89774	A1V	...	1.26	...
...	IRTF/SpeX	2008 Mar 01	18	Prism/0."/5	HD 101060	A0V	Clouds	1.17	...
SIMP J11582077+0435014	IRTF/SpeX	2009 Apr 27	40	SXD/0."/8	HD 97585	A0V	HH,Clouds	1.07	...
SIMP J12003584–2836572	IRTF/SpeX	2008 Feb 29	20	Prism/0."/5	HD 110141	A0V	Good	1.52	...
SIMP J12113013+0406096	G-S/GNIRS	2007 Jan 29	24	XD/0."/3	HD 110466	A2V	...	1.38	...
...	OMM/SIMON	2007 Mar 28	78	Prism/1."/1	HD 123233	A0V	PS	1.50	2
SIMP J12173549+0708334	G-S/GNIRS	2007 Jan 29	24	XD/0."/3	HD 110466	A2V	...	1.33	...

Table 1 – *Continued*

SIMP name	Facility/ Inst.	Obs. Date (UT)	Int. Time (m)	Mode/ Slit	Standard Star	Standard Type ^a	Weather Conditions ^c	Airmass	Comment ^d
SIMP J12184982–1332525	G-S/GNIRS	2007 Jan 07	33	XD/0."/3	HD 101060	A0V	...	1.19	...
SIMP J12255900–1013413	G-S/GNIRS	2007 Mar 25	16	XD/0."/3	HD 119537	A1V	...	1.14	...
SIMP J12565644–1002432	IRTF/SpeX	2009 Apr 28	54	Prism/0."/8	HD 109309	A0V	Cirrus	1.16	...
SIMP J13072984–0558146	G-S/GNIRS	2007 Jan 17	18	XD/0."/3	HD 119537	A1V	...	1.28	...
SIMP J13083106+0818522	IRTF/SpeX	2009 Apr 29	30	Prism/0."/3	HD 116960	A0V	Good	1.04	...
SIMP J13084263+0432441	G-S/GNIRS	2007 Jan 26	16	XD/0."/3	HD 119537	A1V	...	1.26	...
...	OMM/SIMON	2007 Mar 23	56	Prism/1."/1	HD 123233	A0V	Clouds	1.40	2
SIMP J13174922+0448149	IRTF/SpeX	2008 Feb 29	24	Prism/0."/5	HD 116960	A0V	Good	1.04	...
SIMP J13183258–0632057	OMM/SIMON	2007 Mar 30	82	Prism/1."/1	HD 119537	A1V	PS,Cirrus	1.67	...
SIMP J13240776+1906271	G-S/GNIRS	2007 Feb 23	16	XD/0."/3	HD 112476	A1V	...	1.66	...
...	OMM/SIMON	2007 Mar 20	82	Prism/1."/1	HD 109055	A0V	PS	1.15	...
SIMP J13334540–0215599	IRTF/SpeX	2009 Apr 27	30	SXD/0."/8	HD 97585	A0V	HH,Clouds	1.09	...
SIMP J13391950+1523440	G-S/GNIRS	2007 Jan 26	16	XD/0."/3	HD 119537	A1V	...	1.47	...
...	OMM/SIMON	2007 Mar 28	76	Prism/1."/1	HD 101060	A0V	PS	1.17	...
SIMP J13431074–1216256	OMM/SIMON	2007 Mar 29	30	Prism/1."/1	HD 132072	A0V	Clouds	1.89	2
...	IRTF/SpeX	2008 Mar 01	24	Prism/0."/3	HD 122749	A0V	Clouds	1.21	...
...	G-N/NIRI	2008 Mar 21	18/6/6 ^b	Grism/0."/7	HD 105764	A0V	...	1.52	...
SIMP J13432911+1312267	G-S/GNIRS	2007 Apr 04	16	XD/0."/3	HD 121880	A0V	...	1.46	...
SIMP J13441371–1614022	IRTF/SpeX	2009 Apr 29	33	Prism/0."/8	HD 112304	A0V	Good	1.24	...
SIMP J14111847+2948515	IRTF/SpeX	2009 Apr 28	36	Prism/0."/5	HD 122945	A0V	Cirrus	1.02	...
SIMP J14140586+0107102	G-N/NIRI	2008 Mar 23	17/6/6	Grism/0."/7	HD 136831	A0V	...	1.09	...
SIMP J14154242+2635040	IRTF/SpeX	2009 Apr 29	25	Prism/0."/8	HD 122945	A0V	Good	1.02	...
SIMP J14225717+0827539	OMM/SIMON	2006 Jun 06	33	Prism/1."/1	HD 123233	A0V	Good	1.27	...
...	G-S/GNIRS	2007 Mar 19	16	XD/0."/3	HD 140775	A0V	...	1.31	...
SIMP J14520183+1114590	IRTF/SpeX	2009 Apr 28	36	Prism/0."/3	HD 136831	A0V	Cirrus	1.06	...
SIMP J14534687–2744275	G-S/GNIRS	2006 Aug 10	18	XD/0."/3	HD 131223	A0V	...	1.13	...
SIMP J14550283+2619202	IRTF/SpeX	2009 Apr 29	33	SXD/0."/8	HD 140729	A0V	Good	1.08	...
SIMP J15014711–1831272	IRTF/SpeX	2008 Feb 29	18	Prism/0."/5	HD 126818	A0V	Good	1.28	...
SIMP J15102256–1147125	OMM/SIMON	2007 Mar 24	88	Prism/1."/1	HD 122749	A0V	PS	1.90	...
...	IRTF/SpeX	2008 Feb 28	48	SXD/0."/8	HD 132072	A0V	Good	1.18	...
SIMP J15335010+2044470	G-N/NIRI	2008 Sep 24	14/7/7	Grism/0."/7	HD 145647	A0V	...	1.75	...
SIMP J15371974–0800344	OMM/SIMON	2007 Mar 31	68	Prism/1."/1	HD 132230	A1V	Good	1.82	...
...	G-S/GNIRS	2007 Apr 09	16	XD/0."/3	HD 137873	A0V	...	1.23	...
SIMP J16055741+1931115	IRTF/SpeX	2008 Sep 17	20	Prism/0."/3	HD 145647	A0V	BS	1.22	...
SIMP J16133450–0747057	G-S/GNIRS	2007 Feb 27	16	XD/0."/3	HD 144980	A0V	...	1.12	...
...	OMM/SIMON	2007 Mar 30	54	Prism/1."/1	HD 119537	A1V	PS	1.69	...

Table 1 – *Continued*

SIMP name	Facility/ Inst.	Obs. Date (UT)	Int. Time (m)	Mode/ Slit	Standard Star	Standard Type ^a	Weather Conditions ^c	Airmass	Comment ^d
...	G-N/NIRI	2008 Mar 21	21/6/6	Grism/0."/7	HD 159008	A0V	...	1.14	...
SIMP J16150413+1340079	OMM/SIMON	2007 Mar 23	40	Prism/1."/1	HD 123233	A0V	Cirrus	1.18	...
...	G-S/GNIRS	2007 Apr 03	16	XD/0."/3	V* TT Her	A2V (BL)	...	1.47	...
SIMP J16235981–0508066	IRTF/SpEX	2008 Sep 16	20	SXD/0."/8	HD 148968	A0V	Good	1.44	...
SIMP J16270845+0546304	OMM/SIMON	2007 Mar 31	52	Prism/1."/1	HD 80613	A1V	Good	1.31	...
...	IRTF/SpEX	2009 Apr 29	40	Prism/0."/8	HD 145647	A0V	Good	1.08	...
SIMP J16275003+0836036	IRTF/SpEX	2008 Sep 17	15	Prism/0."/3	HD 145647	A0V	Good	1.33	...
SIMP J16280690+0517027	OMM/SIMON	2006 Apr 19	46	Prism/1."/1	HD 99120	A1V	PS	1.32	...
SIMP J16291840+0335371	OMM/SIMON	2006 Sep 11	40	Prism/1."/1	HD 156208	A2V (AT)	Good	1.70	...
...	G-S/GNIRS	2007 Mar 31	16	XD/0."/3	HD 146214	A1V	...	1.30	...
SIMP J16314748–1922461	IRTF/SpEX	2008 Sep 18	16	Prism/0."/3	HD 155379	A0V	Good	1.56	...
SIMP J16443963+2600128	IRTF/SpEX	2008 Sep 18	20	Prism/0."/3	HD 145647	A0V	Good	1.26	...
SIMP J16545081+3747141	IRTF/SpEX	2009 Apr 29	46	SXD/0."/8	HD 191225	A0V	Good	1.20	...
SIMP J17084651+2606449	IRTF/SpEX	2009 Apr 28	24	Prism/0."/5	HD 165029	A0V	Good	1.01	...
SIMP J17553598+3618117	G-N/NIRI	2008 Sep 29	30/7/7 ^b	Grism/0."/7	HD 182761	A0V	...	1.18	...
SIMP J17561080+2815238	G-N/NIRI	2008 Sep 09	30/7/7 ^b	Grism/0."/7	HD 182761	A0V	...	1.06	...
SIMP J17563950+3343002	G-N/NIRI	2008 Sep 13	30/7/7 ^b	Grism/0."/7	HD 182761	A0V	...	1.14	...
SIMP J18115567+2728407	IRTF/SpEX	2008 Sep 16	18	Prism/0."/5	HD 165029	A0V	Good	1.14	...
SIMP J21174252–0611132	OMM/SIMON	2006 Sep 12	24	Prism/1."/1	HD 180782	A1Vn	Good	1.76	1,2
SIMP J21324898–1452544	OMM/SIMON	2006 Sep 11	14	Prism/1."/1	HD 193689	A0V	Good	2.03	...
...	G-N/NIRI	2008 Apr 25	18/6/6 ^b	Grism/0."/7	HD 200414	B9V	...	1.77	...
SIMP J21430506–1544394	IRTF/SpEX	2008 Sep 18	18	Prism/0."/5	HD 202990	A0V	Good	1.26	...
SIMP J21483578+2239427	G-N/NIRI	2008 Apr 27	18/6/6 ^b	Grism/0."/7	HD 210501	A0V	...	1.39	...
SIMP J21503911–0412117	OMM/SIMON	2006 Nov 01	58	Prism/1."/1	HD 205840	A2V	PS	1.59	...
SIMP J21555848+2345307	IRTF/SpEX	2008 Sep 18	18	Prism/0."/5	HD 210501	A0V	Good	1.11	...
SIMP J21570693–0130348	OMM/SIMON	2006 Nov 02	40	Prism/1."/1	HD 198070	A0Vn	HH,PS	1.50	...
SIMP J22030176–0301107	IRTF/SpEX	2008 Sep 16	18	Prism/0."/5	HD 215143	A0Vn	Good	1.09	...
SIMP J22130498+1255078	IRTF/SpEX	2009 Apr 28	30	Prism/0."/5	HD 210501	A0V	Good	1.47	...
SIMP J22153705+2110554	IRTF/SpEX	2008 Sep 17	18	Prism/0."/5	HD 210501	A0V	Good	1.19	...
SIMP J22334328–1331411	OMM/SIMON	2006 Sep 12	8	Prism/1."/1	HD 219833	A0V	Good	1.96	1,2
SIMP J22355244+0418563	OMM/SIMON	2007 Nov 19	56	Prism/1."/1	HD 205840	A2V	PS,Fog	1.34	...
SIMP J22382764+2304114	IRTF/SpEX	2008 Sep 18	24	SXD/0."/8	HD 210501	A0V	Good	1.03	...
SIMP J22393718+1617127	OMM/SIMON	2006 Sep 07	56	Prism/1."/1	GAT 7	A0V	HH	1.18	...
SIMP J22455168+1722276	OMM/SIMON	2007 Oct 05	30	Prism/1."/1	HD 210501	A0V	Cirrus	1.27	...
SIMP J22484809–0126570	IRTF/SpEX	2008 Sep 17	24	Prism/0."/5	HD 215143	A0Vn	Good	1.27	...
SIMP J22493078–1628012	IRTF/SpEX	2008 Sep 17	18	Prism/0."/5	HD 213030	A0V	Good	1.31	...

Table 1 – *Continued*

SIMP name	Facility/ Inst.	Obs. Date (UT)	Int. Time (m)	Mode/ Slit	Standard Star	Standard Type ^a	Weather Conditions ^c	Airmass	Comment ^d
SIMP J22501628+0808245	IRTF/SpeX	2008 Sep 17	18	Prism/0."/3	HD 210501	A0V	Good	1.03	...
SIMP J22543828+1640488	IRTF/SpeX	2008 Sep 17	15	Prism/0."/5	HD 210501	A0V	Good	1.00	...
SIMP J22552905–0725440	OMM/SIMON	2007 Oct 05	3	Prism/1."/1	HD 210501	A0V	Clouds	1.67	...
SIMP J22572115–0140061	OMM/SIMON	2007 Oct 04	32	Prism/1."/1	HD 822	A1V	Good	1.51	...
SIMP J23032925+3150210	IRTF/SpeX	2008 Sep 16	24	Prism/0."/5	HD 222749	B9V	Good	1.03	...
SIMP J23042585+0749010	G-S/GNIRS	2006 Aug 10	18	XD/0."/3	HD 212269	A2V	...	1.54	...
SIMP J23094559+1003122	G-S/GNIRS	2006 Aug 10	27	XD/0."/3	HD 1160	A0V	...	1.40	...
SIMP J23152198+2235417	G-N/NIRI	2008 Sep 30	27/8/13 ^b	Grism/0."/7	HD 210501	A0V	...	1.42	...
SIMP J23185497–1301106	OMM/SIMON	2007 Oct 04	34	Prism/1."/1	HD 822	A1V	Good	1.97	...
SIMP J23221914–1407238	IRTF/SpeX	2008 Sep 17	18	Prism/0."/5	HD 218639	A0V	Good	1.21	...
...	G-N/NIRI	2008 Nov 14	29/9/9 ^b	Grism/0."/7	HD 211278	A0V	...	1.22	...
SIMP J23225888+1300322	OMM/SIMON	2007 Oct 02	60	Prism/1."/1	HD 210501	A0V	Clouds	1.20	...
SIMP J23271573+1517310	IRTF/SpeX	2008 Sep 18	18	Prism/0."/5	BD+14 4774	A0V	Good	1.05	...
SIMP J23302193+1006003	G-S/GNIRS	2006 Aug 11	18	XD/0."/3	HD 1160	A0V	...	1.34	...
SIMP J23324336–1249383	IRTF/SpeX	2008 Sep 18	24	Prism/0."/5	HD 219833	A0V	Good	1.20	...
SIMP J23402648–0745049	IRTF/SpeX	2008 Sep 16	24	Prism/0."/5	HD 219833	A0V	Good	1.14	...
SIMP J23444256+0909020	G-S/GNIRS	2006 Aug 10	18	XD/0."/3	HD 212269	A2V	...	1.30	...
SIMP J23512200+3010540	IRTF/SpeX	2008 Sep 17	18	Prism/0."/3	HD 222749	A0V	Good	1.03	...

Note.

^aAT: Algol type, HB: Horizontal Branch Star, BL: beta Lyr type.

^bIndividual integration times in the *J/H/K* bands.

^cBS: Bright Sky, HH: High Humidity, PS: Poor Seeing.

^d1: The target moved out of the slit at some positions on the nod pattern due to inaccurate pointing and instrument/telescope flexure. 2: The *K* band is saturated.

Table 2 – Log of SIMP photometric follow-up at OMM

Object	Instrument	Obs. Date (UT)	Int. Time (m) ^a	Weather Conditions ^b	Airmass
J0006–1319	SIMON	2008 Jan 26	7.5/8/8	Good	2.42
J0307+0852	SIMON	2008 Jan 27	18/14/16	Good	1.25
J0400–1322	SIMON	2008 Jan 28	18/12/14	Good	1.93
J0423+1212	SIMON	2008 Jan 31	18/8/18	Clouds	1.23
J0429+0607	SIMON	2008 Jan 28	14/11.7/14	Good	1.32
J0430+1035	SIMON	2008 Jan 28	18/15/16	Good	1.37
J0552+0210	SIMON	2008 Jan 24	18/18/18	Fog	1.39
J0851+1043	SIMON	2008 Jan 24	14/14/18	Clouds	1.40
J0921–1534	SIMON	2008 Jan 26	18/16/14	Clouds	2.08
J0936+0528	SIMON	2008 Jan 31	14/14/16	Good	1.34
J0946+1808	SIMON	2008 Jan 26	10.5/12/14	Cirrus	1.33
J0946+0922	SIMON	2008 Jan 26	18/16/16	Cirrus	1.33
J0956–1447	SIMON	2008 Jan 27	16/16/14	Good	2.06
J1004–1127	SIMON	2008 Jan 27	14/0/16	Good	1.91
J1036+0306	SIMON	2008 Jan 31	16/14/14	Clouds	1.38
J1041–0429	SIMON	2008 Jan 31	20/20/18	Clouds	1.57
J1058+1339	SIMON	2008 Jan 26	18/0/0	Clouds	1.18
...	SIMON	2008 Jan 27	0/14/14	Good	1.47
J1147–1032	SIMON	2008 Jan 27	14/14/14	Good	1.79
J1211+0406	SIMON	2008 Jan 28	14/14/14	PS	1.42
J1225–1013	SIMON	2007 Mar 28	10/14/14	PS	1.78
J1307–0558	SIMON	2008 Jan 28	24/16/16	PS	1.61
J1324+1906	SIMON	2008 Jan 26	16/16/14	Clouds	1.14
J1339+1523	SIMON	2008 Jan 28	16/16/16	PS	1.24
J1343+1312	SIMON	2008 Jan 31	0/14/18	Clouds	1.25
J1422+0827	SIMON	2007 Mar 30	12/18/18	Cirrus	1.42
J1537–0800	CPAPIR	2008 Apr 21	12/12/0	Clouds	1.70
J1613–0747	SIMON	2007 Mar 28	18/18/18	PS	1.68
J1615+1340	SIMON	2008 Jan 24	14/14/22	Clouds	1.41

Note.^aIndividual integration times in the *J/H/K* band.^bPS: Poor Seeing

Table 3 – Spectral Indices

Object	Inst. ^a	Median Type	Allers & Liu (2013)				Burgasser et al. (2006b)				
			H ₂ O	H ₂ OD	H ₂ O-1	H ₂ O-2	H ₂ O-J	H ₂ O-H	CH ₄ -J	CH ₄ -H	CH ₄ -K
J0004–2007	3	L1.5±1.5	1.345 (L3.9)	1.008 (···)	0.667 (L1.0)	0.848 (L0.4)	0.916 (L1.0)	0.790 (L2.9)	0.838 (···)	1.084 (···)	1.051 (L2.3)
J0006–1319	1	L7.0±1.0	1.208 ([L1.0])	0.680 (L7.6)	0.577 (L3.5)	0.943 ([M7.6])	0.718 (L6.7)	0.683 (L7.1)	0.911 (···)	1.117 ([T0.7])	1.098 ([L0.1])
...	2	L6.5±2.0	1.382 (···)	0.626 (···)	0.497 (···)	0.846 ([L0.5])	0.855 (L2.5)	0.705 (L6.3)	0.703 (···)	0.986 ([T1.0])	0.929 (L6.6)
J0006–2158	3	L0.5±1.5	1.187 (L0.6)	1.105 (···)	0.962 (···)	0.910 (M8.6)	0.967 (L0.0)	0.813 (L2.0)	0.923 (···)	0.936 ([T1.3])	0.981 ([L5.0])
J0006–0852	2	L1.0±1.0	1.177 (L0.4)	0.958 (L1.2)	0.639 (L1.8)	0.765 (···)	0.916 (L1.0)	0.836 (L1.1)	0.838 (···)	0.974 ([T1.1])	1.044 (L2.6)
J0008+0806	1	L2.5±2.5	1.334 (L3.6)	1.001 (M9.8)	0.598 (L2.9)	0.900 (M8.8)	0.282 ([T4.6])	0.717 (L5.9)	0.962 (···)	0.944 ([T1.2])	1.057 (L2.1)
J0013+0841	1	L0.5±2.0	1.153 (M9.8)	0.895 (L2.8)	0.756 (M8.1)	0.820 (L1.2)	...	0.851 (L0.5)	...	1.114 ([T0.7])	1.171 (···)
J0013–1816	4	L5.5±2.0	1.374 (···)	0.825 (L4.5)	0.576 (L3.5)	0.855 ([L0.2])	0.673 (L8.1)	0.722 (L5.7)	0.816 (···)	0.943 ([T1.2])	0.956 (L5.8)
J0026–0936	4	M8.5±0.5	1.115 (M8.8)	1.016 (···)	0.813 ([M6.2])	0.913 (M8.5)	0.975 (···)	0.904 (···)	0.958 (···)	1.027 (···)	1.038 ([L2.9])
J0049+0440	2	L8.0±2.0	1.400 (···)	0.658 (···)	0.472 (···)	0.871 ([M9.8])	0.704 (L7.2)	0.691 (L6.8)	0.808 (···)	0.985 (T1.0)	0.848 (L8.6)
J0102+0355	2	L8.5±1.5	1.521 (···)	0.653 (···)	0.414 (···)	0.815 ([L1.4])	0.720 (L6.7)	0.604 (L9.8)	0.785 (···)	1.005 (···)	0.861 (L8.3)
J0103+1940	4	L0.0±1.5	1.158 (M9.9)	1.043 (···)	0.737 (M8.8)	0.890 (M9.2)	0.948 (L0.3)	0.909 (···)	0.885 (···)	1.050 (···)	1.052 (L2.3)
J0120+1518	4	L0.0±1.0	1.120 (M9.0)	1.036 (···)	0.698 (L0.0)	0.882 (M9.4)	0.986 (···)	0.863 (L0.0)	0.926 (···)	1.070 (···)	1.084 (L0.8)
J0135+0205	1	T0.0±2.0	1.174 ([L0.3])	0.641 (···)	0.444 (···)	0.973 ([M6.7])	0.613 (L9.7)	0.695 (L6.7)	0.576 (T1.9)	1.106 (T0.7)	0.835 (L8.8)
J0136+0933	2	T2.5±0.5	1.881 (···)	0.565 (···)	0.209 (···)	0.822 ([L1.2])	0.469 (T2.7)	0.495 (T2.5)	0.598 (T1.4)	0.788 (T2.3)	0.559 (T2.1)
J0138–0322	1	T2.5±1.0	1.327 ([L3.5])	0.934 ([L1.8])	0.408 (···)	1.109 (···)	0.436 (T3.2)	0.732 ([L5.3])	0.545 (T2.5)	0.802 (T2.2)	0.713 (T0.7)
J0148+3712	4	L0.5±1.0	1.178 (L0.4)	0.924 (L2.1)	0.625 (L2.2)	0.876 (M9.6)	0.927 (L0.8)	0.849 (L0.6)	0.841 (···)	0.990 ([T1.0])	0.965 ([L5.5])
J0150+3827	4	L8.5±2.0	1.568 (···)	0.646 (···)	0.474 (···)	0.896 ([M9.0])	0.710 (L7.0)	0.661 (L7.9)	0.827 (···)	0.996 (T1.0)	0.815 (L9.2)
J0151+3824	4	L1.5±0.5	1.239 (L1.8)	0.945 (L1.6)	0.657 (L1.3)	0.808 (L1.6)	0.905 (L1.3)	0.791 ([L2.9])	0.892 (···)	1.066 (···)	1.083 (L0.8)
J0155+0950	1	L3.5±1.5	1.245 (L1.8)	0.850 (L3.9)	0.517 (L4.9)	0.802 (L1.8)	0.828 (L3.4)	0.742 (L4.9)	0.854 (···)	1.083 ([T0.7])	1.060 (L1.9)
...	2	L4.0±2.0	1.393 (···)	0.859 (L3.7)	0.549 (L4.2)	0.753 (···)	0.781 (L4.8)	0.708 (L6.2)	0.855 (···)	1.041 (···)	1.058 (L2.0)
J0211–1427	4	L2.0±0.5	1.235 (L1.7)	0.922 (L2.2)	0.628 (L2.2)	0.814 (L1.4)	0.900 (L1.4)	0.809 (L2.2)	0.900 (···)	1.041 (···)	1.045 (L2.6)
J0251–0818	1	L5.0±1.0	1.343 (L3.8)	0.757 (L5.8)	0.571 (L3.6)	0.836 ([L0.7])	0.767 (L5.2)	0.718 (L5.8)	0.841 (···)	0.959 ([T1.1])	0.980 (L5.0)
J0307+0852	2	L1.5±0.5	1.215 (L1.2)	0.805 ([L4.9])	0.652 (L1.5)	0.790 (···)	0.904 (L1.3)	0.839 (L1.0)	0.841 (···)	0.977 ([T1.0])	1.047 (L2.5)
J0316+2650	4	T2.5±0.5	1.974 (···)	0.541 (···)	0.223 (···)	0.942 ([M7.7])	0.439 (T3.1)	0.488 (T2.7)	0.535 (T2.7)	0.758 (T2.6)	0.591 (T1.9)
J0331+1944	1	L0.5±2.0	1.094 (M8.2)	1.088 (···)	0.684 (L0.4)	0.697 (···)	0.872 (L2.1)	0.916 (···)	0.846 (···)	1.026 ([T0.8])	1.238 (···)

Table 3 – *Continued*

Object	Inst. ^a	Median		Allers & Liu (2013)				Burgasser et al. (2006b)				
		Type	H ₂ O	H ₂ OD	H ₂ O-1	H ₂ O-2	H ₂ O-J	H ₂ O-H	CH ₄ -J	CH ₄ -H	CH ₄ -K	
J0357+1529	2	L3.0±1.0	1.231 (L1.6)	0.835 (L4.3)	0.584 (L3.3)	0.766 (···)	0.890 (L1.6)	0.800 (L2.5)	0.829 (···)	0.988 ([T1.0])	1.015 (L3.8)	
J0357-1937	4	M9.5±2.0	1.052 (M7.1)	1.062 (···)	0.713 (M9.6)	0.962 (M7.1)	0.971 (L0.0)	0.879 (···)	0.897 (···)	1.068 (···)	1.087 (L0.7)	
J0358+1039	1	L3.0±1.5	1.271 (L2.4)	0.831 (L4.3)	0.783 ([M7.2])	0.816 (L1.3)	0.884 (L1.8)	0.728 (L5.4)	0.853 (···)	1.110 ([T0.7])	1.030 (L3.2)	
J0400-1322	2	L6.5±2.5	1.374 (···)	0.691 (L7.4)	0.549 (L4.2)	0.793 (···)	0.707 (L7.1)	0.695 (L6.7)	0.871 (···)	1.105 (···)	1.021 (L3.6)	
J0410+1459	4	L1.0±0.5	1.195 (L0.8)	0.954 (L1.3)	0.705 (M9.8)	0.843 (L0.6)	0.898 (L1.4)	0.833 (L1.2)	0.915 (···)	1.040 (···)	1.061 (L1.9)	
J0414+1529	4	M9.5±2.0	1.142 (M9.5)	0.987 (L0.3)	0.790 (M7.0)	0.900 (M8.9)	0.972 (L0.0)	0.910 (···)	0.934 (···)	1.049 (···)	1.047 (L2.5)	
J0417+1634	1	L0.5±0.5	1.067 ([M7.5])	0.997 (M9.9)	0.678 (L0.6)	0.849 (L0.4)	1.034 (···)	0.911 (···)	0.944 (···)	1.025 ([T0.8])	0.992 ([L4.7])	
...	4	L0.5±0.5	1.188 (L0.6)	1.067 (···)	0.681 (L0.6)	0.843 (L0.6)	0.943 (L0.4)	0.838 ([L1.0])	0.901 (···)	1.066 (···)	1.070 ([L1.5])	
J0417-1345	4	L2.5±0.5	1.265 (L2.3)	0.922 (L2.2)	0.704 ([M9.9])	0.844 ([L0.6])	0.856 (L2.5)	0.806 (L2.3)	0.940 (···)	1.025 (···)	1.070 (L1.5)	
J0417-1838	4	L3.5±1.0	1.285 (L2.7)	0.813 (L4.7)	0.631 (L2.1)	0.786 (···)	0.805 (L4.0)	0.754 (L4.4)	0.879 (···)	1.003 (···)	1.037 (L2.9)	
J0418+1121	4	M7.5±1.0	1.074 (M7.7)	1.058 (···)	0.758 (M8.1)	0.989 (M6.3)	1.029 (···)	0.922 (···)	0.972 (···)	1.008 (···)	1.020 ([L3.6])	
J0421-1950	2	L0.5±1.0	1.157 (M9.9)	0.816 ([L4.7])	0.664 (L1.1)	0.805 (L1.7)	0.980 (···)	0.849 (L0.6)	0.796 (···)	0.996 ([T1.0])	1.098 (L0.1)	
J0421-1133	2	L3.0±2.0	1.293 (L2.9)	0.815 (L4.7)	0.726 ([M9.1])	0.727 (···)	1.112 (L0.4)	0.769 (L3.8)	0.929 (···)	0.965 ([T1.1])	1.052 (L2.3)	
J0422+0723	4	L1.0±0.5	1.209 (L1.1)	0.946 (L1.5)	0.645 (L1.7)	0.831 (L0.9)	0.904 (L1.3)	0.803 ([L2.4])	0.894 (···)	1.047 (···)	1.081 (L1.0)	
J0422+1033	1	L0.5±3.0	1.167 (L0.1)	0.950 (L1.4)	0.804 (M6.5)	0.962 (M7.1)	1.001 (···)	0.853 (L0.4)	0.903 (···)	1.003 ([T0.9])	1.011 (L3.9)	
...	4	L2.5±3.0	1.126 (M9.1)	0.916 (L2.4)	1.080 (···)	0.921 ([M8.3])	0.827 (L3.4)	0.922 (···)	1.006 (···)	0.939 ([T1.3])	0.955 ([L5.9])	
J0423+1212	2	L1.0±2.5	1.153 (M9.8)	0.871 (L3.4)	0.675 (L0.8)	0.719 (···)	0.998 (···)	0.852 (L0.5)	0.883 (···)	0.957 ([T1.2])	1.009 (L4.0)	
J0425-1900	2	L0.0±2.5	1.109 (M8.7)	1.008 (···)	0.701 (L0.0)	0.610 (···)	1.087 (···)	0.921 (···)	0.825 (···)	0.934 ([T1.3])	1.033 (L3.1)	
J0429+0607	1	L0.5±0.5	1.172 (L0.2)	0.995 (L0.0)	0.681 (L0.5)	0.859 (L0.1)	0.912 (L1.1)	0.831 (L1.3)	0.894 (···)	1.086 ([T0.7])	1.124 (···)	
...	2	L1.5±1.5	1.142 (M9.5)	0.940 (L1.7)	0.602 (L2.9)	0.636 (···)	0.981 (···)	0.828 (L1.4)	0.874 (···)	1.021 (···)	1.050 (L2.4)	
J0430+1035	2	L1.5±2.0	1.123 (M9.0)	1.028 (···)	0.589 (L3.2)	0.766 (···)	1.165 (L2.1)	0.868 (···)	0.847 (···)	0.982 ([T1.0])	1.091 (L0.5)	
J0432-0639	4	L2.0±1.0	1.205 (L1.0)	0.893 (L2.9)	0.698 (L0.0)	0.803 (L1.8)	0.848 (L2.8)	0.813 (L2.0)	0.928 (···)	1.022 (···)	1.051 (L2.3)	
J0532-3253	2	L1.0±1.5	1.175 (L0.3)	0.931 (L2.0)	0.612 (L2.6)	0.855 (L0.2)	0.942 (L0.5)	0.843 (L0.8)	0.845 (···)	0.960 ([T1.1])	1.045 (L2.6)	
J0552+0210	2	L9.5±2.0	1.039 ([M6.7])	1.011 (···)	0.968 (···)	1.083 (···)	1.003 (···)	0.963 (···)	0.940 (···)	0.963 (T1.1)	0.903 (L7.3)	
J0812+3721	4	L0.5±0.5	1.185 (L0.6)	0.977 (L0.6)	0.735 ([M8.9])	0.854 (L0.3)	0.958 (L0.2)	0.866 (···)	0.967 (···)	1.051 (···)	1.084 (L0.8)	
J0851+1043	2	L3.0±0.5	1.248 ([L2.0])	0.800 ([L5.0])	0.606 (L2.8)	0.782 (···)	0.839 (L3.0)	0.785 (L3.1)	0.862 (···)	1.011 (···)	1.039 (L2.8)	
J0858+2214	1	L1.0±1.5	1.143 (M9.5)	0.873 (L3.4)	0.516 ([L4.9])	0.833 (L0.8)	0.927 (L0.8)	0.851 (L0.5)	0.973 (···)	1.046 ([T0.8])	1.058 (L2.0)	

Table 3 – *Continued*

Object	Inst. ^a	Median Type	Allers & Liu (2013)				Burgasser et al. (2006b)				
			H ₂ O	H ₂ OD	H ₂ O-1	H ₂ O-2	H ₂ O-J	H ₂ O-H	CH ₄ -J	CH ₄ -H	CH ₄ -K
J0858+2710	2	L1.0±0.5	1.199 (L0.9)	0.763 ([L5.8])	0.672 (L0.9)	0.802 (L1.8)	0.731 ([L6.3])	0.841 (L0.9)	0.908 (…)	0.945 ([T1.2])	1.063 (L1.8)
J0915+0514	4	L1.5±1.5	1.312 (L3.2)	0.893 (L2.9)	0.669 (L0.9)	0.853 (L0.3)	0.904 (L1.3)	0.771 (L3.7)	0.956 (…)	1.031 (…)	1.069 (L1.5)
J0921–1534	2	L6.0±0.5	1.386 (…)	0.749 (L6.1)	0.503 (…)	0.835 ([L0.8])	0.852 (L2.6)	0.716 (L5.9)	0.769 (…)	0.982 ([T1.0])	0.965 (L5.6)
J0936+0528	2	L0.0±1.5	1.121 (M9.0)	1.063 (…)	0.763 (M7.9)	0.838 (L0.7)	1.034 (…)	0.922 (…)	0.899 (…)	0.986 ([T1.0])	1.079 (L1.0)
J0940+2946	4	L1.0±2.0	1.331 (L3.6)	1.032 (…)	0.930 (M9.1)	1.036 (…)	0.908 (L1.2)	0.845 (L0.7)	0.930 (…)	1.032 ([T0.8])	1.036 (L3.0)
J0945–0757	4	L2.0±1.5	1.235 (L1.7)	0.844 (L4.1)	0.634 (L2.0)	0.881 (M9.5)	0.881 (L1.9)	0.790 (L3.0)	0.835 (…)	1.057 (…)	1.024 (L3.5)
J0946+1808	1	L0.5±2.0	1.182 (L0.4)	0.998 (M9.9)	0.601 (L2.8)	0.859 (L0.1)	0.830 (L3.3)	0.844 (L0.8)	0.934 (…)	1.030 ([T0.8])	0.962 ([L5.7])
J0946+0922	2	L0.5±1.5	1.093 (M8.2)	1.033 (…)	0.704 (M9.9)	0.831 (L0.9)	1.059 (…)	0.919 (…)	0.875 (…)	0.981 ([T1.0])	1.081 (L1.0)
J0947+0617	1	L0.5±2.0	1.098 (M8.3)	0.959 (L1.1)	0.858 ([M4.5])	0.867 (M9.8)	0.934 (L0.6)	0.885 (…)	0.938 (…)	1.042 ([T0.8])	1.041 (L2.7)
J0951–1343	1	L7.5±2.5	1.441 (…)	0.732 (L6.4)	0.750 ([M8.3])	0.887 ([M9.2])	0.715 (L6.8)	0.680 (L7.2)	0.893 (…)	1.015 (T0.9)	0.799 (L9.5)
J0956–1447	4	T0.0±0.5	1.662 (…)	0.615 (…)	0.375 (…)	0.816 ([L1.4])	0.573 (T0.7)	0.577 (T0.5)	0.702 (…)	1.039 (…)	0.802 (L9.4)
J0956–1910	4	L7.0±1.0	1.425 (…)	0.784 (L5.3)	0.457 (…)	0.807 ([L1.6])	0.726 (L6.5)	0.666 (L7.7)	0.764 (…)	0.997 ([T1.0])	0.906 (L7.2)
J1003–1441	1	L1.5±0.5	1.210 (L1.1)	0.919 (L2.2)	0.758 ([M8.0])	0.840 (L0.6)	0.995 (…)	0.821 (L1.7)	0.924 (…)	1.025 ([T0.8])	1.058 (L2.0)
...	4	L1.0±1.5	1.160 (L0.0)	1.025 (…)	0.732 (M8.9)	0.835 (L0.8)	0.914 (L1.0)	0.820 (L1.7)	0.941 (…)	0.983 ([T1.0])	1.054 (L2.2)
J1004–1127	2	L7.5±2.5	1.415 (…)	0.698 (L7.2)	0.322 (…)	0.772 (…)	0.694 (L7.5)	0.685 (L7.0)	0.642 (T0.3)	0.757 ([T2.6])	0.723 (T0.6)
J1004–1318	2	L4.0±0.5	1.310 (L3.2)	0.803 (L4.9)	0.571 (L3.7)	0.789 (…)	0.812 (L3.8)	0.773 (L3.6)	0.853 (…)	0.984 ([T1.0])	0.994 (L4.6)
J1009+1559	2	L3.0±2.0	1.178 (L0.4)	0.949 (L1.4)	0.551 (L4.2)	0.745 (…)	1.058 (…)	0.872 (…)	0.771 (…)	0.940 ([T1.3])	1.007 (L4.1)
J1013–1946	2	L0.5±1.5	1.093 (M8.2)	1.076 (…)	0.663 (L1.1)	0.803 (L1.8)	0.987 (…)	0.898 (…)	0.862 (…)	1.019 (…)	1.100 (L0.0)
J1014+1900	2	L1.0±2.0	1.098 (M8.4)	0.956 (L1.2)	0.674 (L0.8)	0.729 (…)	0.826 (L3.4)	0.918 (…)	0.872 (…)	0.954 ([T1.2])	1.059 (L2.0)
J1031+3349	4	L3.0±1.0	1.307 (L3.2)	0.887 (L3.1)	0.604 (L2.8)	0.865 ([L0.0])	0.891 (L1.6)	0.785 (L3.1)	0.899 (…)	1.047 (…)	1.067 (L1.6)
J1035+3655	4	M9.0±1.0	1.129 (M9.2)	1.038 (…)	0.779 (M7.4)	0.911 (M8.6)	0.967 (L0.0)	0.896 (…)	0.924 (…)	1.011 (…)	1.032 ([L3.1])
J1036+0306	1	L5.0±2.0	1.273 (L2.4)	0.712 (L6.8)	0.506 (L5.1)	0.862 ([L0.0])	0.965 ([L0.1])	0.725 (L5.5)	0.876 (…)	1.118 ([T0.7])	1.003 (L4.2)
...	2	L4.5±1.0	1.273 (L2.5)	0.814 (L4.7)	0.467 (…)	0.728 (…)	0.795 (L4.3)	0.736 (L5.1)	0.807 (…)	1.079 (…)	1.123 (…)
J1039–2829	3	T3.5±0.5	2.403 (…)	0.542 (…)	0.190 (…)	0.993 ([M6.2])	0.421 (T3.4)	0.447 (T3.4)	0.533 (T2.8)	0.756 (T2.6)	0.395 (T3.3)
J1039+2440	3	L7.5±0.5	1.542 (…)	0.700 (L7.2)	0.600 ([L2.9])	0.710 (…)	0.660 (L8.5)	0.669 (L7.6)	0.929 (…)	1.084 (…)	1.081 ([L1.0])
J1039–1904	4	L1.5±1.5	1.219 (L1.3)	0.892 (L3.0)	0.735 (M8.9)	0.813 (L1.5)	0.909 (L1.2)	0.858 (L0.2)	0.932 (…)	1.036 (…)	1.046 (L2.6)
J1041–0429	2	L3.5±2.0	1.283 (L2.7)	0.786 (L5.3)	0.517 (L4.9)	0.752 (…)	0.841 (L3.0)	0.763 (L4.0)	0.794 (…)	1.081 (…)	1.087 (L0.7)

Table 3 – *Continued*

Object	Inst. ^a	Median	Allers & Liu (2013)					Burgasser et al. (2006b)				
		Type	H ₂ O	H ₂ OD	H ₂ O-1	H ₂ O-2	H ₂ O-J	H ₂ O-H	CH ₄ -J	CH ₄ -H	CH ₄ -K	
J1044+0620	1	L1.0±1.5	1.228 (L1.5)	0.926 (L2.0)	0.723 (M9.2)	0.863 (M9.9)	0.942 (L0.5)	0.772 (L3.7)	0.873 (···)	0.971 ([T1.1])	1.149 (···)	
J1052+1722	1	L3.0±2.0	1.064 ([M7.4])	0.857 (L3.7)	0.648 (L1.5)	0.954 ([M7.3])	0.854 (L2.6)	0.892 (···)	0.913 (···)	1.058 ([T0.7])	0.966 (L5.5)	
...	2	L3.0±1.5	1.312 (L3.3)	0.893 (L2.9)	0.430 (···)	0.793 (···)	0.914 (L1.0)	0.759 (L4.2)	0.718 (···)	1.131 (···)	1.051 (L2.3)	
J1058+1339	1	L0.5±0.5	1.165 (L0.0)	0.984 (L0.3)	0.608 (L2.6)	0.772 (···)	0.726 ([L6.5])	0.787 (L3.0)	0.797 (···)	1.026 ([T0.8])	1.096 (L0.2)	
...	2	L3.5±1.0	1.321 (L3.4)	0.861 (L3.7)	0.478 (···)	0.633 (···)	0.850 (L2.7)	0.762 (L4.1)	0.762 (···)	1.025 (···)	1.066 (L1.7)	
J1102+1629	2	L0.0±1.5	1.119 (M9.0)	0.913 (L2.4)	0.721 (M9.3)	0.894 (M9.1)	0.934 (L0.6)	0.883 (···)	0.895 (···)	0.987 ([T1.0])	1.061 (L1.9)	
J1108+0838	2	L7.0±3.0	1.413 (···)	0.659 (···)	0.475 (···)	0.905 ([M8.8])	0.767 (L5.2)	0.702 (L6.4)	0.796 (···)	0.971 (T1.1)	0.885 (L7.8)	
J1117+1857	2	L2.0±2.0	1.255 (L2.1)	0.975 (L0.7)	0.513 (L5.0)	0.714 (···)	0.988 (···)	0.848 (L0.6)	0.757 (···)	1.051 (···)	1.059 (L2.0)	
J1118-0856	1	L6.5±1.5	1.298 ([L2.9])	0.711 (L6.9)	0.571 (L3.6)	0.917 ([M8.3])	0.745 (L5.9)	0.704 (L6.3)	0.906 (···)	1.052 ([T0.8])	0.909 (L7.2)	
...	3	L7.0±1.0	1.469 (···)	0.684 (L7.6)	0.473 (···)	0.824 ([L1.2])	0.746 (L5.9)	0.691 (L6.8)	0.770 (···)	1.003 (···)	0.919 (L6.9)	
...	4	L7.5±0.5	1.449 (···)	0.696 (L7.3)	0.455 (···)	0.837 ([L0.8])	0.744 ([L5.9])	0.680 (L7.2)	0.785 (···)	1.029 (···)	0.909 (L7.2)	
J1122+0343	1	L4.5±0.5	1.408 (···)	0.832 (L4.3)	0.568 (L3.7)	0.882 ([M9.4])	0.804 (L4.1)	0.701 (L6.4)	0.893 (···)	1.022 ([T0.9])	0.999 (L4.4)	
J1127+1234	2	L3.0±1.5	1.298 (L3.0)	0.769 (L5.7)	0.554 (L4.1)	0.693 (···)	0.868 (L2.2)	0.791 (L2.9)	0.810 (···)	1.004 (···)	1.066 (L1.7)	
J1130+2341	4	L3.5±0.5	1.546 (···)	0.881 (L3.2)	0.579 (L3.5)	0.798 ([L1.9])	0.819 (L3.6)	0.680 ([L7.2])	0.788 (···)	1.066 (···)	1.023 (L3.5)	
J1132-3809	3	L7.0±1.0	1.410 (···)	0.709 (L7.0)	0.455 (···)	0.874 ([M9.7])	0.711 (L6.9)	0.729 (L5.4)	0.780 (···)	0.998 (···)	0.893 (L7.6)	
J1138+0748	1	L1.0±2.5	1.199 (L0.8)	0.485 (···)	0.574 (L3.5)	0.900 (M8.9)	0.551 ([T1.2])	0.951 (···)	0.833 (···)	1.311 ([T2.4])	1.250 (···)	
J1141+1941	2	L1.0±1.5	1.134 (M9.3)	0.928 (L2.0)	0.791 ([M6.9])	0.858 (L0.1)	0.993 (···)	0.843 (L0.8)	0.938 (···)	0.855 ([T1.8])	1.035 (L3.0)	
J1143+1905	3	L5.5±1.0	1.317 (L3.3)	0.772 (L5.6)	0.575 (L3.6)	0.930 ([M8.0])	0.311 ([T4.4])	0.718 (L5.8)	0.738 (···)	1.017 (···)	0.960 (L5.7)	
J1147-1032	2	L3.0±0.5	1.314 (L3.3)	0.769 ([L5.6])	0.595 (L3.1)	0.791 (···)	0.841 (L3.0)	0.763 (L4.0)	0.879 (···)	1.031 (···)	1.038 (L2.9)	
J1147+2153	4	L2.0±1.5	1.227 (L1.5)	0.892 (L2.9)	0.737 (M8.8)	0.865 (M9.9)	0.885 (L1.7)	0.783 (L3.2)	0.932 (···)	0.978 ([T1.0])	1.060 (L1.9)	
J1150+0520	4	L5.0±1.0	1.313 (L3.3)	0.744 (L6.2)	0.529 (L4.7)	0.862 ([L0.0])	0.795 (L4.3)	0.738 (L5.0)	0.795 (···)	1.039 (···)	0.948 (L6.1)	
...	3	L6.5±1.0	1.465 (···)	0.747 (L6.1)	0.503 (···)	0.788 (···)	0.707 (L7.1)	0.726 (L5.5)	0.768 (···)	0.995 ([T1.0])	0.918 (L6.9)	
J1158+0435	4	L8.5±2.0	1.611 (···)	1.078 (···)	0.717 (···)	0.919 (···)	0.697 (L7.4)	0.595 (T0.0)	0.717 (···)	1.078 (T0.7)	0.919 (L6.9)	
J1200-2836	4	L9.0±2.0	1.437 (···)	0.622 (···)	0.387 (···)	0.856 ([L0.2])	0.713 (L6.9)	0.673 (L7.5)	0.761 (···)	0.985 (T1.0)	0.745 (T0.3)	
J1211+0406	1	L2.5±1.0	1.293 (L2.8)	0.959 (L1.1)	0.736 ([M8.8])	0.855 (L0.2)	0.856 (L2.5)	0.804 (L2.4)	0.887 (···)	1.074 ([T0.7])	1.056 (L2.1)	
...	2	L2.5±1.0	1.277 (L2.5)	0.897 (L2.8)	0.635 (L2.0)	0.783 (···)	0.843 (L2.9)	0.770 (L3.8)	0.865 (···)	1.000 (···)	1.067 (L1.6)	
J1217+0708	2	L1.0±0.5	1.206 (L1.0)	1.021 (···)	0.669 (L0.9)	0.800 (L1.9)	0.939 (L0.5)	0.825 (L1.5)	0.860 (···)	1.000 (···)	1.092 (L0.4)	

Table 3 – *Continued*

Object	Inst. ^a	Median	Allers & Liu (2013)				Burgasser et al. (2006b)				
		Type	H ₂ O	H ₂ OD	H ₂ O-1	H ₂ O-2	H ₂ O-J	H ₂ O-H	CH ₄ -J	CH ₄ -H	CH ₄ -K
J1218-1332	2	L7.0±3.0	1.471 (…)	0.791 (L5.2)	0.384 (…)	0.771 (…)	0.932 ([L0.7])	0.675 (L7.4)	0.699 (…)	0.979 (T1.0)	0.928 (L6.7)
J1225-1013	2	T6.0±0.5	2.312 (…)	0.318 (…)	0.052 ([L4.0])	0.273 (…)	0.207 (T5.2)	0.310 (T5.4)	0.332 (T6.0)	0.276 (T6.1)	0.123 (T6.4)
J1256-1002	4	L1.5±2.0	1.029 ([M6.4])	0.942 (L1.7)	0.725 (M9.2)	1.021 ([M5.4])	0.835 (L3.1)	0.931 (…)	0.855 (…)	0.985 ([T1.0])	0.954 ([L5.9])
J1307-0558	2	L3.0±2.5	1.244 (L1.9)	0.759 (L5.9)	0.524 (L4.8)	0.894 ([M9.1])	0.943 (L0.4)	0.789 (L3.0)	0.801 (…)	1.007 (…)	0.913 ([L7.1])
J1308+0818	4	M8.5±0.5	1.107 (M8.6)	1.028 (…)	0.775 (M7.5)	0.922 (M8.3)	0.973 (…)	0.908 (…)	0.966 (…)	0.999 (…)	1.018 ([L3.7])
J1308+0432	1	M9.5±1.5	1.073 (M7.6)	0.956 (L1.2)	0.717 (M9.4)	1.083 ([M3.8])	0.977 (M9.9)	0.890 (…)	0.880 (…)	1.056 ([T0.8])	0.861 ([L8.3])
…	2	L3.0±1.5	1.013 ([M5.9])	1.304 (…)	0.588 (L3.2)	0.598 (…)	1.177 (L2.8)	0.943 (…)	0.764 (…)	1.036 (…)	0.991 (L4.7)
J1317+0448	4	L3.0±1.0	1.280 (L2.6)	0.886 (L3.1)	0.653 (L1.4)	0.793 (…)	0.862 (L2.4)	0.765 (L4.0)	0.907 (…)	1.038 (…)	1.033 (L3.1)
J1318-0632	1	L0.0±1.5	1.123 (M9.0)	0.962 (L1.0)	0.753 (M8.2)	0.814 (L1.4)	1.014 (…)	0.870 (M9.7)	0.880 (…)	1.046 ([T0.8])	0.997 ([L4.5])
J1324+1906	1	T3.5±0.5	…	0.548 (…)	0.515 ([L4.9])	1.094 (…)	0.368 (T3.9)	0.395 (T4.3)	0.608 ([T1.1])	0.645 (T3.5)	0.374 (T3.5)
…	2	T4.0±0.5	2.245 (…)	0.392 (…)	0.114 (…)	0.622 (…)	0.370 (T3.9)	0.391 (T4.3)	0.493 (T3.5)	0.585 (T3.9)	0.352 (T3.6)
J1333-0215	4	L2.5±0.5	1.258 (L2.1)	1.074 (…)	0.968 ([M7.0])	1.042 (…)	0.851 (L2.7)	0.807 (L2.2)	0.968 (…)	1.074 ([T0.7])	1.042 (L2.7)
J1339+1523	1	L0.0±1.5	1.113 (M8.7)	0.890 (L2.9)	0.754 (M8.2)	0.867 (M9.8)	0.976 (M9.9)	0.848 (L0.6)	0.964 (…)	1.089 ([T0.7])	1.067 (L1.6)
…	2	L1.0±1.0	1.182 (L0.5)	1.050 (…)	0.638 (L1.9)	0.830 (L1.0)	0.944 (L0.4)	0.840 (L0.9)	0.838 (…)	0.997 ([T1.0])	1.044 (L2.6)
J1343-1216	1	L9.5±2.0	1.494 (…)	0.471 (…)	0.727 ([M9.1])	0.918 ([M8.3])	0.709 (L7.0)	0.630 (L9.0)	0.821 (…)	1.105 (T0.7)	0.738 (T0.4)
…	3	L6.0±2.5	1.556 (…)	0.827 (L4.4)	0.431 (…)	0.753 (…)	0.698 (L7.3)	0.630 (L9.0)	0.727 (…)	1.087 (…)	1.005 (L4.2)
…	4	L6.0±2.0	1.439 (…)	0.775 (L5.5)	0.407 (…)	0.706 (…)	0.734 (L6.2)	0.629 (L9.0)	0.694 (…)	1.111 (…)	0.983 (L5.0)
J1343+1312	2	L0.5±1.0	1.179 (L0.4)	0.930 (L2.0)	0.715 (M9.5)	0.841 (L0.7)	0.941 (L0.5)	0.843 (L0.8)	0.913 (…)	0.983 ([T1.0])	1.059 (L2.0)
J1344-1614	4	L4.0±2.0	1.316 (L3.3)	1.065 (…)	0.814 (L4.6)	1.072 (L1.4)	0.764 (L5.3)	0.709 (L6.1)	0.814 (…)	1.065 ([T0.7])	1.072 (L1.4)
J1411+2948	4	L8.0±2.0	1.546 (…)	0.766 (L5.7)	0.390 (…)	0.841 ([L0.6])	0.677 (L7.9)	0.606 (L9.7)	0.684 (…)	0.993 (T1.0)	0.910 (L7.1)
J1414+0107	3	L4.5±1.5	1.456 (…)	0.752 (L6.0)	0.544 (L4.3)	0.729 (…)	0.891 (L1.6)	0.757 (L4.3)	0.796 (…)	1.014 (…)	0.975 (L5.2)
J1415+2635	4	L2.0±1.5	1.250 (L2.0)	0.869 (L3.5)	0.700 (L0.0)	0.827 (L1.1)	0.848 (L2.8)	0.780 (L3.3)	0.884 (…)	1.029 (…)	1.079 (L1.0)
J1422+0827	1	L2.0±2.0	1.368 (…)	0.921 (L2.2)	0.700 (M9.9)	0.924 ([M8.2])	0.894 (L1.5)	0.700 ([L6.5])	0.878 (…)	1.110 ([T0.7])	1.012 (L3.9)
…	2	L2.5±1.5	1.311 (L3.2)	0.830 (L4.4)	0.641 (L1.8)	0.789 (…)	0.894 (L1.5)	0.771 (L3.7)	0.904 (…)	1.009 (…)	1.061 (L1.9)
J1452+1114	4	L2.5±0.5	1.280 (L2.6)	0.866 (L3.6)	0.614 (L2.5)	0.805 (L1.7)	0.858 (L2.5)	0.783 (L3.2)	0.864 (…)	1.054 (…)	1.062 (L1.8)
J1453-2744	2	L0.0±2.5	1.151 (M9.7)	1.114 (…)	0.780 (M7.3)	0.814 (L1.5)	1.100 (L0.1)	0.918 (…)	0.909 (…)	0.984 ([T1.0])	1.037 (L2.9)
J1455+2619	4	L2.5±1.0	1.250 (L1.9)	1.048 (…)	0.880 (L1.7)	1.015 (…)	0.845 (L2.8)	0.808 (L2.2)	0.880 (…)	1.048 ([T0.8])	1.015 (L3.8)

Table 3 – *Continued*

Object	Inst. ^a	Median	Allers & Liu (2013)				Burgasser et al. (2006b)				
		Type	H ₂ O	H ₂ OD	H ₂ O-1	H ₂ O-2	H ₂ O-J	H ₂ O-H	CH ₄ -J	CH ₄ -H	CH ₄ -K
J1501-1831	4	L0.5±1.0	1.177 (L0.4)	0.977 (L0.6)	0.713 (M9.6)	0.892 (M9.1)	0.952 (L0.3)	0.881 (···)	0.900 (···)	1.038 (···)	1.010 ([L4.0])
J1510-1147	1	L2.5±2.5	1.159 (M9.9)	0.775 (L5.5)	0.613 (L2.5)	0.766 (···)	0.778 (L4.9)	0.803 (L2.4)	0.809 (···)	1.161 ([T0.8])	1.093 (L0.4)
...	4	L4.5±2.5	1.368 (···)	0.816 (L4.7)	0.529 (L4.7)	0.743 (···)	0.808 (L3.9)	0.687 (L7.0)	0.856 (···)	1.126 (···)	1.083 (L0.9)
J1533+2044	3	L0.5±1.5	1.268 (L2.4)	0.988 (L0.2)	0.668 (L1.0)	0.922 (M8.3)	1.106 (L0.2)	0.866 (···)	0.967 (···)	0.934 ([T1.3])	1.086 (L0.7)
J1537-0800	1	L2.5±2.0	1.241 (L1.8)	1.010 (···)	0.667 (L0.9)	0.820 (L1.2)	0.763 (L5.3)	0.787 (L3.0)	0.918 (···)	0.985 ([T1.0])	1.021 (L3.6)
...	2	L2.5±1.0	1.259 (L2.2)	0.860 (L3.7)	0.596 (L3.0)	0.778 (···)	0.859 (L2.4)	0.781 (L3.3)	0.837 (···)	1.020 (···)	1.070 (L1.5)
J1605+1931	4	L3.0±0.5	1.180 ([L0.4])	0.899 (L2.8)	0.618 (L2.4)	0.788 (···)	0.886 (L1.7)	0.785 (L3.1)	0.915 (···)	1.056 (···)	1.036 (L3.0)
J1613-0747	1	L4.0±1.0	1.419 (···)	0.870 (L3.4)	0.601 (L2.8)	0.754 (···)	0.789 (L4.5)	0.662 ([L7.9])	0.830 (···)	1.034 ([T0.8])	1.000 (L4.3)
...	2	L4.0±2.0	1.340 (L3.8)	0.750 (L6.1)	0.556 (L4.0)	0.755 (···)	0.813 (L3.8)	0.741 (L4.9)	0.834 (···)	1.053 (···)	1.071 (L1.4)
...	3	L4.5±2.0	1.471 (···)	0.834 (L4.3)	0.547 (L4.2)	0.706 (···)	0.768 (L5.2)	0.714 (L6.0)	0.814 (···)	1.060 (···)	1.077 (L1.2)
J1615+1340	1	T5.5±1.0	0.164 (···)	1.298 ([M7.7])	0.127 (T6.2)	0.431 (T3.7)	0.403 (T5.0)	0.344 (T5.6)	0.060 (···)
...	2	T5.5±1.0	2.330 (···)	0.445 (···)	0.052 ([L4.0])	0.404 (···)	0.355 (T4.1)	0.355 (T4.8)	0.328 (T6.0)	0.286 (T6.1)	0.199 (T5.3)
J1623-0508	4	L2.0±1.5	1.219 (L1.3)	1.002 (···)	0.653 (L1.4)	0.869 (M9.8)	0.822 (L3.5)	0.807 (L2.3)	0.867 (···)	1.022 (···)	1.041 (L2.8)
J1627+0546	1	L0.5±0.5	1.187 (L0.6)	0.947 (L1.5)	0.805 ([M6.4])	0.841 (L0.6)	0.939 (L0.5)	0.793 (L2.8)	0.942 (···)	1.044 ([T0.8])	0.943 ([L6.2])
...	4	L0.5±0.5	1.176 (L0.3)	1.001 (···)	0.697 (L0.1)	0.843 (L0.6)	1.003 (···)	0.925 (···)	0.944 (···)	1.032 (···)	1.056 ([L2.1])
J1627+0836	4	L0.0±1.5	1.102 (M8.5)	1.023 (···)	0.679 (L0.6)	0.885 (M9.4)	0.977 (···)	0.887 (···)	0.901 (···)	1.036 (···)	1.070 (L1.5)
J1628+0517	1	L1.0±1.5	1.225 (L1.4)	1.036 (···)	0.724 (M9.2)	0.897 (M9.0)	0.926 (L0.8)	0.828 (L1.4)	0.902 (···)	1.018 ([T0.9])	1.161 (···)
J1629+0335	1	T2.5±1.0	...	0.583 (···)	0.371 (···)	0.829 ([L0.9])	0.463 (T2.8)	0.433 (T3.7)	0.537 (T2.7)	0.835 (T2.0)	0.594 (T1.8)
...	2	T2.0±1.0	1.937 (···)	0.475 (···)	0.191 (···)	0.736 (···)	0.463 (T2.8)	0.457 (T3.3)	0.569 (T2.0)	0.861 (T1.8)	0.607 (T1.7)
J1631-1922	4	M6.0±0.5	1.029 (M6.4)	1.109 (···)	0.925 (···)	1.032 (M5.2)	0.924 ([L0.8])	0.970 (···)	1.013 (···)	1.017 (···)	0.970 ([L5.4])
J1644+2600	4	L1.0±0.5	1.170 (L0.2)	0.978 (L0.6)	0.608 ([L2.7])	0.835 (L0.8)	0.928 (L0.7)	0.827 (L1.4)	0.845 (···)	1.033 (···)	1.008 ([L4.1])
J1654+3747	4	L1.5±1.0	1.248 (L1.9)	1.018 (···)	0.911 (L0.2)	1.032 (···)	0.917 (L1.0)	0.825 (L1.5)	0.911 (···)	1.018 ([T0.9])	1.032 (L3.1)
J1708+2606	4	L4.5±2.0	1.258 (L2.2)	0.813 (L4.7)	0.550 (L4.2)	0.756 (···)	0.785 (L4.6)	0.699 (L6.5)	0.841 (···)	1.124 (···)	1.061 (L1.9)
J1755+3618	3	M8.5±3.0	1.069 (M7.6)	0.975 (L0.7)	0.702 (M9.9)	1.042 (M4.9)	1.014 (···)	0.928 (···)	0.844 (···)	0.949 ([T1.2])	0.925 ([L6.7])
J1756+2815	3	L2.0±0.5	0.032 (···)	0.017 (···)	0.862 ([M4.4])	0.009 (L1.4)	0.865 (L2.3)	0.150 (···)	0.702 (···)	0.138 ([T7.6])	0.004 (···)
J1756+3343	3	L2.0±1.0	1.246 (L1.9)	0.913 (L2.4)	0.580 (L3.4)	0.833 (L0.9)	0.872 (L2.1)	0.832 (L1.2)	0.861 (···)	1.003 (···)	1.060 (L2.0)
J1811+2728	4	L2.5±0.5	1.261 (L2.2)	0.879 (L3.3)	0.585 (L3.3)	0.799 (L1.9)	0.848 (L2.8)	0.745 ([L4.7])	0.852 (···)	1.079 (···)	1.047 (L2.5)

Table 3 – *Continued*

Table 3 – *Continued*

Object	Inst. ^a	Median	Allers & Liu (2013)				Burgasser et al. (2006b)				
		Type	H ₂ O	H ₂ OD	H ₂ O-1	H ₂ O-2	H ₂ O- <i>J</i>	H ₂ O- <i>H</i>	CH ₄ - <i>J</i>	CH ₄ - <i>H</i>	CH ₄ - <i>K</i>
J2322-1407	3	L4.0±1.0	1.361 (…)	0.859 (L3.7)	0.562 (L3.9)	0.784 (…)	0.861 (L2.4)	0.741 (L4.9)	0.779 (…)	1.063 (…)	1.100 ([L0.0])
…	4	L2.0±2.0	1.334 (L3.7)	0.932 (L1.9)	0.506 (…)	0.824 (L1.2)	0.861 (L2.4)	0.736 (L5.1)	0.800 (…)	1.142 (…)	1.091 (L0.4)
J2322+1300	1	L4.5±2.0	1.321 (L3.4)	0.833 (L4.2)	0.638 (L1.8)	0.815 ([L1.4])	0.740 (L6.0)	0.732 (L5.2)	0.929 (…)	1.082 ([T0.7])	0.866 ([L8.2])
J2327+1517	4	L4.0±1.0	1.364 (…)	0.794 (L5.1)	0.598 (L3.0)	0.782 (…)	0.810 (L3.9)	0.738 (L5.0)	0.900 (…)	1.033 (…)	1.008 (L4.1)
J2330+1006	2	L2.0±1.0	1.291 (L2.8)	0.987 (L0.3)	0.646 (L1.6)	0.787 (…)	0.946 (L0.4)	0.814 (L2.0)	0.861 (…)	0.981 ([T1.0])	1.047 (L2.5)
J2332-1249	4	L0.5±0.5	1.172 (L0.2)	0.963 (L1.0)	0.761 ([M8.0])	0.830 (L1.0)	0.929 (L0.7)	0.859 (L0.2)	0.962 (…)	1.024 (…)	1.097 (L0.2)
J2340-0745	4	T6.5±0.5	4.081 (…)	0.230 (…)	0.037 ([L3.5])	1.415 (…)	0.120 (T6.3)	0.252 (T6.3)	0.315 (T6.2)	0.186 (T7.0)	0.096 (T6.9)
J2344+0909	2	L1.0±1.5	1.208 (L1.1)	1.063 (…)	0.749 (M8.4)	0.836 (L0.8)	0.927 (L0.8)	0.865 (L0.0)	0.926 (…)	0.977 ([T1.0])	1.056 (L2.1)
J2351+3010	4	L5.0±1.5	1.336 (L3.7)	0.799 (L5.0)	0.585 (L3.3)	0.802 (L1.8)	0.735 (L6.2)	0.727 (L5.5)	0.866 (…)	1.073 (…)	0.984 (L4.9)

Note.

Spectral types in brackets are not used to calculate the median type.

^a(1) OMM/SIMON; (2) G-S/GNIRS; (3) G-N/NIRI; (4) IRTF/SpEX.

Table 4 – Targets Spectral Classification

Object	Inst. ^a	Obs. Index	Obs. Visual	Adopted NIR	Previous Opt.	Previous NIR	Ref.
		Type	Type	Type	Type	Type	Opt/NIR
J0004–2007	3	L1.5±1.5	M9±2 pec	L0:: pec ²
J0006–1319	1	L7.0±1.0	L6±2 pec	L6:+T7:	...	L5 pec ^b	... /26
...	2	L6.5±2.0	L6±2 pec	L6:+T7:	...	L5 pec ^b	... /26
J0006–2158	3	L0.5±1.5	M8.5±2 pec	M9:: pec
J0006–0852	2	L1.0±1.0	M9±1 pec	M9:+T6: pec	M9	M8.5+T5 ^c	3/2
J0008+0806	1	L2.5±2.5	L0.5±2	L0.5::
J0013+0841	1	L0.5±2.0	L1±2	L1:
J0013–1816	4	L3.5±1.5	L6.5±2 pec	L3:+T4:	L1	L5 pec ^h	28/29
J0026–0936	4	M8.5±0.5	M9±1 pec	M9 pec (red)	M9	...	3/ ...
J0049+0440	2	L8.0±2.0	L8.5±1	L8.5:	...	L9	... /4
J0102+0355	2	L8.5±1.5	L9±1	L9:	...	L9	... /30
J0103+1940	4	L0.0±1.5	M9±1	M9.5: pec ²
J0120+1518	4	L0.0±1.0	M9±1 pec	M9: γ	M9	...	5/ ...
J0135+0205	1	T0.0±2.0	L9±2	L9:	...	L9.5	... /29
J0136+0933	2	T2.5±0.5	T2.5±1	T2.5	...	T2.5	... /1
J0138–0322	1	T2.5±1.0	T2.5±2	T2.5:: ^d	...	T3	... /4
J0148+3712	4	L0.5±1.0	L1±1 pec	L1: pec (blue)
J0150+3827	4	L8.5±2.0	L9.5±1	L9.5:	...	T0	... /4
J0151+3824	4	L1.5±0.5	L1.5±1	L1.5
J0155+0950	1	L3.5±1.5	L4±1	L4	...	L5	... /6
...	2	L4.0±2.0	L4±1	L4	...	L5	... /6
J0211–1427	4	L2.0±0.5	L1.5±1	L2
J0251–0818	1	L5.0±1.0	L5±2	L5:
0307+0852	2	L1.5±0.5	L1.5±1 pec	L1.5 pec (red)	...	L5.5 ^j	... /30
J0316+2650	4	T2.5±0.5	T3±1	T2.5	...	T2.5 ⁱ	... /29
J0331+1944	1	L0.5±2.0	M9.5±2	L0::
J0357+1529	2	L3.0±1.0	L1±1 pec	L1:: pec (blue)	...	L0.5 ^j	... /30

Table 4 – *Continued*

Object	Inst. ^a	Obs. Index	Obs. Visual	Adopted NIR	Previous Opt.	Previous NIR	Ref.
		Type	Type	Type	Type	Type	Opt/NIR
J0357-1937	4	M9.5±2.0	M8±1 pec	M7.5: γ
J0358+1039	1	L3.0±1.5	L2±1	L2: ^e	M5	...	20/ ...
J0400-1322	2	L6.5±2.5	L7±2	L7::
J0410+1459	4	L1.0±0.5	L1±1	L1 pec (red)	L0.5	...	20/ ...
J0414+1529	4	M9.5±2.0	M8.5±1	M8.5:
J0417+1634	1	L0.5±0.5	M9±2	L0: γ	M8	M8.5 (young)	18/21
...	4	L0.5±0.5	M9±1 pec	L0: γ	M8	M8.5 (young)	18/21
J0417-1345	4	L2.5±0.5	L2±1	L2
J0417-1838	4	L3.5±1.0	L2.5±1 pec	L3: pec ¹
J0418+1121	4	M7.5±1.0	M8±1	M8:
J0421-1950	2	L0.5±1.0	M8.5±1 pec	M9: pec (blue)
J0421-1133	2	L3.0±2.0	L3±2 pec	L3: pec (red)
J0422+0723	4	L1.0±0.5	L1±1	L1	L1	...	7/ ...
J0422+1033	1	L0.5±3.0	M9±1	M9.5: pec ²
...	4	L2.5±3.0	M9.5±2	M9.5: pec ²
J0423+1212	2	L1.0±2.5	M9±1 pec	M9.5: pec ²
J0425-1900	2	L0.0±2.5	M6.5±1	M6.5:
J0429+0607	1	L0.5±0.5	M9±1 pec	L0: pec (blue)
...	2	L1.5±1.5	M9.5±1 pec	L0: pec (blue)
J0430+1035	2	L1.5±2.0	M8.5±2 pec	M9:: pec (blue)
J0432-0639	4	L2.0±1.0	L2±1 pec	L2 pec (red)
J0532-3253	2	L1.0±1.5	M9±1 pec	M9.5: pec ²
J0552+0210	2	L9.5±2.0	<M0 pec	<M0 pec
J0812+3721	4	L0.5±0.5	L1±1 pec	L0.5 pec ¹	L3	...	7/ ...
J0851+1043	2	L3.0±0.5	L3±1 pec	L3 pec ¹	L5 ^f	...	5/ ...
J0858+2214	1	L1.0±1.5	L1±1	L1:	L1	...	7/ ...
J0858+2710	2	L1.0±0.5	L2±2 pec	L1.5: pec	L0	...	3/ ...

Table 4 – *Continued*

Object	Inst. ^a	Obs. Index	Obs. Visual	Adopted NIR	Previous Opt.	Previous NIR	Ref.
		Type	Type	Type	Type	Type	Opt/NIR
J0915+0514	4	L1.5±1.5	L2±1	L2:	L3	...	8/ ...
J0921–1534	2	L6.0±0.5	L4±2 pec	L5:: pec ³ (blue)
J0936+0528	2	L0.0±1.5	M9±1	M9:	M9.5	...	8/ ...
J0940+2946	4	L1.0±2.0	L2±1	L2:	L1	L0.5	7/23
J0945–0757	4	L2.0±1.5	L1.5±1	L1.5:
J0946+1808	1	L0.5±2.0	L3±2 pec	L2.5:: pec
J0946+0922	2	L0.5±1.5	M9±2 pec	M9.5: pec (blue)	L0	...	8/ ...
J0947+0617	1	L0.5±2.0	L0±1	L0:	M9	...	3/ ...
J0951–1343	1	L7.5±2.5	L6±2	L6::
J0956–1447	4	T0.0±0.5	L9.5±1	L9.5	...	L9	... /29
J0956–1910	4	L7.0±1.0	L6±1 pec	L6.5: pec (blue)	...	L5 pec ^h	... /29
J1003–1441	1	L1.5±0.5	M9±1	L0.5:
...	4	L1.0±1.5	L0±1	L0.5:
J1004–1127	2	L7.5±2.5	T2.5±1 pec	T2:: pec
J1004–1318	2	L4.0±0.5	L3±1 pec	L3.5 pec (blue)	L0	L1	10/11
J1009+1559	2	L3.0±2.0	L0.5±1	L1:	...	L1.5	... /29
J1013–1946	2	L0.5±1.5	L0±1	L0:
J1014+1900	2	L1.0±2.0	L0.5±2 pec	L0.5:: pec (blue)
J1031+3349	4	L3.0±1.0	L2±1	L2:	...	L2	... /12
J1035+3655	4	M9.0±1.0	M9.5±1	M9.5:	...	M9.5	... /24
J1036+0306	1	L5.0±2.0	L3±2	L3.5: pec (blue)	...	L4 pec (blue)	... /26
...	2	L4.5±1.0	L3±1 pec	L3.5: pec (blue)	...	L4 pec (blue)	... /26
J1039–2829	3	T3.5±0.5	T3±1	T3.5
J1039+2440	3	L7.5±0.5	L5±2 pec	L5:: pec	L5 ^f	...	5/ ...
J1039–1904	4	L1.5±1.5	L2±1	L2:
J1041–0429	2	L3.5±2.0	L2.5±1 pec	L2.5: pec (blue)	...	L1.5 ^j	... /30
J1044+0620	1	L1.0±1.5	L0±1 pec	L0: pec ²

Table 4 – *Continued*

Object	Inst. ^a	Obs. Index	Obs. Visual	Adopted NIR	Previous Opt.	Previous NIR	Ref.
		Type	Type	Type	Type	Type	Opt/NIR
J1052+1722	1	L3.0±2.0	L1±2 pec	L2: pec (blue)	L1.5 ^f	...	5/ ...
...	2	L3.0±1.5	L2±2 pec	L2: pec (blue)	L1.5 ^f	...	5/ ...
J1058+1339	1	L0.5±0.5	L1.5±2 pec	L1.5: pec (blue)
...	2	L3.5±1.0	L1±2 pec	L1.5: pec (blue)
J1102+1629	2	L0.0±1.5	M9.5±1	M9.5:	L0	...	7/ ...
J1108+0838	2	L7.0±3.0	L9±2	L9::	L8.5 ^f	L8	5/29
J1117+1857	2	L2.0±2.0	L1±2 pec	L1:: pec
J1118-0856	1	L6.5±1.5	L6.5±1	L6.5: pec ²	L6	L6 pec (blue)	12/12
...	3	L7.0±1.0	L6±1 pec	L6.5: pec ²	L6	L6±0.5 pec (blue)	12/12
...	4	L7.5±0.5	L5.5±1 pec	L6.5: pec ²	L6	L6 pec (blue)	12/12
J1122+0343	1	L4.5±0.5	L4±2	L4.5:
J1127+1234	2	L3.0±1.5	L1±1	L1.5:	...	L0 ^j	... /30
J1130+2341	4	L3.5±0.5	L2±1 pec	L2.5: pec (blue)	L3 ^f	...	9/ ...
J1132-3809	3	L7.0±1.0	L8.5±1 pec	L8: pec
J1138+0748	1	L1.0±2.5	L2±2	L2:: ^d
J1141+1941	2	L1.0±1.5	M9.5±1	L0:
J1143+1905	3	L5.5±1.0	L8±2 pec	L7:: pec	L9 ^f	...	5/ ...
J1147-1032	2	L3.0±0.5	L3±1	L3
J1147+2153	4	L2.0±1.5	L1.5±1	L1.5:
J1150+0520	3	L5.0±1.0	L6±1 pec	L5.5: pec (blue)	L6	...	7/ ...
...	4	L6.5±1.0	L5.5±1 pec	L5.5: pec (blue)	L6	...	7/ ...
J1158+0435	4	L8.5±2.0	L7±2 pec	sdL7:	sdL7	sdL7	12/12
J1200-2836	4	L9.0±2.0	T0.5±1	T0.5:	...	T0 ^h	... /29
J1211+0406	1	L2.5±1.0	L2.5±1	L2.5	L2	...	8/ ...
...	2	L2.5±1.0	L2.5±1	L2.5	L2	...	8/ ...
J1217+0708	2	L1.0±0.5	L0.5±1	L1	L1	...	8/ ...
J1218-1332	2	L7.0±3.0	L3±2 pec	L4:: pec (blue)

Table 4 – *Continued*

Object	Inst. ^a	Obs. Index	Obs. Visual	Adopted NIR	Previous Opt.	Previous NIR	Ref.
		Type	Type	Type	Type	Type	Opt/NIR
J1225–1013	2	T6.0±0.5	T6±1	T6	...	T6	... /13
J1256–1002	4	L1.5±2.0	M7.5±2 pec	M8:: pec
J1307–0558	2	L3.0±2.5	L4±2 pec	L3.5:: pec (red)	...	L8 (sl. blue)	... /30
J1308+0818	4	M8.5±0.5	L0±1	M9.5:	L0	...	8/ ...
J1308+0432	1	M9.5±1.5	M9±2 pec	M9.5:: pec (blue)
...	2	L3.0±1.5	M8±2 pec	M9.5:: pec (blue)
J1317+0448	4	L3.0±1.0	L2±1	L2.5:
J1318–0632	1	L0.0±1.5	L0.5±1	L0.5:
J1324+1906	1	T3.5±0.5	T4±1	T4	...	T3.5	... /14
...	2	T4.0±0.5	T4±1	T4	...	T3.5	... /14
J1333–0215	4	L2.5±0.5	L2±2	L2.5:	L3	L2	7/23
J1339+1523	1	L0.0±1.5	L0±1	L0:
...	2	L1.0±1.0	M9±1	L0:
J1343–1216	1	L9.5±2.0	L5±2	L5.5: pec (blue)	...	L6.5 pec (blue)	... /26
...	3	L6.0±2.5	L5±1 pec	L5.5: pec (blue)	...	L6.5±2 pec (blue)	... /26
...	4	L6.0±2.0	L5±1 pec	L5.5: pec (blue)	...	L6.5±2 pec (blue)	... /26
J1343+1312	2	L0.5±1.0	L0.5±1	L0.5	L1	...	7/ ...
J1344–1614	4	L4.0±2.0	L3±2	L3.5::
J1411+2948	4	L8.0±2.0	L5±2 pec	L6:: pec ³ (blue)	L3.5 ^f	...	5/ ...
J1414+0107	3	L4.5±1.5	L2±2	L3::	L5.5 ^f	L4	5/15
J1415+2635	4	L2.0±1.5	L1±1	L1:
J1422+0827	1	L2.0±2.0	L2.5±1	L2	L2	L2	7/23
...	2	L2.5±1.5	L2±1	L2	L2	L2	7/23
J1452+1114	4	L2.5±0.5	L2±1	L2.5 pec (blue)	L2	L3	8/23
J1453–2744	2	L0.0±2.5	M9.5±1	M9.5:
J1455+2619	4	L2.5±1.0	L2±1 pec	L2: pec ²	L1	...	7/ ...
J1501–1831	4	L0.5±1.0	M9.5±1	L0:

Table 4 – *Continued*

Object	Inst. ^a	Obs. Index	Obs. Visual	Adopted NIR	Previous Opt.	Previous NIR	Ref.
		Type	Type	Type	Type	Type	Opt/NIR
J1510–1147	1	L2.5±2.5	L4±2	L4: pec (blue)
...	4	L4.5±2.5	L4±2 pec	L4: pec (blue)
J1533+2044	3	L0.5±1.5	M9±2	M9.5:
J1537–0800	1	L2.5±2.0	L3±1	L2.5	...	L4 ^j	... /30
...	2	L2.5±1.0	L2±1	L2.5	...	L4 ^j	... /30
J1605+1931	4	L3.0±0.5	L2.5±1	L2.5
J1613–0747	1	L4.0±1.0	L4±2	L4	...	L3.5 ^j	... /30
...	2	L4.0±2.0	L3.5±1	L4	...	L3.5 ^j	... /30
...	3	L4.5±2.0	L4±1	L4	...	L3.5 ^j	... /30
J1615+1340	1	T5.5±1.0	T6±1	T5.5	...	T6	... /16
...	2	T5.5±1.0	T5.5±1	T5.5	...	T6	... /16
J1623–0508	4	L2.0±1.5	L2±1	L2:	...	L1	... /22
J1627+0546	1	L0.5±0.5	L0±1	L0
...	4	L0.5±0.5	M9.5±1	L0
J1627+0836	4	L0.0±1.5	M9±1	M9:
J1628+0517	1	L1.0±1.5	L0±1	L0:
J1629+0335	1	T2.5±1.0	T2±1	T2	...	T2	... /14
...	2	T2.0±1.0	T2±1	T2	...	T2	... /14
J1631–1922	4	M6.0±0.5	M pec	M pec
J1644+2600	4	L1.0±0.5	L0.5±1	L1	L1	...	7/ ...
J1654+3747	4	L1.5±1.0	L1±1	L1:	L2	L0.5	7/23
J1708+2606	4	L4.5±2.0	L4±1 pec	L4: pec (blue)	...	L5.5 ^j	... /30
J1755+3618	3	M8.5±3.0	M6.5±2	M6.5::
J1756+2815	3	L2.0±0.5	L1±2 pec	L1.5: pec (blue)	sdL1	L1 pec (blue)	12/12
J1756+3343	3	L2.0±1.0	L2±1	L2
J1811+2728	4	L2.5±0.5	L2±2 pec	L2.5 pec (blue)
J2117–0611	1	L3.0±1.0	L2±1	L2.5: pec ²

Table 4 – *Continued*

Object	Inst. ^a	Obs. Index	Obs. Visual	Adopted NIR	Previous Opt.	Previous NIR	Ref.
		Type	Type	Type	Type	Type	Opt/NIR
J2132–1452	1	T4.5±1.5	T4±1	T3.5	...	T4	... /11
...	3	T3.5±0.5	T3.5±1	T3.5	...	T4	... /11
J2143–1544	4	M7.5±0.5	M8.5±1	M8:
J2148+2239	3	T0.5±1.0	T1.5±1	T1:
J2150–0412	1	L0.0±0.5	L1.5±2	L1:: pec ²
J2155+2345	4	L2.5±1.0	L2±1	L2:	...	L2	... /12
J2157–0130	1	L6.5±2.0	L7±2	L7::	...	L4.5 ^j	... /30
J2203–0301	4	M9.5±1.5	M8.5±1 pec	M9: pec (blue)	...	L2 ^j	... /30
J2213+1255	4	M9.5±2.0	M8±2	M8.5:
J2215+2110	4	T1.0±0.5	T1.5±1	T1.5	...	T1 pec ^g	... /27
J2233–1331	1	T0.5±2.0	T1.5±2	T1.5:: ^d	...	T2 (blue)	... /30
J2235+0418	1	L3.0±1.0	L3±1	L3
J2238+2304	4	M9.5±2.0	M9±1	M9:	...	L1.5 ^j	... /30
J2239+1617	1	T3.0±0.5	T3±1	T3	...	T3	... /4
J2245+1722	1	L1.5±2.0	L0.5±1 pec	L0.5: pec (red)
J2248–0126	4	L2.0±0.5	L1±1 pec	L1.5: pec (blue)
J2249–1628	4	L6.0±1.5	L5.5±1 pec	L4:+T1:	...	L5: ^h	... /29
J2250+0808	4	L4.0±1.5	L3±2 pec	L3.5:: pec (blue)	...	L1	... /25
J2254+1640	4	L1.0±0.5	L1±1	L1
J2255–0725	1	L0.5±3.0	L1±2	L1:: ^d pec ²
J2257–0140	1	L2.0±1.0	L0.5±2	L1:: pec (blue)
J2303+3150	4	T3.0±0.5	T3±1	T3	...	T2 (blue)	... /30
J2304+0749	2	M9.5±2.5	M8.5±1	M8.5:	...	HPMS	... /17
J2309+1003	2	L0.0±1.5	L0±1	L0:
J2315+2235	3	M6.0±0.5	M6±2	M6::
J2318–1301	1	T5.5±1.5	T4.5±1	T5:	...	T5	... /11
J2322–1407	3	L4.0±1.0	L1.5±2	L2: pec (blue)	...	L1 pec (blue)	... /26

Table 4 – *Continued*

Object	Inst. ^a	Obs. Index	Obs. Visual	Adopted NIR	Previous Opt.	Previous NIR	Ref.
		Type	Type	Type	Type	Type	Opt/NIR
...	4	L2.0±2.0	L1.5±2 pec	L2: pec (blue)	...	L1 pec (blue)	... /26
J2322+1300	1	L4.5±2.0	L5±2	L5::
J2327+1517	4	L4.0±1.0	L3.5±1	L3.5:	L5 ^f	L3.5	5/25
J2330+1006	2	L2.0±1.0	L2±1 pec	L2 pec ¹
J2332–1249	4	L0.5±0.5	L0.5±1 pec	L0.5: pec
J2340–0745	4	T6.5±0.5	T6.5±1	T6.5	...	T7	... /4
J2344+0909	2	L1.0±1.5	L1.5±1	L1.5:	L1	...	19/ ...
J2351+3010	4	L5.0±1.5	L6±1	L5.5:	L5.5	L5 pec (red)	12/12

Note. The adopted NIR types have uncertainties of ± 0.5 subtype, except for those listed with “:” (± 1 subtype) or “::” ($\geq \pm 1.5$ subtypes). pec¹ are possibly red objects; pec² are possibly blue objects; pec³ are possibly binary objects.

^a(1) OMM/SIMON; (2) G-S/GNIRS; (3) G-N/NIRI; (4) IRTF/SpeX.

^bPossible unresolved $\sim L5+T5.5$ binary noted in Luhman & Sheppard (2014).

^cProbable very tight binary (M8+T5) part of a triple system discovered by Burgasser et al. (2012).

^dVery low quality spectrum.

^eResolved binary by Duchêne et al. (2013), combined spectra obtained.

^fOptical classification based on SDSS colors only.

^gPossible unresolved T0+T2 binary from Kellogg et al. (2015). No peculiarities detected in our spectrum.

^hPossible unresolved L+T binary from Best et al. (2015).

ⁱPossible unresolved T2+T7.5 binary from Best et al. (2015).

^jListed as a candidate UCD by Schneider et al. (2016) with NIR classification based on 2MASS and AllWISE photometry only.

References. (1) Artigau et al. (2006), (2) Burgasser et al. (2012), (3) West et al. (2008), (4) Kirkpatrick et al. (2011), (5) Zhang et al. (2009); (6) Burgasser et al. (2010), (7) Schmidt et al. (2010), (8) Zhang et al. (2010), (9) Sheppard & Cushing (2009), (10) Martín et al. (2010), (11) Marocco et al. (2013), (12) Kirkpatrick et al. (2010), (13) Mace et al. (2013), (14) Deacon et al. (2011), (15) Geißler et al. (2011), (16)Looper et al. (2007), (17) Deacon et al. (2009), (18) Reid et al. (2008), (19) Mauron et al. (2014), (20) Lodieu et al. (2014), (21) Luhman (2006), (22) Thompson et al. (2013), (23) Bardalez Gagliuffi et al. (2014), (24) Deacon et al. (2014), (25) Day-Jones et al. (2013), (26) Luhman & Sheppard (2014), (27) Kellogg et al. (2015), (28) Baron et al. (2015), (29) Best et al. (2015), (30) Schneider et al.

(2016).

Table 5 – Properties of observed UCDs

Object	SpT (NIR)	$\mu_\alpha \cos \delta$	μ_δ	Epochs ^a	V_{\tan} (km s ⁻¹)	$d_{\text{phot}}^{\text{b}}$ (pc)	SDSS		MegaCam			2MASS			MKO			WISE	
		(mas yr ⁻¹)	(mas yr ⁻¹)				<i>i</i>	<i>z</i>	<i>i</i>	<i>z</i>	<i>J</i>	<i>H</i>	<i>K_s</i>	<i>J</i>	<i>H</i>	<i>K</i>	<i>W1</i>	<i>W2</i>	
J23152198+2235417	M6::	21.7 ± 29.6	-192.4 ± 31.3	1,2,3,4	219 ± 86	238.3 ± 41.0	19.91 ± 0.03	18.71 ± 0.02	16.74 ± 0.14	16.30 ± 0.18	15.91 ± 0.29	15.71 ± 0.04	15.75 ± 0.13	
J04253602-1900022	M6.5:	-73.0 ± 10.5	-91.6 ± 11.2	1,2,4,6	72 ± 21	129.5 ± 21.1	20.48 ± 0.04	18.80 ± 0.04	16.26 ± 0.07	15.41 ± 0.07	15.21 ± 0.15	14.88 ± 0.03	14.55 ± 0.05	
J17553598+3618117	M6.5::	-25.9 ± 30.2	37.6 ± 35.1	1,2,4	55 ± 65	254.8 ± 42.8	17.10 ± 0.21	16.10 ± 0.17	16.10 ± 0.29	16.32 ± 0.05	16.02 ± 0.10	
J04182001+1121129	M8:	182.2 ± 12.3	-82.4 ± 8.6	1,2,4,6	60 ± 14	63.7 ± 10.3	18.57 ± 0.03	17.17 ± 0.03	14.90 ± 0.04	14.13 ± 0.05	13.78 ± 0.04	13.61 ± 0.03	13.38 ± 0.03	
J21430506-1544394	M8:	183.7 ± 21.4	-91.7 ± 21.3	1,2,4,6	123 ± 38	126.0 ± 20.9	20.56 ± 0.03	18.97 ± 0.04	16.40 ± 0.12	15.61 ± 0.13	15.39 ± 0.18	15.01 ± 0.04	14.86 ± 0.08	
J04144834+1529007	M8.5:	101.2 ± 14.5	51.1 ± 14.1	1,2,3,4,6	52 ± 18	96.5 ± 15.8	20.20 ± 0.03	18.36 ± 0.02	20.14 ± 0.03	18.64 ± 0.03	16.02 ± 0.08	15.56 ± 0.15	14.72 ± 0.12	14.66 ± 0.03	14.40 ± 0.06	
J22130498+1255078	M8.5:	-99.3 ± 26.4	-141.3 ± 25.2	1,2,3,4	112 ± 42	136.9 ± 22.8	20.58 ± 0.04	18.75 ± 0.04	16.42 ± 0.13	15.78 ± 0.15	15.64 ± 0.31	15.27 ± 0.04	15.16 ± 0.09	
J23042585+0749010	M8.5:	249.8 ± 8.2	-16.6 ± 8.6	1,2,3,4,6	55 ± 11	46.0 ± 7.4	18.60 ± 0.01	16.84 ± 0.01	18.70 ± 0.03	17.12 ± 0.03	14.54 ± 0.03	13.76 ± 0.03	13.33 ± 0.03	13.06 ± 0.02	12.79 ± 0.03	
J09363433+0528243	M9:	15.6 ± 24.6	-116.0 ± 23.1	1,2,3,4,5	62 ± 28	111.8 ± 18.4	19.86 ± 0.05	18.15 ± 0.05	19.83 ± 0.05	...	16.50 ± 0.13	15.77 ± 0.12	15.24 ± 0.17	16.43 ± 0.03	16.02 ± 0.06	15.35 ± 0.04	15.01 ± 0.04	14.84 ± 0.07	
J16275003+0836036	M9:	10.7 ± 12.6	-300.4 ± 8.2	1,2,3,4	71 ± 15	50.0 ± 8.1	19.22 ± 0.02	17.31 ± 0.01	18.88 ± 0.03	17.46 ± 0.03	14.94 ± 0.04	14.12 ± 0.04	13.72 ± 0.05	13.45 ± 0.03	13.09 ± 0.03	
J22382764+2304114	M9:	-209.1 ± 6.5	-253.7 ± 8.3	1,2,3,4,5,6	91 ± 18	58.2 ± 9.4	19.47 ± 0.02	17.68 ± 0.02	19.49 ± 0.03	17.93 ± 0.03	15.38 ± 0.05	14.49 ± 0.05	13.97 ± 0.06	13.70 ± 0.03	13.42 ± 0.03	
J10355478+3655420	M9.5:	-61.7 ± 20.0	-84.6 ± 21.5	2,3,4	28 ± 13	57.3 ± 10.7 ^c	19.09 ± 0.02	18.19 ± 0.03	15.21 ± 0.06	14.51 ± 0.06	13.99 ± 0.05	
J11021199+1629393	M9.5:	179.0 ± 27.4	-109.1 ± 25.0	1,2,3,4	101 ± 35	102.1 ± 16.8	20.57 ± 0.05	18.71 ± 0.04	16.52 ± 0.14	15.57 ± 0.15	15.23 ± 0.14	14.98 ± 0.04	14.76 ± 0.07	
J13083106+0818522	M9.5:	-255.1 ± 10.1	50.1 ± 8.1	1,2,3,4	64 ± 13	51.7 ± 8.4	19.60 ± 0.02	17.82 ± 0.02	15.13 ± 0.05	14.35 ± 0.06	13.85 ± 0.07	13.51 ± 0.03	13.28 ± 0.03	
J14534687-2744275	M9.5:	-164.6 ± 9.5	-63.1 ± 9.4	1,2,6	65 ± 16	77.8 ± 12.7	20.32 ± 0.03	18.76 ± 0.03	16.05 ± 0.07	15.18 ± 0.09	14.68 ± 0.09	14.42 ± 0.03	14.17 ± 0.05	
J15335010+2044470	M9.5:	-94.2 ± 23.7	-65.5 ± 23.9	1,2,3,4	77 ± 35	141.0 ± 23.7	21.32 ± 0.09	19.45 ± 0.08	17.06 ± 0.17	16.30 ± 0.19	15.58 ± 0.21	15.83 ± 0.05	15.46 ± 0.10	
J03314657+1944246	L0::	32.3 ± 8.9	-48.5 ± 9.1	1,2	27 ± 10	97.8 ± 16.1	16.03 ± 0.07	15.50 ± 0.10	14.94 ± 0.11	14.88 ± 0.04	14.78 ± 0.07	
J09475068+0617139	L0:	-236.1 ± 9.2	-157.2 ± 8.9	1,2,3,4	50 ± 10	37.0 ± 6.0	18.67 ± 0.01	16.82 ± 0.01	14.49 ± 0.03	13.67 ± 0.03	13.23 ± 0.03	12.90 ± 0.02	12.67 ± 0.03	
J10135847-1946546	L0:	-201.4 ± 15.5	-78.8 ± 14.0	1,2,4	103 ± 27	100.5 ± 16.5	16.38 ± 0.09	15.80 ± 0.13	15.10 ± 0.13	15.05 ± 0.04	14.84 ± 0.07	
J11411438+1941149	L0:	-63.2 ± 11.3	-210.1 ± 11.4	1,2,3,4	54 ± 13	52.0 ± 8.4	19.46 ± 0.02	17.66 ± 0.02	15.28 ± 0.05	14.45 ± 0.05	14.08 ± 0.06	13.66 ± 0.03	13.41 ± 0.03	
J15014711-1831272	L0:	-122.7 ± 7.4	3.2 ± 8.7	1,2,4,6	44 ± 11	75.9 ± 12.4	20.46 ± 0.03	18.86 ± 0.03	16.02 ± 0.10	15.15 ± 0.10	14.76 ± 0.11	14.50 ± 0.03	14.23 ± 0.05	
J16270845+0546304	L0:	-93.2 ± 27.2	-81.0 ± 25.6	1,2,4	64 ± 30	109.2 ± 18.1	20.17 ± 0.05	...	16.66 ± 0.14	15.71 ± 0.12	15.49 ± 0.23	15.00 ± 0.03	15.02 ± 0.08	
J16280690+0517027	L0:	-22.1 ± 9.0	-119.0 ± 9.5	1,2,3,4	38 ± 10	66.7 ± 10.8	19.93 ± 0.03	18.06 ± 0.02	15.81 ± 0.07	15.09 ± 0.08	14.63 ± 0.11	14.21 ± 0.03	13.95 ± 0.04	
J23094559+1003122	L0:	133.9 ± 22.8	-12.7 ± 9.2	1,2,3,4,6	29 ± 10	45.3 ± 7.3	19.17 ± 0.02	17.47 ± 0.02	19.10 ± 0.30	17.57 ± 0.03	14.93 ± 0.05	14.11 ± 0.06	13.71 ± 0.05	13.42 ± 0.03	13.11 ± 0.03	
J00081285+0806441	L0.5::	9.5 ± 25.7	-265.6 ± 22.7	1,2,3,4	108 ± 32	85.8 ± 14.1	20.84 ± 0.08	19.02 ± 0.05	20.24 ± 0.05	...	16.59 ± 0.16	15.54 ± 0.13	15.16 ± 0.17	14.96 ± 0.04	14.61 ± 0.06	
J10035482-1441534	L0.5:	-196.6 ± 9.4	59.2 ± 10.4	1,2,4	46 ± 11	47.4 ± 7.7	18.86 ± 0.05	...	15.15 ± 0.05	14.31 ± 0.05	13.93 ± 0.07	13.56 ± 0.03	13.32 ± 0.03	
J13183258-0632057	L0.5:	-85.2 ± 11.6	-145.8 ± 11.5	1,2,4	56 ± 15	70.4 ± 11.4	16.05 ± 0.10	15.30 ± 0.11	14.74 ± 0.13	14.42 ± 0.03	14.18 ± 0.04	
J13432911+1312267	L0.5:	-268.9 ± 10.3	-40.3 ± 10.4	1,2,3,4,5,6	85 ± 18	65.7 ± 10.7	20.25 ± 0.03	18.51 ± 0.03	20.28 ± 0.03	18.76 ± 0.03	16.02 ± 0.08	15.44 ± 0.12	14.89 ± 0.12	...	15.35 ± 0.06	14.66 ± 0.04	14.29 ± 0.03	14.03 ± 0.04	
J00132128+0841006	L1:	167.0 ± 24.5	-90.9 ± 22.7	1,2,3,4	74 ± 25	82.3 ± 13.5	20.54 ± 0.05	18.79 ± 0.04	19.92 ± 0.05	...	16.52 ± 0.14	15.71 ± 0.14	15.21 ± 0.15	14.90 ± 0.04	14.63 ± 0.07	
J04223054+0723448	L1:	195.2 ± 8.6	-280.7 ± 8.5	1,2,3,4,6	93 ± 18	57.5 ± 9.3	20.09 ± 0.03	18.22 ± 0.02	20.07 ± 0.04	18.52 ± 0.03	15.77 ± 0.07	14.92 ± 0.07	14.45 ± 0.06	14.09 ± 0.03	13.85 ± 0.04	
J08580549+2214582	L1:	-50.2 ± 15.1	-66.5 ± 6.8	1,2,3	18 ± 6	45.0 ± 7.3	19.55 ± 0.02	17.67 ± 0.02	15.23 ± 0.05	14.42 ± 0.05	13.84 ± 0.05	13.57 ± 0.03	13.32 ± 0.03	
J10091160+1559289	L1:	-200.8 ± 24.3	-63.5 ± 25.6	1,2,3,4	84 ± 28	84.6 ± 13.9	21.12 ± 0.08	19.15 ± 0.05	20.33 ± 0.07	...	16.89 ± 0.20	15.58 ± 0.15	15.45 ± 0.17	15.08 ± 0.04	14.69 ± 0.06	
J12173549+0708334	L1	45.6 ± 20.0	-156.7 ± 18.0	1,2,3,4	62 ± 20	79.7 ± 13.0	20.82 ± 0.04	19.11 ± 0.04	20.78 ± 0.04	19.21 ± 0.04	16.37 ± 0.13	15.76 ± 0.16	15.02 ± 0.15	14.77 ± 0.03	14.56 ± 0.06	
J16443963+2600128	L1	53.6 ± 8.5	153.8 ± 9.0	1,2,3,4	41 ± 10	53.2 ± 8.6	19.86 ± 0.03	17.98 ± 0.02	19.83 ± 0.03	18.28 ± 0.03	15.47 ± 0.05	14.71 ± 0.06	14.21 ± 0.09	13.94 ± 0.03	13.68 ± 0.03	
J16545081+3747141	L1	-114.8 ± 4.3	199.8 ± 5.2	1,2,3	42 ± 8	38.2 ± 6.2	19.31 ± 0.02	17.46 ± 0.01	15.01 ± 0.04	14.18 ± 0.04	13.66 ± 0.04	13.20 ± 0.02	12.96 ± 0.03	
J22543828+1640488	L1:	-84.2 ± 7.5	-229.7 ± 8.1	1,2,3,4,6	67 ± 14	58.0 ± 9.4	19.85 ± 0.03	18.06 ± 0.03	20.11 ± 0.04	18.54 ± 0.03	15.88 ± 0.06	14.83 ± 0.05	14.25 ± 0.06	14.14 ± 0.03	13.87 ± 0.04	
J01512665+3824122	L1.5	166.2 ± 7.1	-70.1 ± 9.7	1,2,4,6	40 ± 9	48.2 ± 7.8	19.67 ± 0.03	18.10 ± 0.03	15.40 ± 0.05	14.62 ± 0.07	13.95 ± 0.05	13.71 ± 0.02	13.48 ± 0.03	

Table 5 – *Continued*

Object	SpT (NIR)	$\mu_\alpha \cos \delta$	μ_δ	Epochs ^a	V_{\tan} (km s ⁻¹)	$d_{\text{phot}}^{\text{b}}$ (pc)	SDSS		MegaCam		2MASS			MKO			WISE		
		(mas yr ⁻¹)	(mas yr ⁻¹)				<i>i</i>	<i>z</i>	<i>i</i>	<i>z</i>	<i>J</i>	<i>H</i>	<i>K_s</i>	<i>J</i>	<i>H</i>	<i>K</i>	<i>W1</i>	<i>W2</i>	
J09455513-0757441	L1.5:	-46.6 ± 15.0	-128.0 ± 9.9	1,2,4	38 ± 11	58.3 ± 9.5	16.17 ± 0.09	15.37 ± 0.09	14.58 ± 0.09	14.24 ± 0.03	13.99 ± 0.04	
J11272648+1234310	L1.5:	-253.0 ± 15.9	186.5 ± 11.3	1,2,3,4	99 ± 22	66.7 ± 10.9	20.44 ± 0.05	18.49 ± 0.04	16.10 ± 0.08	15.36 ± 0.10	14.82 ± 0.08	14.58 ± 0.03	14.28 ± 0.05	
J11473434+2153590	L1.5:	-280.2 ± 20.1	-37.0 ± 19.2	1,2,3,4	104 ± 27	77.6 ± 12.7	21.15 ± 0.07	19.37 ± 0.06	16.74 ± 0.14	15.72 ± 0.14	15.29 ± 0.14	14.92 ± 0.04	14.61 ± 0.06	
J14154242+2635040	L1.5:	-286.7 ± 13.1	-28.3 ± 13.1	1,2,3	85 ± 19	61.9 ± 10.1	20.74 ± 0.05	18.94 ± 0.05	16.37 ± 0.12	15.62 ± 0.15	14.86 ± 0.11	14.42 ± 0.03	14.12 ± 0.04	
J23444256+0909020	L1.5:	314.8 ± 14.0	-139.8 ± 10.0	1,2,3,4,6	56 ± 12	34.5 ± 5.6	19.22 ± 0.02	17.38 ± 0.02	19.26 ± 0.03	17.76 ± 0.03	14.90 ± 0.05	13.96 ± 0.05	13.44 ± 0.04	13.09 ± 0.02	12.85 ± 0.03	
J02110979-1427349	L2	-18.4 ± 9.1	-203.0 ± 8.1	1,2,4,6	39 ± 9	40.4 ± 6.5	19.82 ± 0.03	...	15.44 ± 0.05	14.65 ± 0.07	14.05 ± 0.05	13.62 ± 0.03	13.30 ± 0.03	
J04173264-1454388	L2	-147.4 ± 7.1	-96.2 ± 7.9	1,2,4,6	40 ± 9	48.2 ± 7.8	20.45 ± 0.03	18.98 ± 0.03	15.88 ± 0.07	15.05 ± 0.08	14.55 ± 0.10	13.91 ± 0.03	13.68 ± 0.03	
J09155650+0514212	L2:	-74.3 ± 22.5	-38.6 ± 10.4	1,2,3,4	21 ± 10	52.6 ± 8.5	20.59 ± 0.04	18.73 ± 0.04	19.98 ± 0.05	...	15.90 ± 0.08	15.31 ± 0.09	14.43 ± 0.08	14.12 ± 0.03	13.87 ± 0.04	
J09404793+2946534	L2:	-146.8 ± 12.2	-60.5 ± 8.3	1,2,3,4	30 ± 8	39.5 ± 6.4	19.74 ± 0.02	17.83 ± 0.02	15.29 ± 0.07	14.34 ± 0.07	13.92 ± 0.05	13.51 ± 0.02	13.25 ± 0.03	
J10315064+3349595	L2:	-142.7 ± 7.5	51.1 ± 9.0	1,2,3	33 ± 8	45.8 ± 7.4	20.36 ± 0.04	18.55 ± 0.03	16.09 ± 0.09	15.01 ± 0.07	14.33 ± 0.06	13.89 ± 0.03	13.57 ± 0.04	
J10391406-1904471	L2:	123.6 ± 9.8	107.0 ± 9.5	1,2,4	44 ± 11	57.4 ± 9.3	16.22 ± 0.10	15.33 ± 0.08	14.61 ± 0.12	14.31 ± 0.03	14.06 ± 0.04	
J11384458+0748213	L2::	-192.2 ± 12.7	-182.5 ± 8.5	1,2,3	65 ± 14	51.4 ± 8.3	19.70 ± 0.02	17.96 ± 0.02	15.54 ± 0.07	14.75 ± 0.04	14.26 ± 0.08	14.09 ± 0.03	13.82 ± 0.04	
J14225717+0827539	L2	-170.6 ± 8.6	-571.3 ± 9.5	1,2,3,4,5,6	98 ± 18	34.7 ± 5.6	19.36 ± 0.02	17.57 ± 0.02	19.42 ± 0.03	17.92 ± 0.03	15.10 ± 0.05	14.22 ± 0.03	13.65 ± 0.05	15.05 ± 0.07	14.33 ± 0.03	13.63 ± 0.03	13.23 ± 0.02	12.97 ± 0.03	
J16235981-0508066	L2:	-164.0 ± 7.5	-441.4 ± 7.4	1,2,3,4,6	76 ± 14	34.3 ± 5.5	19.33 ± 0.02	17.43 ± 0.02	19.32 ± 0.03	17.73 ± 0.03	14.94 ± 0.04	14.08 ± 0.03	13.56 ± 0.04	13.26 ± 0.03	12.94 ± 0.03	
J17563950+3343002	L2	-6.2 ± 11.5	65.5 ± 13.0	1,2,4	20 ± 9	64.1 ± 10.4	16.48 ± 0.13	15.64 ± 0.14	14.75 ± 0.09	14.52 ± 0.03	14.30 ± 0.04	
J21555848+2345307	L2:	88.5 ± 9.1	-45.6 ± 9.9	1,2,3,4,5,6	21 ± 6	44.7 ± 7.2	20.43 ± 0.05	18.69 ± 0.04	20.47 ± 0.03	18.88 ± 0.03	15.99 ± 0.08	14.95 ± 0.08	14.27 ± 0.07	13.82 ± 0.03	13.52 ± 0.03	
J12113013-0406096	L2.5:	-78.2 ± 10.5	-221.0 ± 13.0	1,2,3,4,5	40 ± 9	35.8 ± 5.8	20.12 ± 0.03	18.29 ± 0.03	20.26 ± 0.04	18.67 ± 0.03	15.53 ± 0.06	14.55 ± 0.04	14.02 ± 0.08	15.58 ± 0.04	14.61 ± 0.07	13.99 ± 0.02	13.47 ± 0.03	13.14 ± 0.03	
J13174922+0448149	L2.5:	-136.3 ± 9.0	-58.6 ± 9.1	1,2,3,4	32 ± 8	45.7 ± 7.4	20.71 ± 0.06	18.72 ± 0.04	20.84 ± 0.04	19.24 ± 0.03	16.22 ± 0.10	15.14 ± 0.08	14.46 ± 0.09	13.96 ± 0.03	13.67 ± 0.03	
J13334540-0215599	L2.5:	-279.5 ± 11.8	-113.6 ± 7.4	1,2,3,4	54 ± 11	38.0 ± 6.2	19.56 ± 0.03	17.70 ± 0.02	15.38 ± 0.04	14.37 ± 0.04	13.85 ± 0.05	13.54 ± 0.03	13.27 ± 0.03	
J15371974-0800344	L2.5:	-7.6 ± 11.6	-304.2 ± 10.4	1,2,5,6	80 ± 17	55.2 ± 9.0	20.87 ± 0.04	19.37 ± 0.04	16.44 ± 0.14	15.36 ± 0.12	14.75 ± 0.12	16.06 ± 0.14	15.37 ± 0.11	14.33 ± 0.03	14.08 ± 0.05
J16055741+1931115	L2.5:	52.1 ± 12.0	-252.1 ± 12.5	1,2,3,4,5,6	48 ± 11	39.3 ± 6.4	20.13 ± 0.04	18.30 ± 0.04	20.14 ± 0.03	18.61 ± 0.03	15.58 ± 0.05	14.72 ± 0.07	14.08 ± 0.05	13.65 ± 0.03	13.34 ± 0.03	
J11470302-1032547	L3	128.0 ± 18.1	-174.2 ± 16.5	1,2,4,5	55 ± 15	53.7 ± 8.8	20.65 ± 0.05	...	16.49 ± 0.12	15.57 ± 0.11	14.84 ± 0.13	16.61 ± 0.04	15.51 ± 0.03	14.90 ± 0.04	14.40 ± 0.03	14.12 ± 0.05	
J14140586+0107102	L3::	-357.1 ± 26.6	-165.4 ± 20.5	1,2,3,4	117 ± 29	62.5 ± 10.2	21.76 ± 0.14	19.63 ± 0.09	16.74 ± 0.20	15.74 ± 0.19	15.25 ± 0.20	14.66 ± 0.03	14.45 ± 0.05	
J22355244+0418563	L3	-295.4 ± 8.8	-167.4 ± 8.4	1,2,3,4	51 ± 10	31.8 ± 5.1	20.31 ± 0.05	18.14 ± 0.03	15.37 ± 0.04	14.38 ± 0.03	13.79 ± 0.04	13.24 ± 0.03	12.98 ± 0.03	
J13441371-1614022	L3.5::	78.9 ± 17.5	-152.0 ± 16.5	1,2,4	58 ± 18	71.5 ± 11.8	16.65 ± 0.14	15.82 ± 0.15	16.16	15.08 ± 0.04	14.84 ± 0.07	
J23271573+1517310	L3.5:	-66.1 ± 10.5	-162.3 ± 10.7	1,2,3,4,6	40 ± 10	48.5 ± 7.9	20.94 ± 0.08	19.08 ± 0.06	21.04 ± 0.05	19.36 ± 0.04	16.29 ± 0.11	15.35 ± 0.09	14.77 ± 0.13	14.17 ± 0.03	14.00 ± 0.04	
J01550354+0950003	L4	342.7 ± 11.7	-91.9 ± 12.6	1,2,3,4,6	34 ± 7	20.4 ± 3.3	19.60 ± 0.03	17.66 ± 0.02	19.60 ± 0.03	17.93 ± 0.03	14.83 ± 0.04	13.76 ± 0.03	13.14 ± 0.04	12.56 ± 0.02	12.21 ± 0.02	
J16133450-0747057	L4	-209.0 ± 11.4	-344.7 ± 10.7	1,2,4,5,6	104 ± 21	54.3 ± 8.9	21.48 ± 0.06	19.69 ± 0.04	16.68 ± 0.14	15.51 ± 0.11	14.96 ± 0.13	16.93 ± 0.07	15.93 ± 0.05	15.17 ± 0.03	14.55 ± 0.03	14.34 ± 0.05	
J11220855+0343193	L4.5:	-327.1 ± 16.8	59.0 ± 19.8	1,2,3,4	44 ± 11	27.9 ± 4.5	20.41 ± 0.05	18.50 ± 0.04	15.65 ± 0.07	14.71 ± 0.06	13.95 ± 0.06	13.27 ± 0.03	12.99 ± 0.03	
J02512861-0818254	L5:	112.1 ± 12.7	-121.5 ± 10.3	1,2,3,4	43 ± 11	55.2 ± 9.0	21.09 ± 0.08	19.16 ± 0.06	16.57 ± 0.12	15.47 ± 0.09	14.94 ± 0.12	14.66 ± 0.03	14.56 ± 0.05	
J23225888+1300322	L5::	335.6 ± 10.7	-453.1 ± 10.2	1,2,3,4	102 ± 19	38.0 ± 6.2	20.53 ± 0.10	18.62 ± 0.07	16.35 ± 0.12	15.30 ± 0.10	14.56 ± 0.12	14.20 ± 0.03	13.75 ± 0.04	
J23512200+3010540	L5.5:	258.1 ± 8.1	10.7 ± 7.8	1,2,3,4,6	30 ± 6	24.1 ± 3.9	20.89 ± 0.06	18.56 ± 0.03	20.80 ± 0.04	18.92 ± 0.03	15.85 ± 0.10	14.57 ± 0.07	14.02 ± 0.06	13.23 ± 0.02	12.85 ± 0.03	
J09514402-1343474	L6::	-159.9 ± 15.9	29.7 ± 14.5	1,2,4	35 ± 10	44.9 ± 7.3	16.16 ± 0.10	15.51 ± 0.12	14.55 ± 0.11	14.56 ± 0.03	14.29 ± 0.05	
J04005763-1322024	L7::	-137.1 ± 11.7	-169.7 ± 10.4	1,2,4,5,6	31 ± 7	30.4 ± 4.9	21.58 ± 0.05	19.58 ± 0.04	16.58 ± 0.13	15.50 ± 0.12	14.54 ± 0.10	16.78 ± 0.07	15.55 ± 0.06	14.74 ± 0.03	13.94 ± 0.03	13.61 ± 0.03	
J21570693-0130348	L7::	279.2 ± 13.9	-30.3 ± 12.3	1,2,3,4	46 ± 10	34.4 ± 5.6	21.21 ± 0.08	19.49 ± 0.07	16.39 ± 0.11	15.54 ± 0.13	14.75 ± 0.11	14.18 ± 0.03	13.88 ± 0.04	
J00492826+0440575	L8.5:	314.5 ± 14.1	227.8 ± 9.3	1,2,3,4,6	37 ± 8	20.1 ± 3.3	21.61 ± 0.13	18.52 ± 0.04	18.87 ± 0.03	15.85 ± 0.07	14.67 ± 0.07	14.17 ± 0.07	13.43 ± 0.03	12.96 ± 0.03	
J01020186+0355405	L9:	360.5 ± 18.7	88.3 ± 16.2	1,2,3,4,6	47 ± 11	26.6 ± 4.3	22.70 ± 0.35	19.37 ± 0.07	22.67 ± 0.07	19.88 ± 0.04	16.74 ± 0.13	15.66 ± 0.11	15.08 ± 0.12	14.22 ± 0.03	13.65 ± 0.04	
J01352531+0205232	L9:	103.2 ± 16.9	-491.7 ± 15.9	1,2,3,4	70 ± 15	29.6 ± 4.8	22.10 ± 0.13	19.20 ± 0.05	16.62 ± 0.13	15.48 ± 0.10	15.12 ± 0.12	14.28 ± 0.03	13.88 ± 0.04	

Table 5 – *Continued*

Table 5 – *Continued*

Object	SpT (NIR)	$\mu_\alpha \cos \delta$	μ_δ	Epochs ^a	V_{\tan} (km s ⁻¹)	$d_{\text{phot}}^{\text{b}}$ (pc)	SDSS		MegaCam			2MASS			MKO			WISE	
		(mas yr ⁻¹)	(mas yr ⁻¹)				<i>i</i>	<i>z</i>	<i>i</i>	<i>z</i>	<i>J</i>	<i>H</i>	<i>K_s</i>	<i>J</i>	<i>H</i>	<i>K</i>	<i>W1</i>	<i>W2</i>	
J04210053–1950245	M9: pec (blue)	76.3 ± 8.3	–162.4 ± 8.8	1,2,4	74 ± 17	86.8 ± 14.1	15.86 ± 0.06	15.35 ± 0.09	14.86 ± 0.12	14.54 ± 0.03	14.29 ± 0.04	
J04302219+1035438	M9:: pec (blue)	–96.7 ± 24.2	–206.5 ± 23.9	1,2,4,5,6	185 ± 60	170.8 ± 30.3	20.79 ± 0.05	19.24 ± 0.05	16.88 ± 0.17	15.99 ± 0.18	15.60 ± 0.16	17.31 ± 0.08	16.75 ± 0.12	16.37 ± 0.07	15.77 ± 0.05	15.76 ± 0.16	
J22030176–0301107	M9: pec (blue)	–162.6 ± 19.9	–149.7 ± 18.0	1,2,3,6	95 ± 27	90.5 ± 14.8	20.13 ± 0.04	18.36 ± 0.03	20.16 ± 0.03	18.59 ± 0.03	16.11 ± 0.10	15.33 ± 0.11	15.15 ± 0.13	14.67 ± 0.03	14.38 ± 0.06	
J09465378+0922432	M9.5:: pec (blue)	–96.3 ± 23.1	–9.0 ± 20.7	1,2,3,4,5	58 ± 28	125.7 ± 21.1	20.91 ± 0.05	19.03 ± 0.04	16.86 ± 0.21	15.83 ± 0.16	15.36	16.89 ± 0.09	16.45 ± 0.06	16.00 ± 0.07	15.39 ± 0.04	15.21 ± 0.10	
J13084263+0432441	M9.5:: pec (blue)	–23.4 ± 21.6	–184.8 ± 19.8	1,2,3,4	90 ± 29	101.7 ± 16.6	20.41 ± 0.04	18.52 ± 0.02	20.38 ± 0.06	18.85 ± 0.03	16.07 ± 0.10	15.95 ± 0.17	15.58 ± 0.25	15.05 ± 0.03	14.75 ± 0.06	
J04292691+0607368	L0: pec (blue)	117.1 ± 10.8	–246.0 ± 9.9	1,2,4,5,6	103 ± 22	79.5 ± 13.0	20.11 ± 0.03	18.46 ± 0.03	15.92 ± 0.06	15.47 ± 0.10	15.03 ± 0.09	15.92 ± 0.02	15.51 ± 0.06	14.93 ± 0.02	14.63 ± 0.03	14.33 ± 0.05	
J10144907+1900041	L0.5:: pec (blue)	4.6 ± 8.3	–143.0 ± 8.3	1,2,3,4	47 ± 12	69.4 ± 11.3	19.23 ± 0.03	17.52 ± 0.02	15.90 ± 0.06	15.16 ± 0.06	14.98 ± 0.10	14.48 ± 0.03	14.15 ± 0.05	
J01481626+3712421	L1: pec (blue)	121.2 ± 7.9	–43.0 ± 8.2	1,2,4,6	43 ± 11	70.1 ± 11.4	20.37 ± 0.04	18.77 ± 0.04	16.03 ± 0.08	15.25 ± 0.10	15.00 ± 0.11	14.60 ± 0.03	14.28 ± 0.05	
J03570493+1529270	L1:: pec (blue)	103.2 ± 7.0	–288.4 ± 7.3	1,2,3,4,6	64 ± 13	44.2 ± 7.2	19.73 ± 0.02	17.76 ± 0.02	19.84 ± 0.32	18.74 ± 1.20	15.10 ± 0.05	14.34 ± 0.05	13.99 ± 0.07	13.54 ± 0.03	13.28 ± 0.03	
J22572115–0140061	L1:: pec (blue)	518.2 ± 25.5	–219.0 ± 20.2	1,2,3,4	242 ± 54	90.7 ± 15.0	20.12 ± 0.03	18.36 ± 0.02	16.23 ± 0.11	15.60 ± 0.15	15.24 ± 0.17	15.08 ± 0.04	14.84 ± 0.08	
J10580444+1339474	L1.5: pec (blue)	–316.8 ± 20.6	–90.1 ± 20.8	1,2,3,4,5	149 ± 38	95.5 ± 15.9	20.90 ± 0.07	18.84 ± 0.04	16.43 ± 0.11	15.84 ± 0.14	15.89 ± 0.23	16.51 ± 0.05	16.11 ± 0.04	15.42 ± 0.04	15.21 ± 0.04	15.06 ± 0.09	
J17561080+2815238	L1.5: pec (blue)	–620.6 ± 7.9	–412.7 ± 7.8	1,2,4	135 ± 24	38.2 ± 6.2	14.71 ± 0.03	14.14 ± 0.04	13.81 ± 0.04	13.38 ± 0.02	13.07 ± 0.03	
J22484809–0126570	L1.5: pec (blue)	228.2 ± 26.3	150.9 ± 23.7	1,2,3,4,6	106 ± 31	81.6 ± 13.4	20.82 ± 0.06	18.90 ± 0.04	20.59 ± 0.05	19.07 ± 0.04	16.54 ± 0.12	15.62 ± 0.12	15.67 ± 0.24	14.97 ± 0.04	14.72 ± 0.07	
J10520466+1722433	L2: pec (blue)	185.2 ± 20.1	–309.0 ± 18.5	1,2,3,4	124 ± 30	72.6 ± 11.9	21.25 ± 0.10	19.19 ± 0.06	16.71 ± 0.11	16.04 ± 0.14	15.53 ± 0.16	14.94 ± 0.04	14.57 ± 0.06	
J23221914–1407238	L2: pec (blue)	403.2 ± 10.0	–235.6 ± 10.2	1,2,4,6	146 ± 28	66.2 ± 10.8	20.26 ± 0.11	18.56 ± 0.03	15.99 ± 0.07	15.52 ± 0.11	15.10 ± 0.14	14.69 ± 0.03	14.37 ± 0.05	
J10414238–0429259	L2.5: pec (blue)	–246.3 ± 18.6	–292.4 ± 17.4	1,2,4,5	113 ± 26	62.2 ± 10.1	16.41 ± 0.10	15.65 ± 0.10	15.08 ± 0.15	16.58 ± 0.07	15.97 ± 0.12	15.25 ± 0.12	14.71 ± 0.03	14.34 ± 0.05	
J11303803+2341480	L2.5: pec (blue)	–463.1 ± 23.1	–70.2 ± 19.4	1,2,3,4	175 ± 40	78.7 ± 13.0	21.27 ± 0.08	19.13 ± 0.04	16.65 ± 0.13	15.87 ± 0.12	15.74 ± 0.18	14.98 ± 0.03	14.85 ± 0.07	
J14520183+1114590	L2.5 pec (blue)	234.9 ± 16.7	–302.3 ± 15.5	1,2,3,4	81 ± 18	44.7 ± 7.2	20.15 ± 0.03	18.18 ± 0.02	15.52 ± 0.07	14.85 ± 0.07	14.34 ± 0.10	13.92 ± 0.03	13.62 ± 0.03	
J10044030–1318186	L3: pec (blue)	–117.8 ± 16.9	–171.0 ± 25.7	1,2,4	25 ± 8	25.5 ± 4.1	14.69 ± 0.04	13.88 ± 0.04	13.36 ± 0.04	12.78 ± 0.02	12.50 ± 0.02	
J18115567+2728407	L3: pec (blue)	–120.6 ± 10.9	7.1 ± 10.8	1,2,4,5,6	30 ± 9	53.2 ± 8.6	20.64 ± 0.04	19.10 ± 0.05	16.19 ± 0.10	15.33 ± 0.10	14.88 ± 0.10	14.45 ± 0.03	14.10 ± 0.04	
J10360307+0306160	L3.5: pec (blue)	–421.9 ± 15.3	–15.4 ± 15.9	1,2,3,4,5	99 ± 21	49.5 ± 8.0	20.63 ± 0.06	18.71 ± 0.04	15.98 ± 0.10	15.48 ± 0.11	14.82 ± 0.13	16.26 ± 0.04	15.41 ± 0.07	14.86 ± 0.05	14.40 ± 0.03	14.04 ± 0.04	
J22501628+0808245	L3.5:: pec (blue)	212.5 ± 11.2	–257.6 ± 9.4	1,2,3,4,6	67 ± 14	42.5 ± 6.9	20.24 ± 0.04	18.14 ± 0.03	20.28 ± 0.04	18.42 ± 0.03	15.59 ± 0.06	14.98 ± 0.07	14.56 ± 0.08	14.04 ± 0.03	13.71 ± 0.04	
J12184982–1332525	L4: pec (blue)	–274.6 ± 22.4	68.7 ± 15.6	1,2,4,6	82 ± 21	61.2 ± 10.0	21.80 ± 0.09	19.35 ± 0.05	16.32 ± 0.11	15.92 ± 0.16	15.24 ± 0.16	14.91 ± 0.03	14.60 ± 0.06	
J15102256–1147125	L4: pec (blue)	–220.7 ± 8.9	54.2 ± 7.3	1,2,3,4,6	42 ± 9	38.8 ± 6.3	20.52 ± 0.05	18.48 ± 0.03	20.49 ± 0.03	18.77 ± 0.03	15.66 ± 0.06	14.88 ± 0.05	14.26 ± 0.07	13.77 ± 0.03	13.61 ± 0.04	
J17084651+2606444	L4: pec (blue)	–61.3 ± 19.6	–319.4 ± 19.3	1,2,3,4	82 ± 20	53.1 ± 8.6	21.20 ± 0.07	19.08 ± 0.05	16.37 ± 0.11	15.50 ± 0.10	15.32 ± 0.15	14.54 ± 0.03	14.29 ± 0.04	
J09213274–1534290	L5:: pec ³ (blue)	–199.3 ± 10.3	–64.8 ± 9.0	1,2,4,5	41 ± 9	41.3 ± 6.7	16.40 ± 0.11	15.30 ± 0.09	14.77 ± 0.10	16.40 ± 0.05	15.43 ± 0.03	15.03 ± 0.05	14.24 ± 0.03	13.93 ± 0.04	
J11501322+0520124	L5.5: pec (blue)	–259.4 ± 16.1	–228.8 ± 26.6	1,2,3,4	58 ± 15	35.3 ± 5.7	21.32 ± 0.07	18.92 ± 0.04	16.25 ± 0.14	15.46 ± 0.14	15.02 ± 0.17	14.03 ± 0.03	13.68 ± 0.04	
J13431074–1216256	L5.5: pec (blue)	–381.3 ± 13.2	–265.5 ± 12.9	1,2,4,6	102 ± 21	46.1 ± 7.5	21.08 ± 0.04	19.14 ± 0.04	16.27 ± 0.10	15.46 ± 0.09	15.23 ± 0.18	14.55 ± 0.03	14.26 ± 0.04	
J14111847+2948515	L6:: pec ³ (blue)	36.3 ± 18.7	–274.1 ± 16.9	1,2,3,4	52 ± 13	39.5 ± 6.4	21.01 ± 0.07	18.71 ± 0.04	16.20 ± 0.09	15.43 ± 0.11	15.09 ± 0.11	14.46 ± 0.03	14.01 ± 0.04	
J09564583–1910227	L6.5: pec (blue)	–100.7 ± 7.4	32.9 ± 6.9	1,2,4	12 ± 3	23.0 ± 3.7	15.21 ± 0.05	14.32 ± 0.04	13.85 ± 0.05	13.33 ± 0.02	12.92 ± 0.03	
(g) Binary UCDs																			
J00064916–0852457	M9:+T6: pec	–62.5 ± 10.8	–320.2 ± 9.3	1,2,3,4	56 ± 12	36.4 ± 5.9	18.23 ± 0.01	16.40 ± 0.01	18.21 ± 0.10	...	14.14 ± 0.03	13.55 ± 0.03	13.13 ± 0.04	12.76 ± 0.02	12.35 ± 0.03	
J00135882–1816462	L3:+T4:	–9.1 ± 18.2	–182.3 ± 18.3	1,2,4	51 ± 15	58.6 ± 9.5	19.81 ± 0.05	16.54 ± 0.14	15.89 ± 0.18	15.04 ± 0.13	14.55 ± 0.03	14.14 ± 0.05
J22493078–1628012	L4:+T1:	378.6 ± 9.5	127.8 ± 9.5	1,2,4,6	91 ± 18	47.8 ± 7.8	21.28 ± 0.04	19.13 ± 0.04	16.12 ± 0.09	15.26 ± 0.09	14.83 ± 0.11	14.08 ± 0.03	13.75 ± 0.04	
J00062287–1319503	L6:+T7:	–236.9 ± 15.2	–426.5 ± 13.8	1,2,4,5,6	87 ± 18	37.5 ± 6.1	16.67 ± 0.13	15.55 ± 0.11	15.12 ± 0.13	16.70 ± 0.11	15.81 ± 0.09	14.86 ± 0.04	14.24 ± 0.03	13.75 ± 0.04	
(h) Peculiar UCDs																			
J05522359+0210585	<M0 pec	–62.4 ± 30.7	31.7 ± 27.4	1,2,3,4,5	20.81 ± 0.05	19.49 ± 0.05	16.85 ± 0.19	15.87 ± 0.15	15.73 ± 0.22	17.21 ± 0.10	16.30 ± 0.06	15.72 ± 0.04	15.23 ± 0.05	15.25 ± 0.09	
J16314748–1922461	M pec	–59.2 ± 7.1	–72.6 ± 6.8	1,2,4	15.54 ± 0.05	14.54 ± 0.06	14.01 ± 0.06	13.75 ± 0.03	13.55 ± 0.04	

Table 5 – *Continued*

Object	SpT (NIR)	$\mu_\alpha \cos \delta$	μ_δ	Epochs ^a	V_{\tan} (km s ⁻¹)	$d_{\text{phot}}^{\text{b}}$ (pc)	SDSS		MegaCam		2MASS			MKO			WISE	
		(mas yr ⁻¹)	(mas yr ⁻¹)				<i>i</i>	<i>z</i>	<i>i</i>	<i>z</i>	<i>J</i>	<i>H</i>	<i>K_s</i>	<i>J</i>	<i>H</i>	<i>K</i>	<i>W1</i>	<i>W2</i>
J12565644-1002432	M8:: pec	-62.5 ± 16.8	-284.3 ± 15.3	1,2,4	129 ± 31	93.9 ± 15.3	16.67 ± 0.18	15.71 ± 0.14	14.86 ± 0.13	14.45 ± 0.03	14.22 ± 0.05
J00063158-2158225	M9:: pec	0.6 ± 28.2	118.9 ± 28.0	1,2,4	72 ± 36	128.4 ± 21.3	16.83 ± 0.18	16.24 ± 0.24	15.44 ± 0.17	15.50 ± 0.04	15.14 ± 0.08
J01031050+1940463	M9.5: pec ²	-46.3 ± 32.2	-129.0 ± 29.3	1,2,3,4,6	95 ± 47	147.0 ± 25.1	21.20 ± 0.13	19.25 ± 0.08	21.00 ± 0.03	19.50 ± 0.03	16.56 ± 0.10	16.50 ± 0.19	15.96 ± 0.30	15.41 ± 0.04	15.55 ± 0.12
J04223302+1033189	M9.5: pec ²	79.7 ± 9.8	-174.9 ± 8.7	1,2,4,6	74 ± 17	81.1 ± 13.2	19.38 ± 0.03	18.03 ± 0.03	15.65 ± 0.06	15.12 ± 0.09	14.65 ± 0.07	14.46 ± 0.03	14.26 ± 0.05
J04232040+1212118	M9.5: pec ²	27.7 ± 9.3	-56.8 ± 9.0	1,2,4,5	23 ± 8	76.4 ± 12.5	15.69 ± 0.07	15.22 ± 0.09	14.98 ± 0.15	15.83 ± 0.03	15.15 ± 0.03	14.66 ± 0.05	14.41 ± 0.03	14.13 ± 0.05
J05320830-3253328	M9.5: pec ²	-52.9 ± 20.5	139.7 ± 19.0	1,2,4,6	66 ± 23	92.7 ± 15.1	20.79 ± 0.04	19.10 ± 0.04	16.32 ± 0.12	15.89 ± 0.19	15.43 ± 0.23	14.88 ± 0.03	14.55 ± 0.05
J00045499-2007410	L0:: pec ²	238.4 ± 28.4	-61.4 ± 28.2	1,2,4	139 ± 46	119.2 ± 19.9	16.52 ± 0.14	16.24 ± 0.24	15.75 ± 0.22	15.48 ± 0.04	15.21 ± 0.09
J10441549+0620138	L0: pec ²	128.0 ± 17.7	-35.1 ± 16.5	1,2,3,4	53 ± 18	84.0 ± 13.7	20.41 ± 0.04	18.43 ± 0.03	16.08 ± 0.09	15.52 ± 0.11	15.16 ± 0.18	14.74 ± 0.03	14.45 ± 0.06
J13391950+1523440	L0: pec	-128.8 ± 13.3	-145.1 ± 13.3	1,2,3,5	75 ± 19	81.3 ± 13.3	20.38 ± 0.04	18.60 ± 0.03	16.10 ± 0.09	15.39 ± 0.10	15.04 ± 0.12	16.20 ± 0.03	15.54 ± 0.04	14.90 ± 0.02	14.70 ± 0.03	14.38 ± 0.05
J08125319+3721048	L0.5 pec ¹	12.7 ± 7.2	-152.3 ± 6.8	1,2,3,4	43 ± 10	59.4 ± 9.6	20.20 ± 0.03	18.33 ± 0.02	15.75 ± 0.07	14.98 ± 0.08	14.28 ± 0.07	14.04 ± 0.03	13.81 ± 0.04
J23324336-1249383	L0.5: pec	183.2 ± 21.2	-84.8 ± 20.8	1,2,4,6	108 ± 34	113.1 ± 19.0	21.43 ± 0.07	19.86 ± 0.16	16.56 ± 0.13	16.23 ± 0.22	15.51 ± 0.18	15.34 ± 0.04	15.21 ± 0.10
J11171536+1857037	L1:: pec	-222.6 ± 21.0	-117.2 ± 19.5	1,2,3,4	101 ± 28	84.6 ± 13.9	20.82 ± 0.05	18.99 ± 0.04	20.23 ± 0.05	...	16.61 ± 0.14	15.66 ± 0.13	15.10 ± 0.13	14.98 ± 0.04	14.69 ± 0.06
J21503911-0412117	L1:: pec ²	8.0 ± 15.8	-89.1 ± 15.8	1,2,3,4	33 ± 14	78.3 ± 12.8	20.99 ± 0.07	19.05 ± 0.05	16.14 ± 0.09	15.46 ± 0.14	15.33 ± 0.18	14.65 ± 0.03	14.52 ± 0.06
J22552905-0725440	L1:: pec ²	269.5 ± 16.7	-382.6 ± 15.8	1,2,3,4	172 ± 37	77.5 ± 12.8	20.28 ± 0.05	18.18 ± 0.03	16.08 ± 0.08	15.41 ± 0.11	15.22 ± 0.16	14.80 ± 0.04	14.50 ± 0.07
J08583693+2710518	L1.5: pec	96.8 ± 13.0	-180.8 ± 12.8	1,2,3,4	33 ± 8	34.3 ± 5.6	19.40 ± 0.02	17.61 ± 0.02	15.05 ± 0.05	14.23 ± 0.05	13.66 ± 0.05	13.13 ± 0.02	12.84 ± 0.03
J14550283+2619202	L2: pec ²	181.8 ± 10.3	-138.7 ± 14.2	1,2,3,4	41 ± 10	37.7 ± 6.1	19.56 ± 0.02	17.71 ± 0.02	15.14 ± 0.05	14.53 ± 0.06	13.87 ± 0.06	13.42 ± 0.02	13.15 ± 0.03
J23302193+1006003	L2: pec ¹	183.3 ± 14.3	-94.5 ± 13.6	1,2,3,4,6	57 ± 15	58.7 ± 9.6	20.72 ± 0.06	18.89 ± 0.05	20.81 ± 0.05	19.26 ± 0.04	16.36 ± 0.14	15.32 ± 0.13	14.65 ± 0.09	14.36 ± 0.03	14.11 ± 0.05
J09463358+1808211	L2.5: pec	-61.3 ± 10.9	-181.0 ± 12.5	1,2,3,5	62 ± 16	68.6 ± 11.2	20.69 ± 0.04	19.02 ± 0.05	16.34 ± 0.07	15.36 ± 0.09	15.10 ± 0.10	16.81 ± 0.08	15.53 ± 0.03	14.91 ± 0.04	14.66 ± 0.03	14.55 ± 0.06
J21174252-0611132	L2.5: pec ²	126.4 ± 11.6	-161.7 ± 13.8	1,2,3,4	58 ± 14	59.2 ± 9.6	20.01 ± 0.05	18.27 ± 0.04	16.14 ± 0.08	15.16 ± 0.08	14.92 ± 0.11	14.51 ± 0.03	14.23 ± 0.05
J04175143-1838320	L3: pec ¹	144.2 ± 10.2	111.8 ± 10.6	1,2,4,6	36 ± 9	41.5 ± 6.7	20.57 ± 0.05	18.98 ± 0.05	16.33 ± 0.12	15.31 ± 0.11	14.60 ± 0.10	13.80 ± 0.03	13.56 ± 0.03
J08511977+1043470	L3: pec ¹	-138.0 ± 17.2	108.2 ± 18.5	1,2,3,4,5	50 ± 15	60.0 ± 9.8	21.79 ± 0.10	19.60 ± 0.05	16.79 ± 0.15	15.78 ± 0.14	15.09 ± 0.12	16.92 ± 0.04	15.89 ± 0.03	15.09 ± 0.03	14.65 ± 0.03	14.36 ± 0.05
J10390822+2440446	L5:: pec	-84.5 ± 14.0	-69.6 ± 14.4	1,2,3,4	22 ± 8	41.9 ± 6.8	21.73 ± 0.12	19.41 ± 0.06	16.76 ± 0.14	15.72 ± 0.13	15.04 ± 0.11	14.35 ± 0.03	13.96 ± 0.04
J11181292-0856106	L6.5 pec ²	-632.8 ± 10.1	-272.3 ± 8.6	1,2,4	86 ± 16	26.3 ± 4.3	15.74 ± 0.09	14.77 ± 0.06	14.18 ± 0.08	13.57 ± 0.03	13.21 ± 0.03
J11430272+1905440	L7:: pec	6.7 ± 20.7	-265.2 ± 21.7	1,2,3,4	45 ± 12	35.7 ± 5.8	22.79 ± 0.28	19.76 ± 0.08	16.77 ± 0.18	15.80 ± 0.15	15.01 ± 0.14	14.42 ± 0.03	13.96 ± 0.04
J11322058-3809562	L8: pec	170.7 ± 5.8	-142.8 ± 6.7	1,2	23 ± 5	21.4 ± 3.5	15.96 ± 0.08	14.82 ± 0.07	14.21 ± 0.07	13.49 ± 0.02	13.02 ± 0.03
J10043728-1127342	T2:: pec	217.7 ± 28.1	-134.9 ± 26.1	1,2,4,5	39 ± 12	32.3 ± 5.3	21.60 ± 0.05	...	16.97 ± 0.19	15.96 ± 0.17	15.59 ± 0.24	16.80 ± 0.04	15.73 ± 0.03	15.16 ± 0.04

Note. pec¹ are possibly red objects; pec² are possibly blue objects; pec³ are possibly binary objects.

^aEpochs included in the measurements of proper motion: (1) WISE; (2) 2MASS; (3) SDSS; (4) SIMP; (5) OMM; (6) CFHT.

^bUnless otherwise noted, photometric distances are based on WISE W2 band and polynomial fits for M_{W2} from Dupuy & Liu (2012). Binarie distances are calculated by adding the flux of both unresolved components.

^cPhotometric distance based on 2MASS H band and polynomial fits for M_H from Dupuy & Liu (2012).

^dResolved binary by Duchêne et al. (2013). Rejected as a Hyades member by Lodieu et al. (2014).